Universitat
de les Illes Balears

DOCTORAL THESIS
2024

Dynamics of social interactions

David Abella Bujalance

Universitat de les Illes Balears

IFISC

DOCTORAL THESIS 2024

Doctoral programme in Physics

Dynamics of social interactions

David Abella Bujalance

Thesis Supervisor: José Javier Ramasco Sukia
Thesis Supervisor: Maxi San Miguel
Thesis Tutor: Cristóbal López Sánchez

Doctor by the Universitat de les Illes Balears

Supervisors:
José Javier Ramasco Sukia
Maxi San Miguel

David Abella Bujalance.
Dynamics of social interactions. ©
Palma de Mallorca, June 2024

A en Manuel Miranda
pel seu suport i ajuda
durant tots aquests anys.
Sempre estaràs amb mi.
i recordare sempre
el que em vas ensenyar.

Dr José Javier Ramasco of the Consejo Superior de Investigaciones Científicas (CSIC) and Dr Maxi San Miguel of the Universitat de les Illes Balears (UIB)

WE DECLARE:

That the thesis titles *Dynamics of social interactions*, presented by David Abella Bujalance to obtain a doctoral degree, has been completed under my supervision and meets the requirements to opt for an International Doctorate.

For all intents and purposes, I hereby sign this document.

Signature

Dr. José Javier Ramasco Sukia
Thesis Supervisor

Dr. Maxi San Miguel
Thesis Supervisor

Palma de Mallorca, June 2024

Acknowledgements

M'agradaria agrair aquesta tesi a totes les persones que m'han ajudat a fer-la possible. En primer lloc, vull agrair a la meva família, per tot el suport que m'han donat durant tots aquests anys. En especial, vull agrair a la meva mare, per tot el que ha fet per mi, i per tot el que ha hagut de patir per mi. També vull agrair a la meva parella, per tot el suport que m'ha donat, i per tot el que m'ha ajudat a tirar endavant. I finalment, vull agrair a tots els meus amics, per tot el suport que m'han donat, i per tots els bons moments que hem passat junts.

Des d'un primer moment, vull agrair a la meva directora, la professora Marta Arias, per haver-me donat l'oportunitat de fer aquest projecte, i per tot el suport que m'ha donat durant tot el projecte. També vull agrair al meu tutor, el professor Jordi Casas, per tot el suport que m'ha donat durant tot el projecte. I finalment, vull agrair a tots els professors que m'han ensenyat durant tots aquests anys, per tot el que m'han ensenyat, i per tot el que m'han ajudat a tirar endavant.

Tambe afegir que aquest projecte no hagués estat possible sense l'ajuda de tots els companys que han fet possible que aquest projecte sigui una realitat. Jo que soc un dels que ha fet possible que aquest projecte sigui una realitat, vull agrair a tots els companys que han fet possible que aquest projecte sigui una realitat, per tot el suport que m'han donat durant tot el projecte.

Resum

En els sistemes complexos distribuïts, els sistemes de memòria transaccional distribuïda (DTM) són una eina molt útil per a la programació concurrent. Aquests sistemes permeten als desenvolupadors de software escriure codi concurrent sense haver de preocupar-se per la gestió de la memòria compartida. A més, els DTM ofereixen una interfície molt senzilla per a la programació concurrent, ja que permeten als desenvolupadors de software escriure codi concurrent de forma semblant a com ho farien si el codi fos seqüencial. Tot i això, els DTM no són una eina perfecta, ja que tenen un rendiment molt inferior al de les estructures de dades distribuïdes. A més, els DTM no són capaços de gestionar estructures de dades distribuïdes de forma eficient. Per aquest motiu, els DTM no són una eina adequada per a la programació de sistemes distribuïts.

Resumen

En los sistemas complejos distribuidos, los sistemas de memoria transaccional distribuida (DTM) son una herramienta muy útil para la programación concurrente. Estos sistemas permiten a los desarrolladores de software escribir código concurrente sin tener que preocuparse por la gestión de la memoria compartida. Además, los DTM ofrecen una interfaz muy sencilla para la programación concurrente, ya que permiten a los desarrolladores de software escribir código concurrente de forma similar a como lo harían si el código fuera secuencial. Sin embargo, los DTM no son una herramienta perfecta, ya que tienen un rendimiento muy inferior al de las estructuras de datos distribuidas. Además, los DTM no son capaces de gestionar estructuras de datos distribuidas de forma eficiente. Por este motivo, los DTM no son una herramienta adecuada para la programación de sistemas distribuidos.

Abstract

In complex systems distributed transactional memory (DTM) systems are a very useful tool for concurrent programming. These systems allow software developers to write concurrent code without having to worry about managing shared memory. In addition, DTM systems offer a very simple interface for concurrent programming, as they allow software developers to write concurrent code in a similar way to how they would if the code were sequential. However, DTM systems are not a perfect tool, as they have a much lower performance than distributed data structures. In addition, DTM systems are not able to manage distributed data structures efficiently. For this reason, DTM systems are not a suitable tool for programming distributed systems.

Contents

1 Introduction and positioning . . . 1
1.1 Scientific Landscape . . . 1
1.2 Challenges of Computational Social Science . . . 1
1.2.1 Data availability . . . 2
1.2.2 Data analysis . . . 2
1.2.3 Modeling . . . 2
1.2.4 Applications . . . 2
1.3 Terminology and general concepts . . . 2
1.4 Datasets . . . 2

2 Models, temporal patterns and aging . . . 5
2.1 Introduction . . . 5
2.2 Simple and Complex Contagion . . . 5
2.3 Threshold model . . . 5
2.4 The Sakoda-Schelling model . . . 6
2.5 Bursty Human Dynamics . . . 6
2.6 Aging mechanism . . . 6
2.7 Aging in Simple Contagion Models . . . 7

I Aging in threshold models

3 Aging in binary state dynamics: The threshold model . . . 11
3.1 Introduction . . . 11
3.2 Aging and the Threshold model . . . 13
3.3 Dynamics on Complex networks . . . 13
3.3.1 Numerical results . . . 13
3.3.2 General mathematical description . . . 18
3.3.3 Analytical results . . . 20

3.4 Dynamics on a Moore lattice . . . 23
3.5 Conclusions . . . 26

4 Aging effects in the Schelling segreggation model . . . 27
4.1 Introduction . . . 27
4.2 Model . . . 29
4.3 Metrics of segregation . . . 30
4.4 Results . . . 30
4.4.1 Phase diagram . . . 30
4.4.2 Segregated phase: final state . . . 31
4.4.3 Segregated phase: coarsening dynamics . . . 33
4.4.4 Aging breaks the asymptotic time-translational invariance . . . 35
4.5 Summary and discussion . . . 37

5 Ordering dynamics in the Symmetrical Threshold model . . . 39
5.1 Introduction . . . 39
5.2 Symmetrical Threshold model . . . 40
5.2.1 Mean-field . . . 40
5.2.2 Random networks . . . 42
5.3 Symmetrical Threshold model in a Moore Lattice . . . 45
5.3.1 Original model without aging . . . 46
5.4 Summary and conclusions . . . 47

6 Aging implications in the Symmetrical Threshold model . . . 51
6.1 Introduction . . . 51
6.2 Symmetrical Threshold model with aging . . . 51
6.2.1 Mean-field . . . 52
6.2.2 Random networks . . . 53
6.3 Symmetrical Threshold model in a Moore Lattice . . . 56
6.3.1 The role of aging . . . 56
6.4 Summary and conclusions . . . 57

II Real estate market dynamics

7 Dynamics of the real state market . . . 65
7.1 Theorems . . . 65
7.1.1 Several equations . . . 65
7.1.2 Single Line . . . 65
7.2 Definitions . . . 65
7.3 Notations . . . 65
7.4 Remarks . . . 66
7.5 Corollaries . . . 66
7.6 Propositions . . . 66
7.6.1 Several equations . . . 66

7.6.2 Single Line 66
7.7 Examples 66
7.7.1 Equation Example 66
7.7.2 Text Example 66
7.8 Exercises 66
7.9 Problems 66
7.10 Vocabulary 67

8 Assessing the real state market segmentation 69
8.1 Table 69
8.2 Figure 69

Index 83

Appendices 85

A Effect of a higher vacancy density ρ_v in the coarsening dynamics of the Schelling model 85

B Generalized master equation for binary state dynamics with aging 87

List of Figures

3.1 Average density ρ of adopters for an Erdős-Rényi graph 14

3.2 Cascade spreading for the Threshold model 14

3.3 Cascade dynamics and fall to the full-adopt state ($\rho \sim 1$) 15

3.4 Average time to reach the steady state τ 16

3.5 Cascade dynamics of the Threshold model in graphs 17

3.6 Exponent for the Threshold model 21

3.7 Exponent γ for the Threshold model with exogenous aging 23

3.8 Cascade spreading of the Threshold model in a lattice 24

3.9 Cascade dynamics snapshots in a lattice 25

4.1 Average interface density and segregation coefficient 31

4.2 Fraction of unsatisfied agents and roughness 32

4.3 Average interface density evolution 34

4.4 Coarsening towards the segregated state 35

4.5 Two-times autocorrelation 36

5.1 **Phases of the Symmetrical Threshold model.** (a) Phase diagram of the Symmetrical Threshold model in a Complete graph of $N = 2500$ nodes. Dotted and dashed lines correspond to $T = (1 - |m_0|)/2$ and $T = (1 + |m_0|)/2$, respectively. Average performed over 5000 realizations. (b) Potential representation from Eq. (**??**) for a set of values of the threshold T, shown in different colors. 41

5.2 **Phase diagram in random networks.** Phase diagram of the Symmetrical Threshold model in an ER (a) and a RR (b) graph, both of $N = 4 \cdot 10^4$ nodes and mean degree $\langle k \rangle = 8$. The color map indicates the value of the average final magnetization m_f. The red dashed line is the HMF prediction of the mixed-ordered critical line. The black solid lines correspond to the AME prediction of the borders of Phase II. (c) Average final magnetization m_f as a function of the initial magnetization m_0 for different T values (indicated with different colors and markers) in the RR graph. The average is performed over 5000 realizations. The dotted and solid lines are the HMF (for $T = 1/8 - 4/8$) and AME predictions (for all T), respectively. 42

5.3 **Symmetrical Threshold model dynamics in random networks.** Evolution of the average interface density $\rho(t)$ (a), the average magnetization $m(t)$ (b), the mean internal time $\bar{\tau}(t)$ (c), and the persistence $p(t)$ (d) for the Symmetrical Threshold model. The average is computed over 5000 surviving trajectories (simulations stop when the system reaches the absorbing ordered states). Results for different values of T are plotted with diverse markers and colors: red ($T = 0.12$) and blue ($T = 0.24$) belong to Phase I, green ($T = 0.36$) and grey ($T = 0.49$) belong to Phase II and purple ($T = 0.86$) belongs to Phase III. Solid colored lines are the AME integrated solutions, using Eqs. (5.6)-(5.8). The initial magnetization is $m_0 = 0.5$. The system is on an ER graph with $N = 4 \cdot 10^4$ and mean degree $\langle k \rangle = 8$. The dashed green line in (a) shows $\rho(t) \sim \rho_0 e^{-t}$, the dashed purple line in (c) shows $\bar{\tau}(t) = t$ and the dashed lines in (d) show $p(t) \sim e^{-\alpha t}$, where $\alpha = 1$ (red) and $\alpha = 3/4$ (blue) We compute the relative difference, Δ, between the simulation and the integrated solution (until simulation ends): For all T, $\Delta_\rho < 5\%$, $\Delta_m < 1\%$ and $\Delta_{\bar{\tau}} < 5\%$ (except for $T = 0.86$ where $\Delta_{\bar{\tau}} = 11\%$). 44

5.4 **Aging effects in the complete graph.** Evolution of the average magnetization $m(t)$ (a) and the mean internal time $\bar{\tau}(t)$ (b) in a complete graph of $N = 2500$ nodes. Results are shown for the Symmetrical Threshold Model (pluses) and the version with aging (crosses) obtained from simulations. Different colors correspond to different values of the threshold T: red ($T = 0.1$) belongs to Phase I, green ($T = 0.5$) belongs to Phase II, and purple ($T = 0.9$) to Phase III. The initial magnetization is fixed at $m_0 = 0.5$. The solid and dashed lines correspond to the numerically integrated solutions from Eq. 6.3 for the original model ($p_A(j) = 1$) and the version with aging ($p_A(j) = 1/(t+2)$), respectively. The dashed lines in (b) show $\bar{\tau}(t) = t$ (purple) and the solution from the recursive relation in Eq. (**??**) (red). As computed in Fig. 5.3, for the non-aging version, $\Delta_m, \Delta_{\bar{\tau}} < 4\%$ (except for $T = 0.86$ where $\Delta_{\bar{\tau}} = 10\%$) and for the aging version, $\Delta^a_m, \Delta^a_{\bar{\tau}} < 9\%$ (except for $T = 0.86$ where $\Delta^a_{\bar{\tau}} = 15\%$). 46

5.5 **Symmetrical Threshold model in a Moore lattice.** (a) Phase diagram of the Symmetrical Threshold model in a Moore lattice of size $N = L \times L$, with $L = 100$. The color map indicates the value of the average final magnetization m_f. Solid black lines are the borders of Phase II (first and last value of T where the system reaches the absorbing ordered state for each m_0), computed from the numerical simulations. (b) Average final magnetization m_f as a function of the initial magnetization m_0 for the discrete values of the threshold T (indicated with different colors and markers) in a Moore lattice of the same size. Average performed over 5000 realizations. . . . 47

5.6 **Dynamical regimes in a Moore lattice.** Evolution of the average interface density $\rho(t)$ (a-b), the average magnetization $m(t)$ (c-d), and the persistence $p(t)$ (e-f) for the Symmetrical model in a Moore lattice starting from a random configuration with $m_0 = 0.5$ (a-c-e) and $m_0 = 0$ (b-d-f). We plot 50 different trajectories in solid lines and the average of 5000 surviving trajectories (simulations stop when the system reaches the absorbing ordered states) in different markers. Different colors and markers indicate different threshold values: red ($T = 1/8$) and blue ($T = 2/8$) belong to Phase I, green ($T = 3/8$) and black ($T = 4/8$), and purple ($T = 5/8, 7/8$) belong to Phase III. The average magnetization $m(t)$ is computed according to the two symmetric absorbing states. System size is fixed at $N = L \times L$, $L = 200$. The dashed lines in (a) are $\rho \sim \exp(-\alpha \cdot t)$ with $\alpha = 0.5$ (black) and $\alpha = 0.8$ (green), in (b) are $\rho(t) \sim at^{-1/2}$ with $a = 0.36$ (black) and $a = 0.2$ (green), in (e-f) is $p(t) \sim \exp(-\ln(t)^2)$ (blue). 48

6.1 **Phase diagram modified by aging.** Phase diagram of the Symmetrical Threshold with aging model in an ER graph of $N = 4 \cdot 10^4$ nodes and $\langle k \rangle = 8$. The blue, red, and green dotted lines show the borders of Phase II (first and last value of T where the system reaches the absorbing ordered state for each m_0) computed from numerical simulations evolving until $t_{\max} = 10^3$, 10^4 and 10^5 time steps, respectively. Black solid lines show AME solution integrated 10^5 time steps. Phase I^*, II and III correspond with the orange, white and gray areas, respectively. The solid purple lines are the mixed-ordered and ordered-frozen critical lines for the non-aging version of the model. . . . 53

6.2 **Symmetrical threshold model with aging dynamics in random networks.** Evolution of the average interface density $\rho(t)$ (a) and the average magnetization $m(t)$ (b) for the Symmetrical Threshold model with aging. The average is computed over 5000 surviving trajectories (simulations stop when the system reaches the absorbing ordered states) for different values of T, shown by different markers and colors: red ($T = 0.12$) and blue ($T = 0.24$) belong to Phase I^*, green ($T = 0.36$) and grey ($T = 0.49$) belong to Phase II and purple ($T = 0.86$) belong to Phase III. The inset in (a) shows a close look to the evolution for $T = 0.12$, in linear-log scale. Solid colored lines are the AME integrated solutions for 10^4 time steps, using Eqs. 5.6 - 5.7. The initial magnetization is $m_0 = 0.5$. The system is on an ER graph with $N = 4 \cdot 10^4$ and mean degree $\langle k \rangle = 8$. The dashed green line in (a) shows $\rho(t) \sim \rho_0 t^{-1}$. As computed in Fig. 5.3, for all T, $\Delta_\rho^a < 12\%$, $\Delta_m^a < 15\%$. . . 59

6.3 **Phase I^* slow decay and minority consensus.** Magnetization $m(t)$ (a) and interface density $\rho(t)$ (c) trajectories for different values of the threshold T ($m_0 = -0.2$) using the Symmetrical Threshold model with aging. (b) Final magnetization histogram of 1000 trajectories for the same system at $T = 0.25$. Different colors indicate different values of T. The inset at (b) shows a close look at the logarithmic-like decay, shown in linear-log scale. The system is an ER graph with $N = 4 \cdot 10^4$ and mean degree $\langle k \rangle = 8$. 59

6.4 **Phase I^* dependence with the network mean degree.** Critical threshold T_c dependence with the mean degree $\langle k \rangle$ for the Symmetrical Threshold model with aging for an ER graph with $N = 4 \times 10^4$ nodes for an initial magnetization of $m_0 = 0.25$ (a) and $m_0 = 0.75$ (b). The blue and red markers indicate the borders of phases I and II, which coincide for a sufficiently large value of the mean degree. The hatched area corresponds to the fulfillment of the inequality in the legend. 60

6.5 **Symmetrical Threshold model with aging in a Moore lattice.** (a) Phase diagram of the Symmetrical Threshold model with aging in a Moore lattice of $N = L \times L$, with $L = 100$. The blue, red and green dotted lines show the borders of Phase II (first and last value of T where the system reaches the absorbing ordered state for each m_0) from numerical simulations evolving until $t_{\max} = 10^3$, 10^4 and 10^5 time steps, respectively. Phase I^*, II and III correspond with the orange, white and gray areas, respectively. The solid purple lines are the mixed-ordered and ordered-frozen critical lines for the Symmetrical threshold model (from Fig. 5.5) (b) Average magnetization at time $t_{\max}$ ($m_f(t_{\max})$) as a function of the initial magnetization m_0 for different values of the threshold T (indicated with different colors and markers) in a Moore lattice of $N = L \times L$, with $L = 100$. The numerical simulations are obtained until $t_{\max} = 10^4$ time steps. Average performed over 5000 realizations. 60

6.6 **Modified dynamical regimes by aging in a Moore lattice** Evolution of the average interface density $\rho(t)$ (a-b), the average magnetization $m(t)$ (c-d), and the persistence $p(t)$ (e-f) for the Symmetrical model with aging in a Moore lattice starting from a random configuration with $m_0 = 0.5$ (a-c-e) and $m_0 = 0$ (b-d-f). We plot 30 different trajectories in solid lines and the average of over 5000 surviving trajectories in symbols. Colors and symbols indicate different threshold values: red ($T = 1/8$) and blue ($T = 2/8$) belong to Phase I^*, green ($T = 3/8$), and black ($T = 4/8$) belong to Phase II, and purple ($T = 5/8, 7/8$) belong to Phase III. The average magnetization is computed according to the two symmetric absorbing states. The insets in (a-b) show a close look at the evolution for $T = 0.12$, in linear-log scale. System size is fixed at $N = L \times L$, $L = 200$. The dashed lines in (a) are $\rho \sim t^{-\alpha}$ with $\alpha = 0.5$ (black) and $\alpha = 0.8$ (green), and in (c) are $p(t) \sim t^{-1}$ (red). Simulations stop when the system reaches the absorbing ordered states. 61

6.7 **System evolution at $T = 0.5$ and $m_0 = 0$.** Evolution of a single realization for $T = 0.5$ and $m_0 = 0$ using the Symmetrical threshold model (a) and the version with aging (b). Snapshots are taken after $1, 10, 60, 440$ and 3300 time steps in (a) and after $1, 60, 3300, 2 \cdot 10^5$ and $5 \cdot 10^6$ time steps in (b), increasing from left to right. System size is fixed to $N = L \times L$, $L = 256$. 62

8.1 Figure caption. 69

8.2 Floating figure. 70

A.1 Average interface density $\langle \rho(t) \rangle$ as a function of time steps for different values of the tolerance parameter T fr the Schelling model (**a**) and the version with aging (**b**). The different plots show a the evolution at a different value of the vacancy density, increasing from left to right $\rho_v = 0.005, 0.15, 0.2, 0.3$ and 0.45. Average performed over 10^3 realisations with system size $100\ x\ 100$. 85

A.2 Snapshots of the system at the final segregated state (after 10^6 MC steps) for the Schelling model (**a**) and the version with (**b**). System size $200\ x\ 200$ with $\rho_v = 0.45$ and $T = 0.29$. 86

A.3 Cluster coefficient of vacancies as a function of the vacancy density ρ_v for the Schelling model (**a**) and the version with (**b**) for different values of the tolerance T. 86

B.1 Schematic representation of the transitions to or from the set $s_{k,m,j}$ $(j > 0)$. We show the central node with some neighbors for different values m and j. Purple nodes are susceptible or non-adopters or spin-down, and yellow are infected or adopters or spin-up. 88

List of Tables

8.1 Table caption. 69
8.2 Floating table. 70

List of publications

1. David Abella, Maxi San Miguel, and José J. Ramasco. "Aging effects in Schelling segregation model". In: *Scientific Reports* 12 (2022), page 19376. DOI: 10.1038/s41598-022-23224-7

2. David Abella, Maxi San Miguel, and José J. Ramasco. "Aging in binary-state models: The Threshold model for complex contagion". In: *Phys. Rev. E* 107 (2 Feb. 2023), page 024101. DOI: 10.1103/PhysRevE.107.024101. URL: https://link.aps.org/doi/10.1103/PhysRevE.107.024101

3. Aging in Symmetrical Threshold Models

4. Idealista model for complex systems housing

5. Idealista spatial segmentation of the real state market

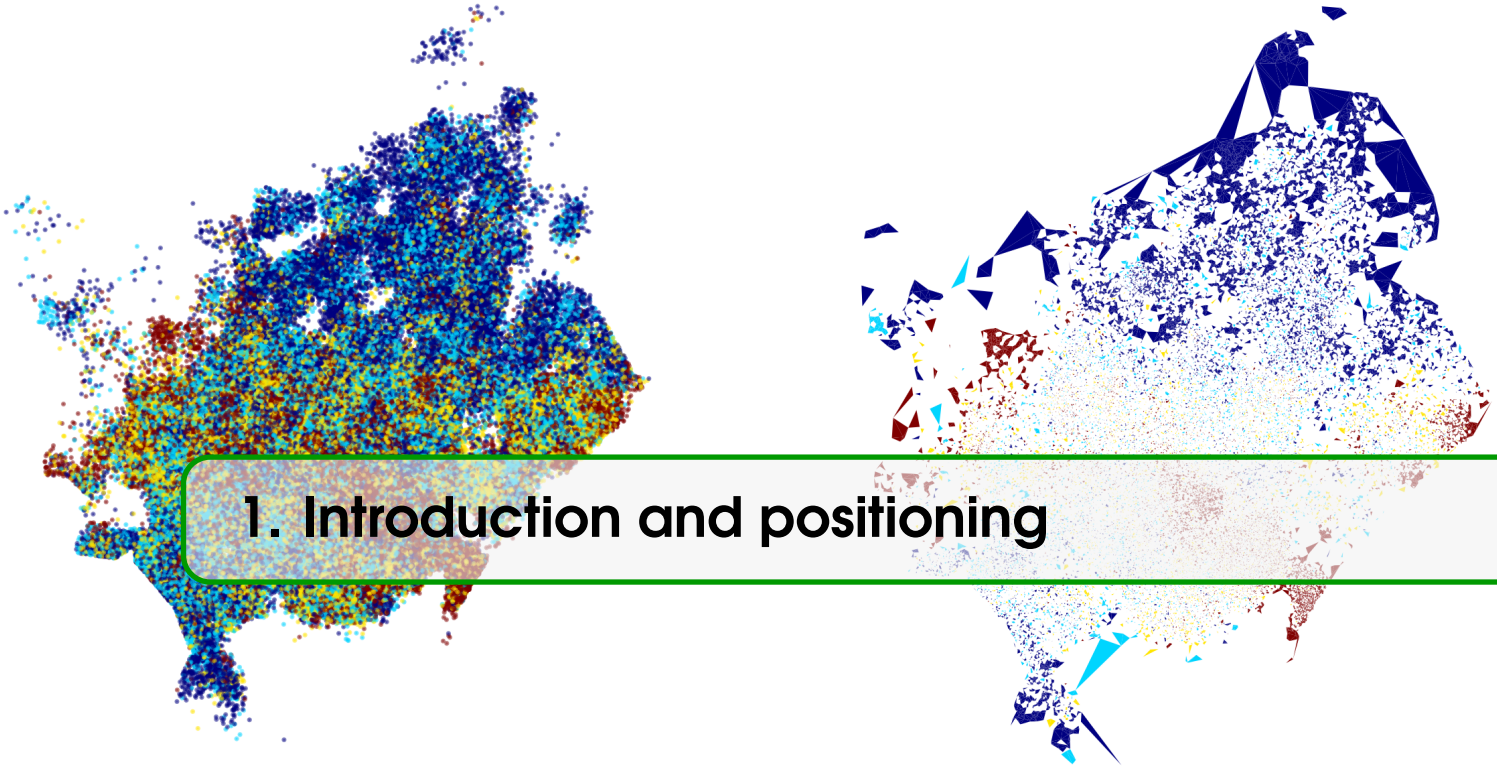

1. Introduction and positioning

1.1 Scientific Landscape

- How complex systems are studied from a physics perspective, and how the study of complex systems has evolved into the study of social systems.

- Human complex systems ....

- Nevertheless there are some challenges that are unique to the study of social systems, and that are not present in the study of physical systems and the main problem is the data availability.

- After the digital revolution, the amount of data that is generated by human activities has increased exponentially, and this data is being used to study human behavior and social systems.

- Big data is a term that is used to describe the large amount of data that is generated by human activities, and that is being used to study human behavior and social systems.

- To deal with big data, computational social science has emerged as a new field of study that uses computational methods to study human behavior and social systems.

- Also network science has emerged as a new field of study that uses network theory to study human behavior and social systems.

- This perspective is important because it allows us to understand phenomena from a different perspective, and to develop new methods to study human behavior and social systems.

- For example, the study of information spreading as a dynamical system on networks has allowed us to understand how information spreads in social networks, and to develop new methods to study information spreading in social networks.

- In particular, human interactions exhibit complex activity patterns that are difficult to understand and to model, and that are not present in the study of physical systems.

1.2 Challenges of Computational Social Science

- The study of human behavior and social systems is a complex problem that requires the use of computational methods to study human behavior and social systems.

- There are some challenges that are unique to the study of human behavior and social systems, and that are not present in the study of physical systems.

1.2.1 Data availability

- The main problem is the data availability, and the fact that the data that is generated by human activities is not always available for study.

- Notice that the data sources typically used for the study of human behavior does not come from controlled experiments, but from the digital traces that are generated by human activities.

1.2.2 Data analysis

- The second problem is the data analysis, and the fact that the data that is generated by human activities is not always easy to analyze.

- The data source to analyze usually is a piece of a larger dataset, so we need to be careful to avoid biases in the analysis driven by the data size.

- Temporal windows are also a problem, because when we analyze the dynamics of a system, we need to be careful to avoid biases in the analysis driven by the temporal window.

1.2.3 Modeling

- The third problem is the modeling, and the fact that the data that is generated by human activities is not always easy to model.

- Deterministic models are not always useful to model human behavior, and we need to use stochastic models to model human behavior.

- Also, mechanistic models and data driven models is something that we need to consider when we model human behavior.

- Another possibility is to use agent-based models to model human behavior.

1.2.4 Applications

- Computational social science has many applications, and it is being used to study human behavior and social systems.

- Sociotechnical systems, social networks, and human dynamics are some of the applications of computational social science.

- fake news detection, information spreading, and social influence are some of the applications of computational social science.

1.3 Terminology and general concepts

- In this section, we introduce some terminology and general concepts that are used in the study of human behavior and social systems.

Complex networks, interface density, and community structure are some of the concepts that are used in the study of human behavior and social systems.

binary state models, random networks, configuration models, and preferential attachment are some of the models that are used in the study of human behavior and social systems.

1.4 Datasets

- We used the idealista dataset

- The strong point of the idealista dataset is that it contains information about the real estate market in Spain, and that it is a large dataset that contains information about the real estate market in Spain.

- The missing point of the idealista dataset is that it contains information about the real estate market in Spain, and that it is a large dataset that contains information about the real estate market in Spain.

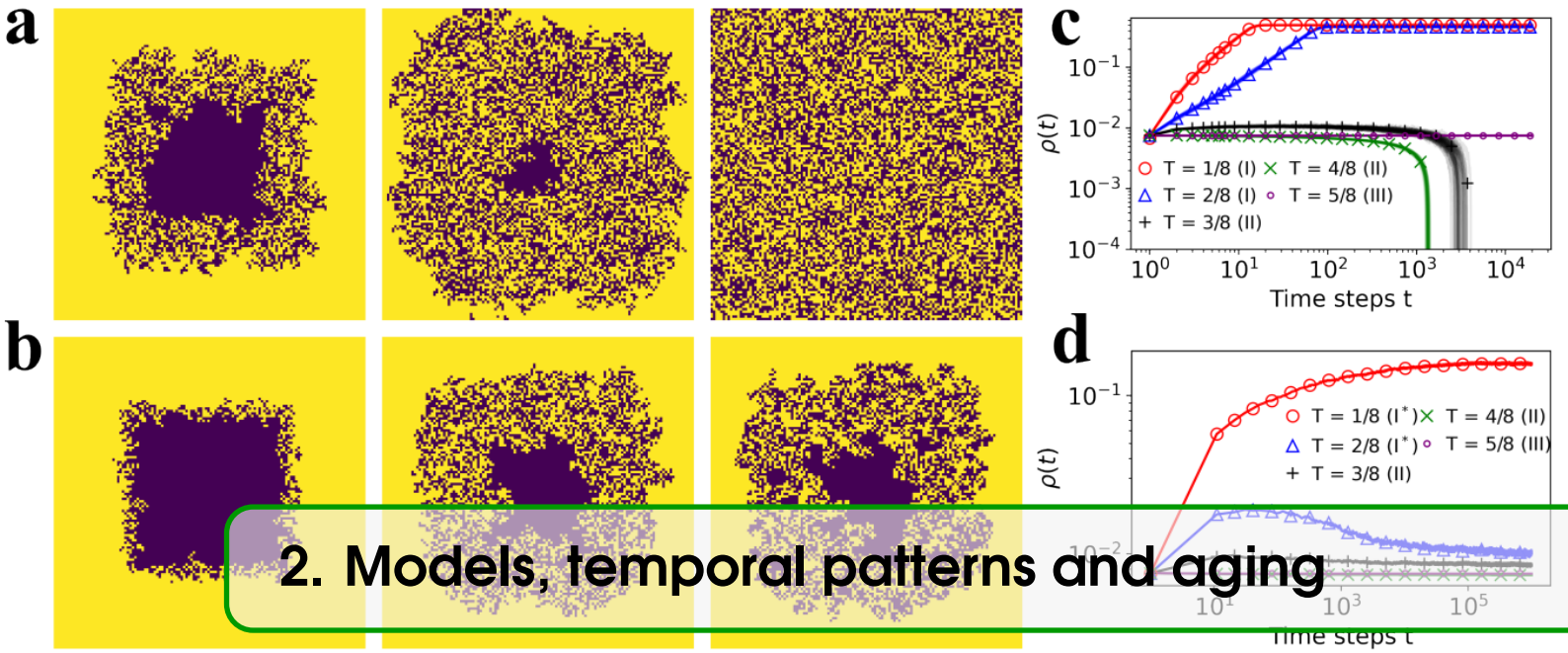

2. Models, temporal patterns and aging

2.1 Introduction

- Modeling human dynamics in opinion formation processes, or technology adoption process has been object of study for many years.

- The contagion of ideas is a process that has been studied for many years, and it is a process that is present in many social systems.

...

2.2 Simple and Complex Contagion

- The contagion of ideas is a process that has been studied for many years, and it is a process that is present in many social systems.

- Simple contagion is used to describe the process of contagion of ideas that is driven by the number of contacts that an individual has with other individuals.

- Complex contagion is used to describe the process of contagion of ideas that is driven by the number of contacts that an individual has with other individuals, and by the number of contacts that the individuals that the individual has contact with have with other individuals.

2.3 Threshold model

- The threshold model is used to describe processes of complex contagion based on the idea that individuals have a threshold that needs to be reached in order to adopt an idea.

- Watts (2002) proposed a simple model to study the dynamics of complex contagion based on the idea that individuals have a threshold that needs to be reached in order to adopt an idea.

- Should I describe what is a phase transition? Maybe with a foot note.

- This model exhibits a phase transition from a regime where the adoption of an idea is rare to a regime where the adoption of an idea is common. This phase transition is discontinuous.

- This model has been studied for many social networks and many variants of the model have been proposed...

2.4 The Sakoda-Schelling model

- Thomas C. Schelling (1975) proposed a model to study the dynamics of segregation based on the idea that individuals have a threshold that needs to be reached in order to move to a different location.

- This model become very popular because it was able to reproduce the segregation patterns that are observed in many cities, just as an emergent phenomena from individual decisions.

- On the other hand, this model was already studied by Sakoda in 1971, in a paper that was published in Japanese, and that was not known by the scientific community. In this work, the author proposed a model to study the dynamics of segregation based on the idea that individuals have a threshold that needs to be reached in order to move to a different location.

- Schelling model is a particular case of the Sakoda model.

- This model exhibits a phase transition from a regime where the segregation is low to a regime where the segregation is high. This phase transition is discontinuous.

- Despite the many variants of the model that have been proposed, the phase transition emergent in this model is very robust.

2.5 Bursty Human Dynamics

- All models previously described are based in an important assumption regarding to its dynamics: the interactions between individuals occur at a constant rate.

- This constant rate assumption is assuming that the stochastic interactions follow a Poisson process.

- However, from the analysis of many datasets of human interactions, it has been observed that the interactions between individuals are not constant, but bursty.

- The bursty behaviour is characterized by power law interevent time distributions, and it is present in many human activities, such as e-mail communication, face-to-face interactions, and phone calls.

- The modeling of bursty human dynamics is important because it allows us to understand how the bursty behaviour of human interactions affects the dynamics of social systems.

- Previous literature has several approaches to model bursty human dynamics: temporal networks, activity-driven models, aging ...

2.6 Aging mechanism

- The aging mechanism is a mechanism that has been proposed to model the bursty behaviour of human interactions.

- Aging mechanism is based on the idea that the probability of an individual to interact with another individual decreases with the time since the last interaction.

- Attachment to previous beliefs or habits is a common feature in human behavior. Granovetter (1973) discussed

- Instead of the constant rate assumption, the aging mechanism assumes that the interactions between individuals occur at a rate that decreases with the time since the last interaction.

- The focus on this approach is to include the bursty dynamics in the individuals attempts to interact with others, rather than in the interactions themselves (as in the activity-driven models or temporal networks).

2.7 Aging in Simple Contagion Models

- Aging in the Voter model has been studied by many authors, and it has been shown that the aging mechanism affects the dynamics of the model.

- The aging mechanism has been shown to affect the dynamics of the Voter model, and to change the phase transition of the model.

- Aging in the noisy voter model is able to change the phase transition of the model, and to make the phase transition continuous.

- Aging in the SI model is able to change the cascade size distribution of the model, and to make the cascade size distribution follow a power law (see the work of Karsai et al. 2011).

Aging in threshold models

3 Aging in binary state dynamics: The threshold model . . . 11

3.1 Introduction . . . 11
3.2 Aging and the Threshold model . . . 13
3.3 Dynamics on Complex networks . . . 13
3.4 Dynamics on a Moore lattice . . . 23
3.5 Conclusions . . . 26

4 Aging effects in the Schelling segreggation model . . . 27

4.1 Introduction . . . 27
4.2 Model . . . 29
4.3 Metrics of segregation . . . 30
4.4 Results . . . 30
4.5 Summary and discussion . . . 37

5 Ordering dynamics in the Symmetrical Threshold model . . . 39

5.1 Introduction . . . 39
5.2 Symmetrical Threshold model . . . 40
5.3 Symmetrical Threshold model in a Moore Lattice 45
5.4 Summary and conclusions . . . 47

6 Aging implications in the Symmetrical Threshold model . . . 51

6.1 Introduction . . . 51
6.2 Symmetrical Threshold model with aging . . . 51
6.3 Symmetrical Threshold model in a Moore Lattice 56
6.4 Summary and conclusions . . . 57

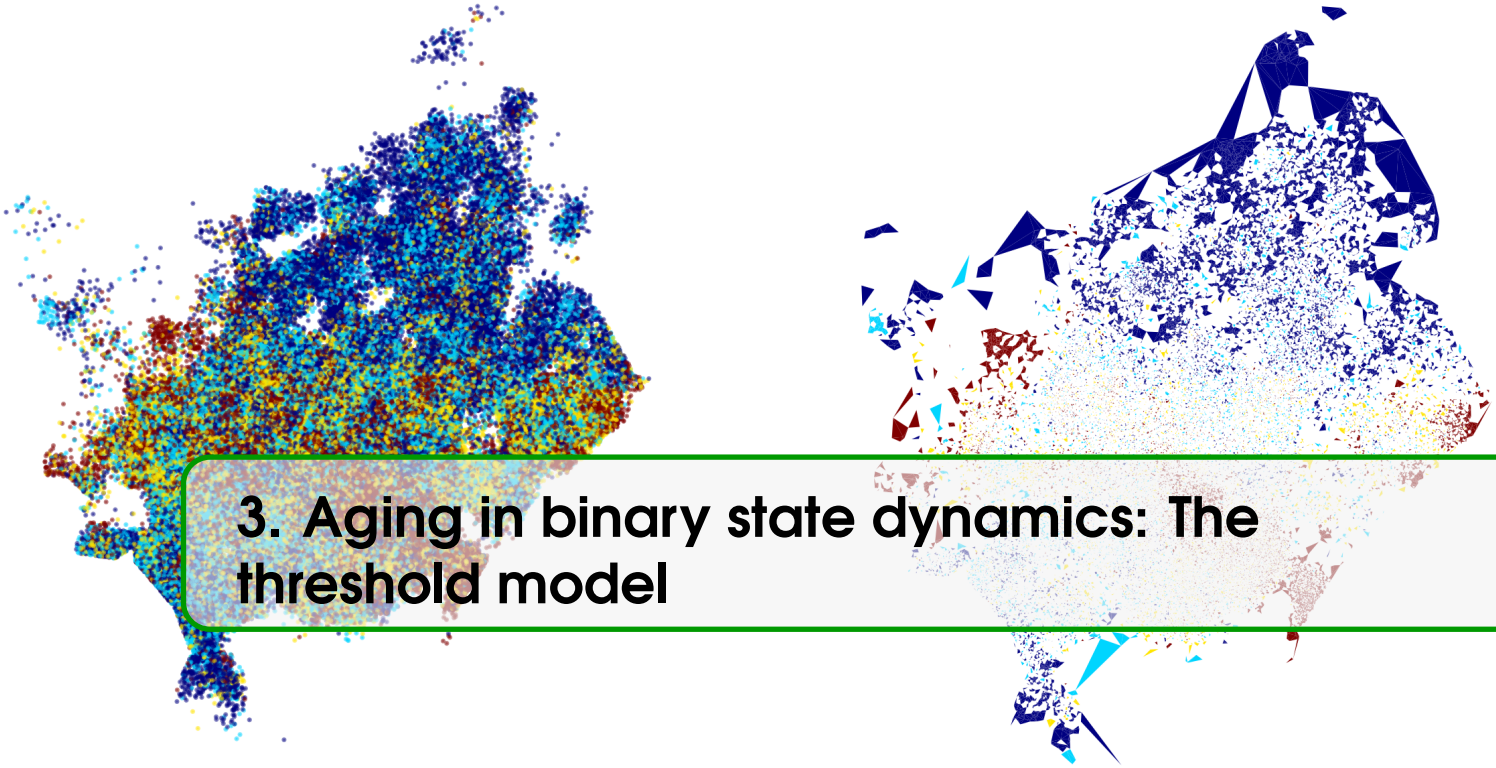

3. Aging in binary state dynamics: The threshold model

We study the non-Markovian effects associated with aging for binary-state dynamics in complex networks. Aging is considered as the property of the agents to be less prone to change state the longer they have been in the current state, which gives rise to heterogeneous activity patterns. In particular, we analyze aging in the Threshold model, which has been proposed to explain the process of adoption of new technologies. Our analytical approximations give a good description of extensive Monte Carlo simulations in Erdős-Rényi, random-regular and Barabási-Albert networks. While aging does not modify the cascade condition, it slows down the cascade dynamics towards the full-adoption state: the exponential increase of adopters in time from the original model is replaced by a stretched exponential or power law, depending on the aging mechanism. Under several approximations, we give analytical expressions for the cascade condition and for the exponents of the adopters' density growth laws. Beyond random networks, we also describe by Monte Carlo simulations the effects of aging for the Threshold model in a two-dimensional lattice.

3.1 Introduction

Stochastic binary-state models are a versatile tool to describe a variety of natural and social phenomena in systems formed by many interacting agents. Each agent is considered to be in one of two possible states: susceptible/infected, adopters/non-adopters, democrat/republican, etc, depending on the context of the model. The interaction among agents is determined by the underlying network and the dynamical rules of the model. There are many examples of binary-state models, including processes of opinion formation (47, 90, 116, 132), disease or social contagion (62, 107), etc. Extended and modified versions of these models can lead to very different dynamical behaviors than in the original model. As examples, the use of multi-layer (6, 38, 39) or time-dependent networks (143), higher-order interactions (7, 24, 76), non-linear collective phenomena (23, 109), noise (20) and non-Markovian (26, 110, 136, 142) effects induce significant changes to the dynamics.

A well-known binary-state model is the Threshold model (147), introduced by M. Granovetter (62), for rumor propagation, adoption of new technologies, riots, stock market herds, political and environmental campaigns, etc. These are examples of *Complex Contagion* processes (25, 75) in which contagion, at variance with *Simple Contagion* (such as in the Voter and SIS models), requires simultaneous exposure to multiple adopter

neighbors and a threshold fraction of neighboring agents that have already undergone contagion. Complex contagion implies a process of group or many-agent interactions built from a combination of pairwise interactions. The discontinuous phase transition and the cascade condition exhibited by the Threshold model were predicted with analytical tools in Ref. (147). This model has been extensively studied in regular lattices and small-world networks (25), random graphs (57), modular and community structure (54), clustered networks (69, 70), hypergraphs (7), homophilic networks (40), etc. Moreover, recent studies also include variants of the adoption rules including the impact of opinion leaders (91) and seed-size (131), on-off threshold (41) and the competition between simple and complex contagion (32, 40, 94). Additionally, the Threshold model has been confronted with several sources of empirical data (**Centola-2010**, 65, 82, 84, 85, 98, 119, 141).

Theoretical and computational studies of stochastic binary-state models, including the Threshold model, usually rely on a Markovian assumption for its dynamics. However, there is strong empirical evidence against this assumption in human interactions. For example, bursty non-Markovian dynamics with heavy-tail inter-event time distributions, reflecting temporal activity patterns, have been reported in many studies (8, 78, 83, 87, 121, 153). The understanding of these non-Markovian effects is in general a topic of current interest (110, 111, 136, 142). In particular, for the Threshold model, memory effects have been included as past exposures' memory (42), message-passing algorithms (128), memory distributions for retweeting algorithms (58) and timers (102).

Aging is an important non-Markovian effect that we address in this paper for binary-state models. Aging accounts for the influence that the persistence time of an agent in a given state modifies the transition rate to a different state (18, 26, 45, 114, 134), so that, the longer an agent remains in a given state, the smaller is the probability to change it. Aging effects have been already shown to modify binary-state dynamics very significantly. For example, aging is able to produce coarsening towards a consensus state in the Voter model (45, 111), to induce continuous phase transitions in the noisy Voter model (9, 110) or to modify the phase diagram and non-equilibrium dynamics of Schelling segregation model (1).

In the specific context of innovation adoption, other mechanisms of inertia or resistance to adopt the technology have been already introduced. In fact, the original approach of Rogers (117) considers a fraction of "laggards" that will resist innovating until a large majority of the population has already adopted it. Similar articles highlight the importance of timing interactions (13) and the effect of "contrarians" (tendency to act against the majority), which has an important impact on the dynamics (49, 59). In Ref. (59), it is discussed how different technologies may show different adoption cascades regarding the balance between advertisement and resistance to change.

In this paper, we provide a general theoretical framework to discuss aging effects building upon a general Markovian approach for binary-state models (55, 56). We build a general master equation for any binary-state model with temporal activity patterns and we propose two different aging mechanisms giving rise to heterogeneous activity patterns, characterized by flat-tail inter-event time distributions. As an example, we apply this framework to the Threshold model for Complex Contagion. Theoretical predictions are matched with extensive Monte Carlo simulations in different networks. In addition, the role of both aging mechanisms is also studied in a two-dimensional Moore lattice.

The paper is organized as follows. In the next section, we describe the original Threshold model and introduce exogenous and endogenous aging in the model. In section 3.3, numerical results are reported and contrasted with theoretical predictions

for different complex networks. For completeness, in section 3.4 the case of a 2D-lattice is analyzed. The final section contains a summary and a discussion of the results. The derivation of the Approximate Master Equation for general binary-state dynamics with aging effects is given in the Appendix.

3.2 Aging and the Threshold model

In the standard Threshold model (62, 147), one considers a network of N interacting agents. Each node of the network represents an agent i with a binary-state variable $\sigma_i = \{0,1\}$ and a given threshold T $(0 < T < 1)$. The state indicates if the agent has adopted a technology (or joined a riot, spread a meme or fake news, etc.) or not. We use the wording of a technology adoption process for the rest of the paper. If a node i (with k neighbors) has not adopted ($\sigma_i = 0$) the technology, becomes adopter ($\sigma_i = 1$) if the fraction m/k of neighbors adopters exceeds the threshold T. Adopter nodes cannot go back to the non-adopter state.

In the Threshold model with aging, each agent has an internal time $j = 0,1,2,...$ (in Monte-Carlo units) as in Refs. (1, 9, 26, 45, 46, 110, 111, 114, 134). As initial condition, we set $j = 0$ for all nodes. In Monte Carlo simulations, we follow a Random Asynchronous Update in which agents are activated in discrete time steps with probability $p_A(j) = 1/(j+2)$. When a non-adopter agent is activated, he/she changes state according to the threshold condition $m/k > T$. We will consider two different aging mechanisms, endogenous and exogenous aging (45), which account for the power law inter-event time distributions empirically observed in human interactions (8). For endogenous aging, the internal time measures the time spent in the current state: If an agent in an updating attempt is not activated or does not adopt, the internal time increases by one unit. Therefore, the longer an agent has remained without adopting the technology, the more difficult it is for him/her to adopt it.

For exogenous aging, the internal time accounts for the time since the last attempt to change state: In each updating attempt in which the agent is activated, the internal clock resets to $j = 0$ even if there is no adoption. In this case, aging is understood as a resistance to adopt the technology the longer the agent has not been induced to consider adoption by some external influence.

3.3 Dynamics on Complex networks

In this section we discuss the Threshold model with endogenous and exogenous aging in three different complex networks: random-regular (149), Erdős-Rényi (44) and Barabási-Albert (11).

3.3.1 Numerical results

For the networks considered, the Threshold model undergoes a discontinuous phase transition at a certain critical value T_c, which is called cascade condition (147). For $T < T_c$, a small initial seed of adopters triggers a global cascade where, on average, a significant proportion of agents in the system adopt the technology (change from $\sigma_i = 0$ to 1). In our analysis, the initial condition is set to favor cascades: one agent i with degree $k_i = z$ is selected randomly and all him/her neighbors are initially adopters, as in Ref. (25, 131). For $T > T_c$, there are few cascade occurrences and none of them is global. The cascade condition dependence with the average degree z of the underlying network has been studied in Refs. (57, 147). For the two aging mechanisms considered, Monte Carlo simulations in random graphs show that the T_c dependence on z is very similar to the one for the model without aging (see Fig. 3.1). Therefore,

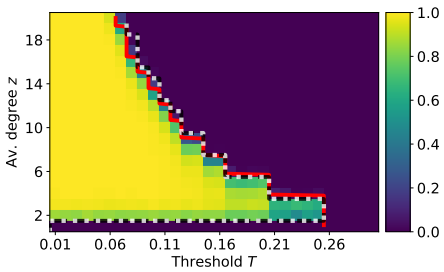

Figure 3.1: Average density ρ of adopters for an Erdős-Rényi graph of mean degree z using a model with threshold T. Color-coded values of ρ are from Monte Carlo simulations of the model without aging in a graph with $N = 10,000$ agents. Black dashed and white dotted lines correspond to T_c value obtained numerically for the model with exogenous and endogenous aging, respectively. Monte Carlo simulations are averaged over $M = 5 \times 10^4$ realizations. The red solid line is the analytical approximation of the cascade boundary, from Eq. (3.17), which is the same with and without aging.

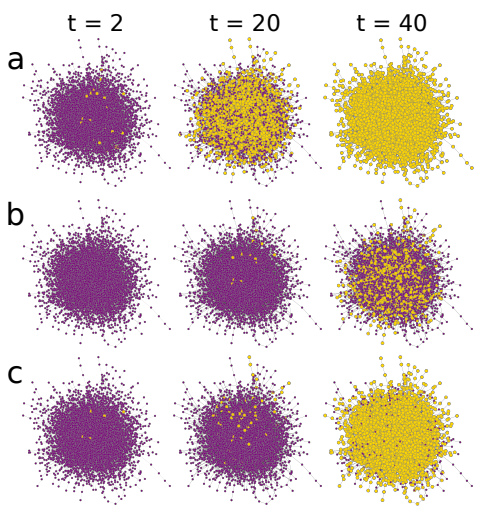

Figure 3.2: Cascade spreading for the original Threshold model (a), and the versions with endogenous (b) and exogenous (c) aging. Yellow nodes are adopters and purple nodes are non-adopters. Time increases from left to right. Monte Carlo simulations are performed in an Erdős-Rényi network with mean degree $z = 3$ and $T = 0.22$. System size is $N = 8,000$.

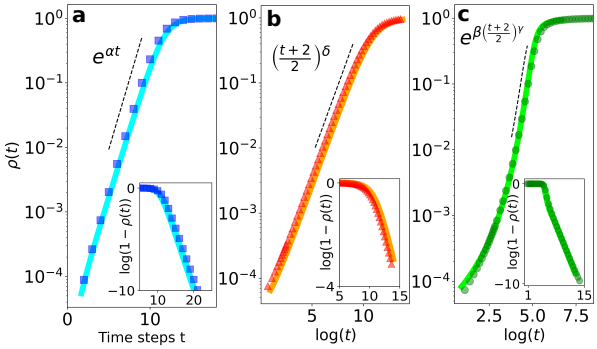

Figure 3.3: Cascade dynamics and fall to the full-adopt state ($\rho \sim 1$) of the Threshold model without aging (a) and the versions with endogenous (b) and exogenous (c) aging effects. At (b-c), the evolution is plotted as a function of the logarithm of time $\log(t)$ in Monte Carlo steps, as in the insets. The underlying network is a 3-regular random graph and the threshold is $T = 0.2$. The exponent values are $\alpha \simeq 1.0$, $\beta \simeq 1.14$, $\gamma \simeq 0.38$ and $\delta \simeq 1.0$. Numerically integrated solutions of Eq. (3.4) (solid lines) describe accurately the numerical results. Monte Carlo simulations are averaged over $M = 5 \times 10^4$ realizations in a network of $N = 1.6 \times 10^5$ nodes.

for large connected networks, tends to the same cascade condition derived for the original Threshold model (which for ER graphs is $T_c = 1/z$ (147)). This result is not obvious a priory because aging has been shown to modify the final state in several models (1, 9, 26, 45, 46, 110, 111, 114, 134). This is discussed in detail in Appendix **??**.

Even though aging in the Threshold model does not modify the cascade condition, it has a large impact in the complex contagion cascade dynamics (Fig.3.2). From Monte Carlo simulations in a random regular graph we find that, without aging, the average fraction of adopters follows an initial exponential increase with time (see Fig. 3.2a and 3.3a),

$$\rho(t) \sim \rho_0 e^{\alpha t}, \tag{3.1}$$

where ρ_0 is the initial fraction of adopters (seed). This behavior is universal for all values of the control parameters z and T below the cascade condition. In addition, we investigated the approach to the full-adopt state ($\rho = 1$) and we found that the number of non-adopters follows an exponential decay $1 - \rho(t) \sim e^{-t}$ for all values of the control parameters (see inset in Fig.3.3a).

When aging is introduced, the cascade dynamics are much slower than an exponential law (see Fig. 3.2b). For endogenous aging, all agents non-adopters have the same activation probability $p_A(j)$, which decreases at each time step. This gives rise to cascade dynamics well-fitted by a power law increase (see Fig. 3.3b),

$$\rho(t) \sim \rho_0 \left(\frac{t+2}{2}\right)^{\delta}. \tag{3.2}$$

For exogenous aging, we observe a slow adoption spread at the beginning followed by a cascade where almost all agents adopt the technology (Fig. 3.2c). This behavior is well-fitted with a stretched exponential increase of the number of adopters (see Fig. 3.3c),

$$\rho(t) \sim \rho_0 e^{\beta\left((t+2)/2\right)^{\gamma}}. \tag{3.3}$$

For both aging mechanisms, in the last stages of evolution, a few "stubborn" non-adopters remain, although the environment favors the adoption. Due to the chosen

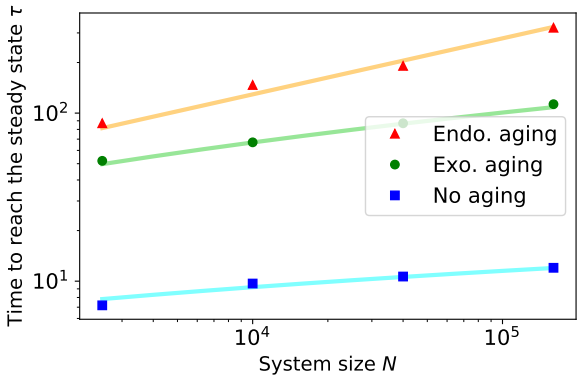

Figure 3.4: Average time to reach the steady state ($\rho > 0.9$) τ as a function of the system size N for the original Threshold model and the versions with endogenous and exogenous aging. The underlying network is a 5-regular random graph and the threshold is $T = 0.12$. Monte Carlo simulations are averaged over $M = 5 \times 10^4$ realizations. Solid lines are the system size-dependent timescale: For the original model, $\tau_{\text{NOAG.}} = (1/\alpha)\log(N)$, for the endogenous ($\tau_{\text{ENDO}} = 2N^{1/\delta} - 2$) and for the exogenous aging ($\tau_{\text{EXO}} = 2(\log(N)/\beta)^{1/\gamma} - 2$), which follows from the dynamics from Eq. (3.1), (3.2) and (3.3). The exponents α, β, γ and δ are fitted exponents.

activation probability, the number of non-adopters decay with a power law $1-\rho(t) \sim 1/(t+2)$ in both cases (see insets at Fig. 3.3(b-c)).

Comparing the evolution of the original model with one of the versions with aging, we observe an important separation of time scales. While for the original model, the time to reach the steady state follows a logarithmic increase with the system size, the versions with endogenous and exogenous aging show a power law and a power-logarithmic dependence, respectively (see Fig.3.4). Therefore, the time scale separation between the original model and the versions with aging increases as we increase the system size, and thus, the aging effects are more relevant for large systems.

The power law and the stretched exponential dynamics for endogenous and exogenous aging, respectively, are observed for all parameter values z and T below the cascade condition ($T < T_c$) and for all system sizes. This is shown in Fig. 3.5 for a random regular, Erdős-Rényi and Barabási-Albert networks. In particular, we show that the time-dependent behavior for different system sizes collapses to a single curve when time is scaled with the system size-dependent timescale (previously analyzed in Fig. 3.4) that follows from either the power law dynamics ($\tau_{\text{ENDO}} = 2N^{1/\delta} - 2$) or the stretched exponential law ($\tau_{\text{EXO}} = 2(\log(N)/\beta)^{1/\gamma} - 2$). Notice that the scaling of the y-axis is necessary for Fig.3.5(d-f) to show a linear dependence (for all system sizes) due to the stretched exponential increase.

A different question is the dependence of the exponents of the power law and stretched exponential with the parameters z and T. Numerical results from fitted Monte Carlo simulations for $\alpha(z,T)$, $\delta(z,T)$ and $\gamma(z,T)$ are shown in Figs. 3.6 and 3.7. For a random-regular graph, as apparent from Fig. 3.5, the exponents do not depend on the parameter T up to T_c (so the exponents are dependent only on z, $\alpha(z)$, $\gamma(z)$ and $\delta(z)$), while for Erdős-Rényi and Barabási-Albert networks the value of the exponents decrease with T when approaching T_c, indicating a slowing down of the dynamics. Also, for these two latter networks, the exponents present a maximum value at a certain value of z. This maximum value at a certain z for a fixed T can be understood as being between the two critical lines of Fig. 3.1.

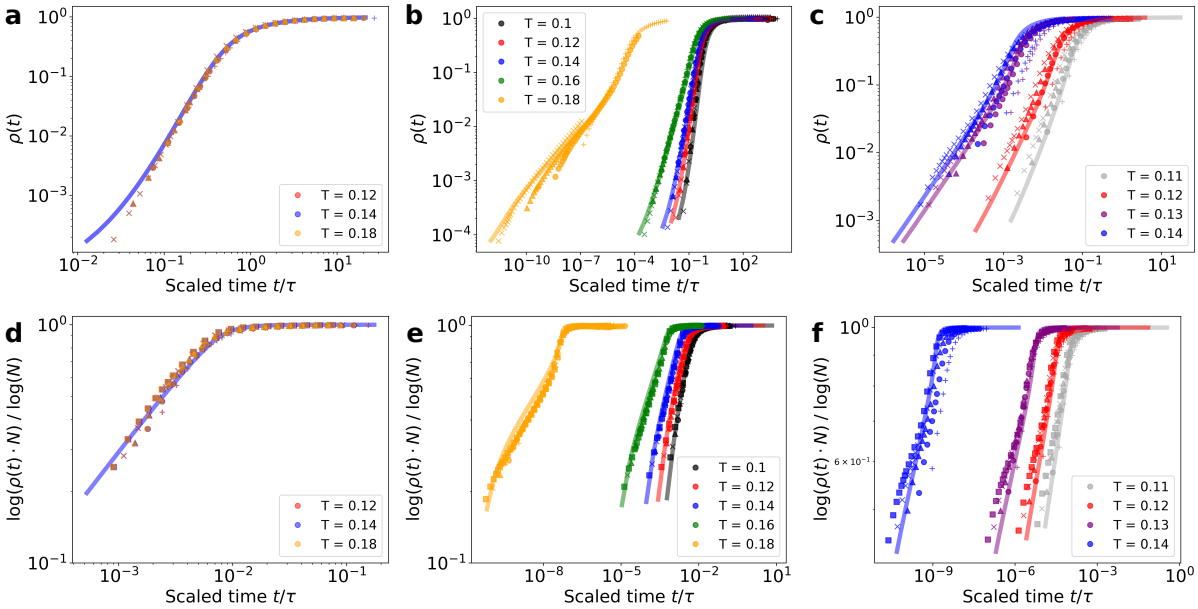

Figure 3.5: Cascade dynamics of the Threshold model with endogenous (a - c) and exogenous (d - f) aging. From the left column to the right: a random regular graph with degree $z = 5$ (a and d), an Erdős-Rényi graph with average degree $z = 5$ (b and e) and a Barabási-Albert graph with average degree $z = 8$ (c and f). Different colors indicate different values of T and markers correspond to different system sizes: $N = 2,500$ (plus), $10,000$ (circles), $40,000$ (triangles), $160,000$ (crosses) and $640,000$ (squares). Time is scaled according to the system size for each model: $\tau_{\text{EXO}} = 2(\log(N)/\beta)^{1/\gamma} - 2$, $\tau_{\text{ENDO}} = 2N^{1/\delta} - 2$, where β,γ and δ are the fitted exponents from the behavior according to Eq. (3.2) and (3.3). Solid lines are obtained from the solutions of Eq. (3.13). Monte Carlo simulations are averaged over $M = 5 \times 10^4$ realizations.

3.3.2 General mathematical description

To account for the non-Markovian dynamics introduced by the aging mechanism, we need to go beyond the standard mathematical descriptions of the Threshold model (54, 56, 57). We do so using a Markovian description by enlarging the number of variables (110, 111). Namely, we classify the agents with degree k, number of adopter neighbors m and age j as different sets in a compartmental model in a general framework for binary-state dynamics in complex networks (55, 56, 147). Assuming a local tree-like network structure, as the one generated using the configuration model for a generic degree distribution p_k (97, 99) or Erdős-Rényi model, we derive a general master equation [1] for binary-state dynamics with temporal activity patterns in complex networks considering the following possible transitions (see Appendix B for details):

- A susceptible (infected) node changes state and resets internal age with probability $F(k,m,j)$ ($R(k,m,j)$);
- A susceptible (infected) node remains in the same state and resets internal age to zero ($j \to 0$) with probability $F_R(k,m,j)$ ($R_R(k,m,j)$);
- A susceptible (infected) node remains in the same state and ages ($j \to j+1$) with probability $F_A(k,m,j)$ ($R_A(k,m,j)$).

See a schematic representation in Fig. B.1. Note that we introduce here epidemics notation of susceptible/infected nodes (55, 56), but it is immediately translated to the non-adopter/adopter situation of our model. For the specific case of the Threshold model, dynamics are monotonic and $R(k,m,j)=0$ (no adopter becomes a non-adopter). Moreover, when an agent becomes an adopter, there are neither resetting nor aging events $R_R(k,m,j) = R_A(k,m,j) = 0$. This means as well that equations for the non-adopters $s_{k,m,j}$ and adopters $i_{k,m,j}$ nodes are independent. Thus, we can write the following rate equations for the evolution of the fraction $s_{k,m,j}(t)$ of k-degree non-adopters nodes with m infected neighbors and age j:

$$\begin{aligned}
\frac{ds_{k,m,j}}{dt} &= -s_{k,m,j} - (k-m)\,\beta^s\, s_{k,m,j} \\
&\quad + (k-m+1)\,\beta^s\, s_{k,m-1,j-1} \\
&\quad + F_A(k,m,j-1)\, s_{k,m,j-1}, \\
\frac{ds_{k,m,0}}{dt} &= -s_{k,m,0} - (k-m)\,\beta^s\, s_{k,m,0} \\
&\quad + \sum_{l=0} F_R(k,m,l)\, s_{k,m,l},
\end{aligned} \tag{3.4}$$

where β^s is a non-linear function of $s_{k',m',j'}$ for all values of k',m' and j' (see Eq. (B.4)). The remaining step is to define explicitly the transition probabilities for our aging mechanisms. For both exogenous and endogenous aging, the adoption probability is the probability that an agent is activated and has a fraction of adopters that exceeds the threshold T, which means that

$$F(k,m,j) = p_A(j)\,\theta(m/k - T), \tag{3.5}$$

where $\theta(\cdot)$ is the Heaviside step function.

The reset and aging probabilities for endogenous and exogenous aging mechanisms are different. The simplest case is endogenous aging where there is no reset $F_R(k,m,j)=0$

[1] We use here the term "master equation" for consistency with Refs. [55, 56], but the word "master" has a different meaning than the one used to describe an equation for the probability distribution [108]

and agents increase by one the age with probability

$$\begin{aligned} F_A(k,m,j) &= 1 - F(k,m,j) \\ &= 1 - p_A(j)\,\theta\,(m/k - T)\,. \end{aligned} \tag{3.6}$$

When aging is exogenous, the reset probability is the probability to activate and not adopt

$$F_R(k,m,j) = p_A(j)\,(1 - \theta\,(m/k - T))\,. \tag{3.7}$$

Thus, agents that age are just the ones that do not activate, $F_A(k,m,j) = 1 - p_A(j)$.

Using these definitions, we have integrated numerically Eq. (3.4) for the Threshold model with both endogenous and exogenous aging. Numerical solutions give good agreement with Monte Carlo simulations (see Fig. 3.3). However, in a general network, considering a cutoff for the degree $k = 0,\ldots,k_{\max}$ and age $j = 0,\ldots,j_{\max}$, the number of differential equations to solve is $(k_{\max}+1)\,(k_{\max}+1)\,(j_{\max}+1)$ according to the three subindexes of the variable $s_{k,m,j}$. This number grows with the largest degree square and largest age considered and thus, some further approximations are needed to obtain a convenient reduced system of differential equations.

As an ansatz, we assume that timing interactions can be effectively decoupled from the adoption process so the solution of Eq. (3.4) can be written as

$$s_{k,m,j}(t) = s_{k,m}(t)\,G_j(t), \tag{3.8}$$

where $s_{k,m}$ is the fraction of non-adopters with degree k and m infected neighbors $s_{k,m} = \sum_j s_{k,m,j}$ and there is an age distribution $G_j(t)$, independent of the adoption process.

If we sum over the variable age j in Eq. (3.4), we can rewrite the following rate equations for the variables $s_{k,m}$

$$\begin{aligned} \frac{ds_{k,m}}{dt} = &-\langle p_A\rangle\,\theta(m-kT)\,s_{k,m} \\ &-(k-m)\,\beta^s\,s_{k,m} + (k-m+1)\,\beta^s\,s_{k,m-1}, \end{aligned} \tag{3.9}$$

where aging effects are just included in $\langle p_A\rangle(t)$:

$$\langle p_A\rangle(t) = \sum_{j=0}^{\infty} p_A(j)\,G_j(t). \tag{3.10}$$

Using the definition of the fraction of k-degree agents adopters $\rho_k(t)$,

$$\rho_k(t) = 1 - \sum_{j=0}^{\infty}\sum_{m=0}^{k} s_{k,m,j}, \tag{3.11}$$

and along lines of Ref. (56), we use the exact solution

$$s_{k,m} = (1 - \rho_k(0))\,B_{k,m}[\phi], \tag{3.12}$$

where $B_{k,m}[\phi]$ is the binomial distribution with k attempts, m successes and with success probability ϕ. From this point, we derive from Eq. (3.9) a reduced system of

two coupled differential equations for the fraction of adopters $\rho(t) = \sum_k p_k \rho_k(t)$ and an auxiliary variable $\phi(t)$ (see details in Ref. (56)):

$$\begin{aligned} \frac{d\rho}{dt} &= \langle p_A \rangle [h(\phi) - \rho], \\ \frac{d\phi}{dt} &= \langle p_A \rangle [g(\phi) - \phi], \end{aligned} \tag{3.13}$$

where $\phi(t)$ can be understood as the probability that a randomly chosen neighbor of a non-adopter node is an adopter at time t. The functions $h(\phi)$ and $g(\phi)$ are nonlinear functions of this variable ϕ

$$\begin{aligned} h(\phi) &= \sum_{k=0}^{\infty} p_k \left(\rho_k(0) + (1 - \rho_k(0)) \sum_{m=kT}^{k} B_{k,m}[\phi] \right), \\ g(\phi) &= \sum_{k=0}^{\infty} \frac{k}{z} p_k \left(\rho_k(0) + (1 - \rho_k(0)) \sum_{m=kT}^{k} B_{k-1,m}[\phi] \right). \end{aligned} \tag{3.14}$$

When $\langle p_A \rangle$ is replaced by a constant, Eqs. (3.13) reduce to previous results for the original model (54).

Determining the distribution $G_j(t)$ is not easy. For endogenous aging, all non-adopters have the same age at each time step and $G_j(t) = \delta(j - t)$ (where $\delta(\cdot)$ is the Dirac delta function). Therefore, $\langle p_A \rangle = 1/(t+2)$. The numerical solution of Eq. (3.13) gives a good agreement with Monte Carlo simulations (see Fig. 3.5(a-c)). For the case of exogenous aging, the reset of the internal clock makes more difficult a choice for $G_j(t)$. Inspired on the stretched exponential behavior of $\rho(t)$ observed from Monte Carlo simulations, we propose $\langle p_A \rangle = 1/(t+2)^{\mu}$. For $\mu = 0.75$, the numerical solutions of Eq. (3.13) gives a very good agreement with our Monte Carlo simulations (see Fig. 3.5 (d-f)).

3.3.3 Analytical results

To obtain an analytical result for the cascade condition and for the exponents of the predicted exponential, stretched-exponential and power law cascade dynamics that we fitted from Monte Carlo simulations, we need to go a step beyond the numerical solution of our approximated differential equations (Eqs. (3.4) and (3.13)).

For a global cascade to occur, it is needed that the variable $\phi(t)$ grows with time. If we assume a small initial seed ($\rho_k(0) \to 0$), Eq. (3.13) can be rewritten as in Ref. (57)

$$\frac{d\phi}{dt} = \langle p_A \rangle \left(-\phi + \sum_{k=1}^{\infty} \frac{k}{z} p_k \sum_{m=kT}^{k} B_{k-1,m}[\phi] \right). \tag{3.15}$$

Rewriting the sum term as $\sum_{l=0}^{\infty} C_l \phi^l$, with coefficients

$$C_l = \sum_{k=l}^{\infty} \sum_{m=0}^{l} \binom{k-1}{l} \binom{l}{m} (-1)^{l+m} \frac{k}{z} p_k \, \theta(m/k - T), \tag{3.16}$$

we linearize Eq. (3.15) around $\phi = 0$:

$$\frac{d\phi}{dt} \approx \langle p_A \rangle (C_1 - 1) \phi. \tag{3.17}$$

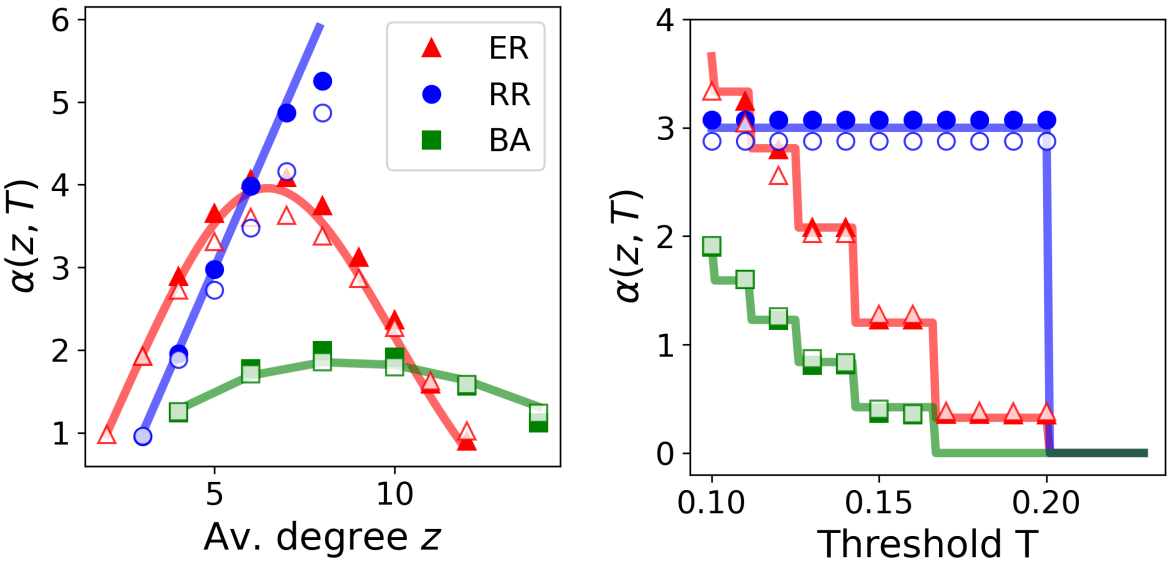

Figure 3.6: Exponent α for the original Threshold model (empty markers) and δ for the version with endogenous aging (filled markers) for different values of the average degree z (and $T = 0.1$) (left) and as a function of T for fixed z (right). Different markers indicate results from Monte Carlo simulations with different topologies: red triangles indicate an Erdős-Rényi (ER) graph, blue circles indicate a random regular (RR) graph and green squares indicate a Barabási-Albert (BA) graph. In the right panel, the average degree is fixed $z = 5$ for ER and RR, and $z = 8$ for the BA. Predicted values by Eq. (3.22) (solid lines) fit the results for each topology. System size is fixed at $N = 4 \times 10^6$ for the original model and $N = 3.2 \times 10^5$ for the version with aging.

The solution for Eq. (3.17) is then

$$\phi(t) = \rho_0 \, e^{(C_1-1)\int_0^t \langle p_A \rangle(s)\, ds}, \tag{3.18}$$

given that $\phi(0) = \rho_0$.

Since $\langle p_A \rangle(t)$ is always positive, global cascades occur when $(C_1 - 1) > 0$. This cascade condition does not depend on the aging term $\langle p_A \rangle(t)$ and thus, it is the same as for the Threshold model without aging. In Fig. 3.1, the red solid line is the result of this analytical calculation, and it is in good agreement with the numerical results.

Linearization is also useful to determine the time dependence of the cascade process. Assuming a small initial seed and rewriting the term $h(\phi)$ as $\sum_{l=0}^{\infty} K_l \phi^l$, the linearized equation for the fraction of adopters $\rho(t)$ becomes

$$\frac{d\rho}{dt} \approx \langle p_A \rangle (K_1 - 1)\, \phi, \tag{3.19}$$

where the coefficients K_l are

$$K_l = \sum_{k=l}^{\infty} \sum_{m=0}^{l} \binom{k}{l} \binom{l}{m} (-1)^{l+m} p_k \, \theta\left(m/k - T\right). \tag{3.20}$$

A solution for the fraction of adopters $\rho(t)$ can be obtained from Eqs. (3.18) and (3.19). For the case of the Threshold model without aging, setting $\langle p_A \rangle = 1$, the solution is an exponential cascade dynamics

$$\rho(t) = \rho_0 \, e^{(C_1-1)t}. \tag{3.21}$$

Therefore, the number of adopters $\rho(t)$ follows an exponential increase with exponent $\alpha(z,T)$:

$$\alpha(z,T) = C_1 - 1 = \sum_{k=0}^{\lfloor 1/T \rfloor} \frac{k\,(k-1)}{z} p_k - 1, \tag{3.22}$$

where C_1 is computed from Eq. (3.16).

For endogenous aging, the same derivation is valid to determine the exponents $\delta(z,T)$. Using $\langle p_A \rangle = 1/(t+2)$, the fraction of adopters follows a power law dependence,

$$\rho(t) = \rho_0 \left(\frac{t+2}{2}\right)^{(C_1-1)}. \tag{3.23}$$

The exponent reported for the power law cascade dynamics $\delta(z,T)$ turns out to be, therefore, the same exponent as the one for the exponential behavior where there is no aging: $\delta(z,T) = \alpha(z,T) = C_1 - 1$. Fig. 3.6 compares the prediction of Eq. (3.22) with the results computed from Monte Carlo simulations. There is a good agreement for both Barabási-Albert and Erdős-Rényi networks for all values of T and z. For a random-regular graph, the predicted dependence, $\alpha(z) = z - 2$, is not a good approximation for large z. This is because the presence of small cycles increases importantly in a random-regular graph as the average degree z grows (148) and the locally-tree assumption made for the derivation of the rate equations (Eq. (3.4)) is not valid anymore. A different approach is necessary for clustered networks (as in Ref.(86) for the Threshold model).

For exogenous aging, an analytical expression for the exponent $\gamma(z,T)$ is not obtained following this methodology. Still, we can fit the exponent from the numerical solutions in Fig. 3.5 (d-f). Fig.3.7 shows a good comparison between the exponent calculated from the numerical solutions (from the AME) and the one calculated from Monte Carlo simulations. The dependence of $\gamma(z,T)$ with the parameters z and T is qualitatively similar to the dependence of $\alpha(z,T)$.

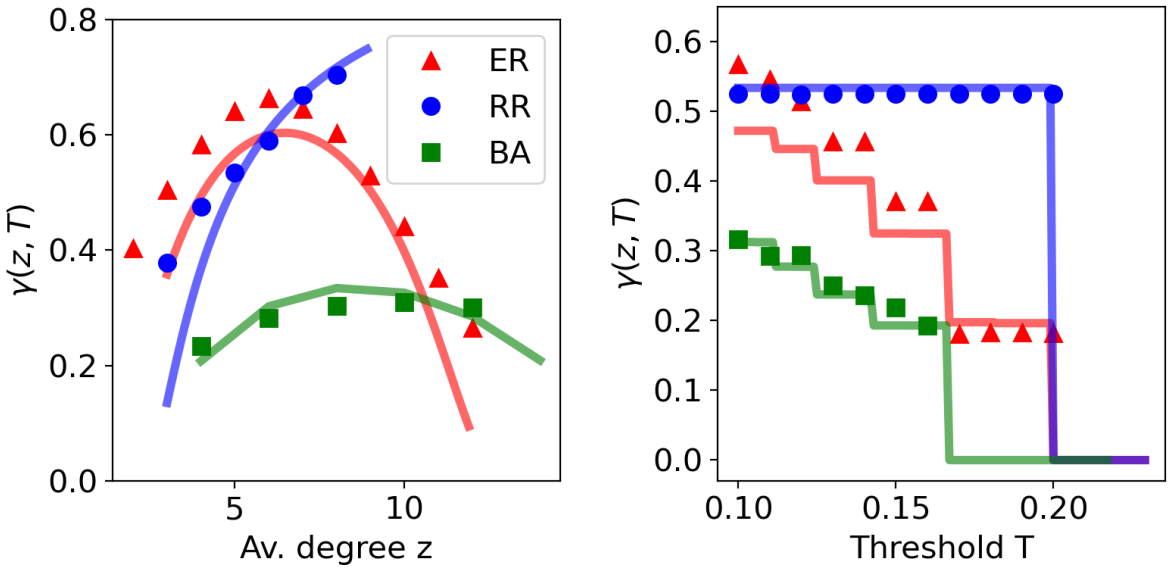

Figure 3.7: Exponent γ for the Threshold model with exogenous aging for different values of the average degree z ($T = 0.1$) (left) and as a function of T for fixed z (right). Different markers indicate results from Monte Carlo simulations with different topology: red triangles indicate an Erdős-Rényi (ER) graph, blue circles indicate a random regular (RR) graph and green squares indicate a Barabási-Albert (BA) graph. In the right panel, the average degree is fixed $z = 5$ for ER and RR, and $z = 8$ for the BA. Predicted values by numerical integration of Eqs. (3.13) (solid lines) fit approximately the results for each topology. System size is fixed at $N = 3.2 \times 10^5$.

3.4 Dynamics on a Moore lattice

The Threshold model in a two-dimensional regular lattice with a Moore neighborhood (nearest and next nearest neighbors) is known to have a critical threshold (cascade condition) $T_c = 3/8$ (25). Below this value, cascade dynamics follows a power law increase in the density of adopters $\rho(t) \sim t^2$, which does not depend on the threshold value T. In Fig. 3.8a, we show a typical realization of this model: From an initial seed, the adoption radius increases linearly with time until all agents adopt the technology.

When aging is considered, cascade dynamics become much slower and a dependence on T appears. When the aging mechanism is exogenous, Monte Carlo simulations indicate cascade dynamics following a power law $\rho(t) \approx t^{\zeta(T)}$. Qualitatively, we observe that while in the case without aging there was a soft interface between adopter and non-adopters, aging causes a strong roughening in the interface and the presence of non-adopters inside the bulk (see Fig. 3.8b). In addition, the exponent values fitted from Monte Carlo simulations allow us to collapse curves for different system sizes (see Fig. 3.9a). Due to finite size effects, the interface between adopters and non-adopters eventually reaches the borders of the system and the remaining non-adopters, in the bulk, will slowly adopt with the density of adopters following the functional shape $\rho(t) = 1 - 1/(t+2)$.

Fig.3.8c shows the dynamics towards global adoption for endogenous aging. In comparison with the case of exogenous aging, we do not observe strong interface roughening between adopters and non-adopters, because non-adopters are not present in the bulk. Monte Carlo simulations indicate a very slow increase of the density of adopters ρ, similar to a power-logarithmic growth $\rho(t) \approx (\log(t))^{\nu}$, with a threshold dependent exponent $\nu(T)$ (Fig. 3.9b). Unfortunately, we were not able to

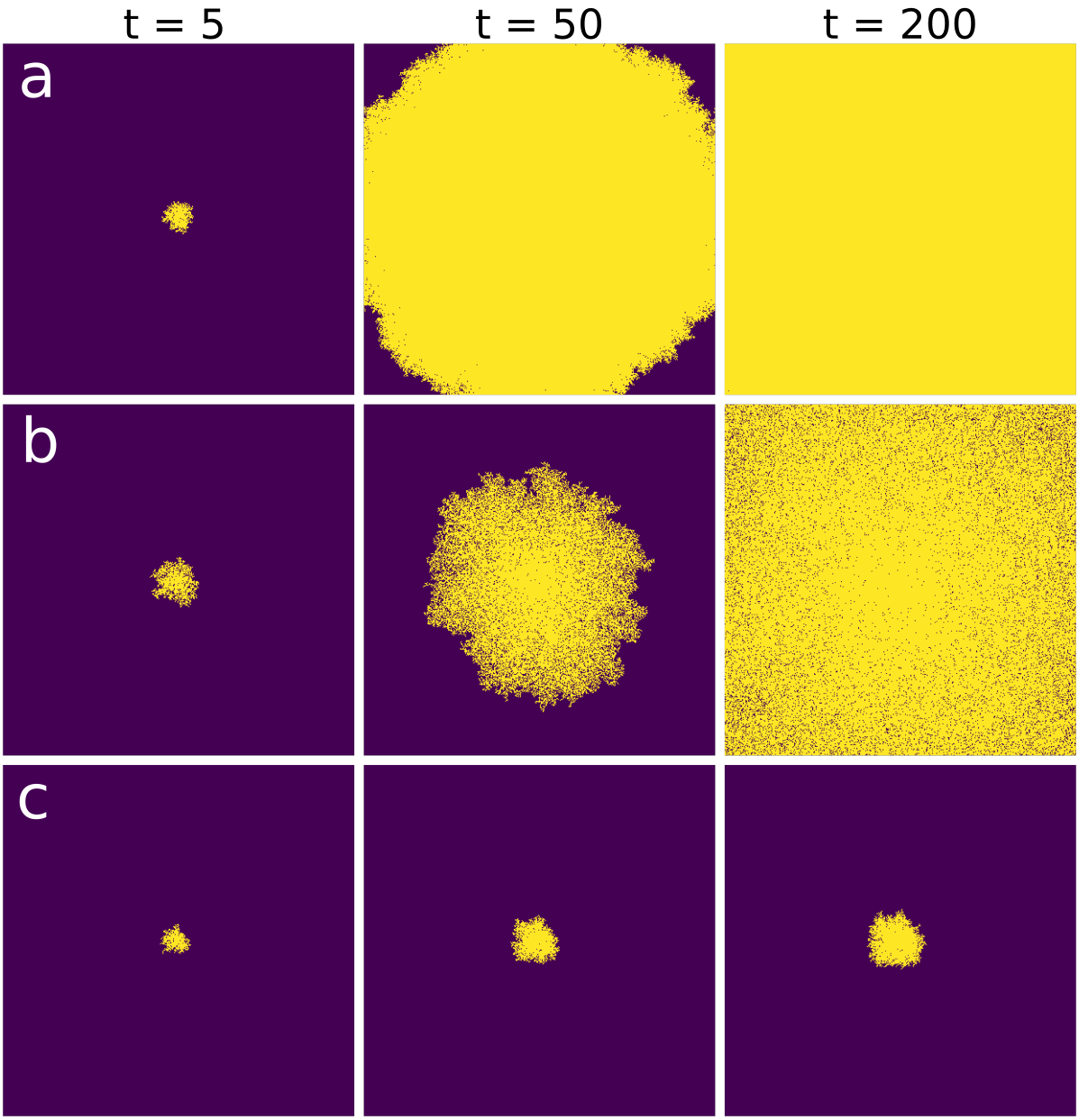

Figure 3.8: Cascade spreading of the original Threshold model (a) and the versions with exogenous (b) and endogenous (c) aging on a Moore neighborhood lattice with size $N = L \times L$, $L = 405$. Yellow and purple nodes are adopters and non-adopters, respectively. Time increases from left to right. Initial seeds are selected favoring cascades: one agent and all him/her neighbors are set as adopters at the center of the system.

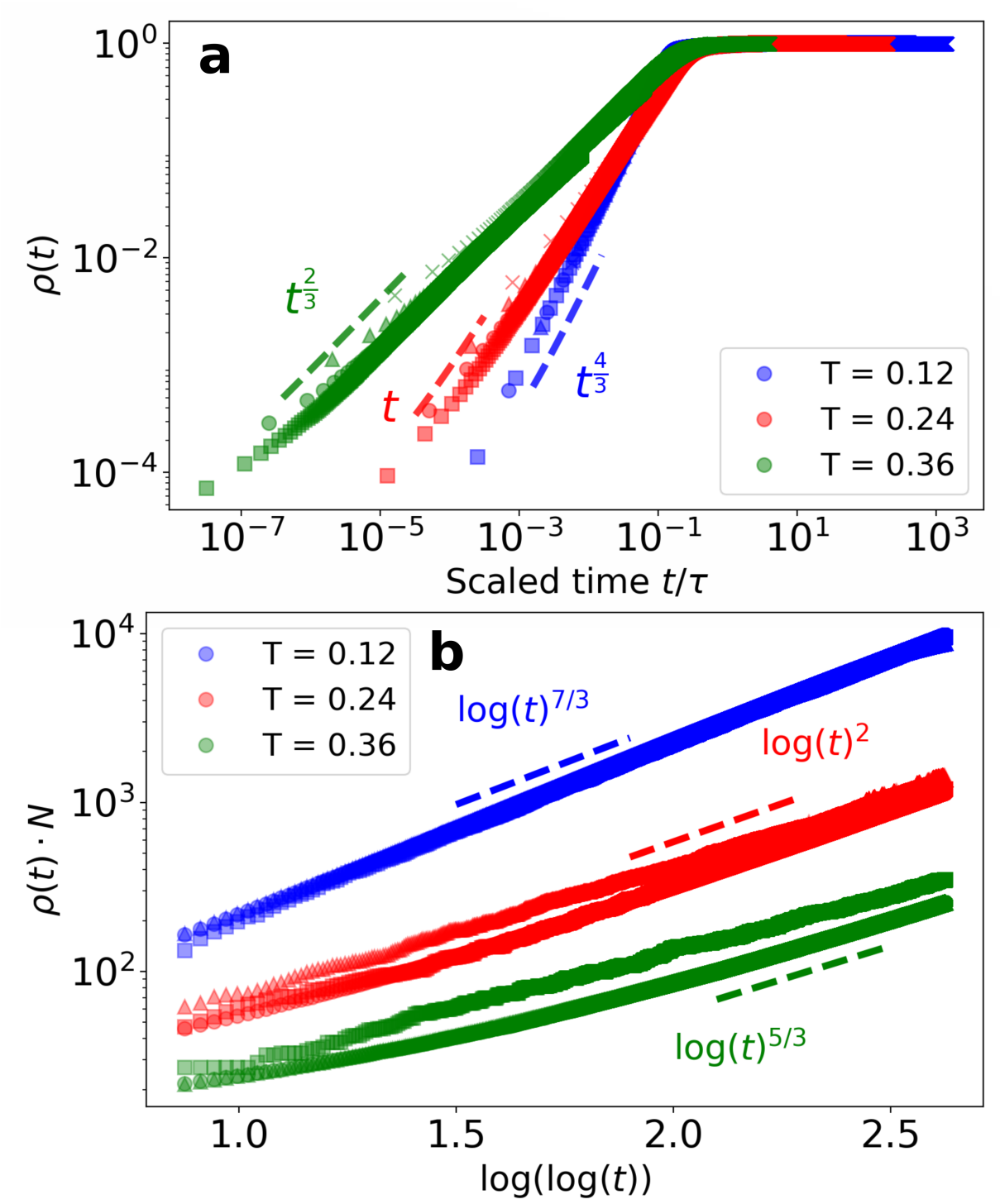

Figure 3.9: Cascade dynamics of the Threshold model with exogenous (a) and endogenous (b) aging on a Moore neighborhood lattice. Different colors indicate different values of the threshold T. Different markers indicate the results of Monte Carlo simulations with different system size $N = L \times L$: $L = 50$ (crosses), 100 (triangles), 200 (circles) and 400 (squares). In (a), time is scaled according to size $\tau = L^{2/\zeta}$. Discontinuous solid lines indicate a power law behavior with exponent $\zeta = 4/3$ (blue), 1 (red) and $2/3$ (green). In (b), the system sizes are not scaled due to the slow dynamics. Discontinuous solid lines indicate a power-logarithmic behavior, $\rho(t)N \sim \log(t)^{\nu}$, with exponent $\nu = 7/3$ (blue), 2 (red) and $5/3$ (green).

find an analytical framework for the Threshold model in a Moore lattice. Our general approximation used for complex networks assumes a tree-like network, and it is not appropriate for this case.

3.5 Conclusions

We have addressed in this work the role of aging in general models with binary-state agents interacting in a complex network. Temporal activity patterns are incorporated by means of a variable that represents the internal time of each agent. We have developed an approximate Master Equation for this general situation. In this framework, we have explicitly studied the effect of aging in the Threshold model as a paradigmatic example of Complex Contagion processes. Aging implies a lower probability to change state when the internal time increases. We considered two aging mechanisms: endogenous aging, in which the internal time measures the persistence time in the current state, and exogenous aging, in which the internal time measures the time since the last update attempt.

Our theoretical framework with some approximations to attain analytical results provide a good description of the results from Monte Carlo simulations for Erdős-Rényi, random-regular and Barabási-Albert networks. For these three types of complex networks, we found that the cascade condition T_c (critical value of the threshold parameter T as a function of mean degree z of the network) for the full spreading from an initial seed is not changed by the aging mechanisms. However, aging modifies in non-trivial ways cascade dynamics of the process. The exponential growth with exponent $\alpha(z,T)$ of the density of adopters in the absence of aging becomes a power law with exponent $\delta(z,T)$ for endogenous aging, and a stretched exponential characterized by an exponent $\gamma(z,T)$ for exogenous aging. We have analyzed the exponents' dependence with the order parameters $\alpha(z,T)$, $\delta(z,T)$, $\gamma(z,T)$ and shown that $\delta(z,T) = \alpha(z,T)$.

Our general theoretical framework, based on the assumption of a tree-like network, is not appropriate for a regular lattice. In this case, we have been only able to run Monte Carlo simulations. Our results indicate that exogenous aging gives rise to adoption dynamics characterized by an increase in the interface roughness, by the presence of non-adopters in the bulk, and by a power law growth of the density of adopters with exponent $\zeta(T)$, while in the absence of aging $\zeta = 2$ independently of T. Endogenous aging, on the other hand, produces very slow (logarithmic-like) dynamics, with a threshold-dependent exponent $\nu(T)$.

This work highlights the importance of non-Markovian dynamics in general binary-state dynamics and, specifically, in the Threshold model. For the problem of innovation adoption that this model addresses, we show how persistence times have an important impact on the adoption cascade. In fact, in the lattice, for $T = 2/8$ and exogenous aging we recover a linear evolution for the number of adopters as in Ref. (59) for a mean-field model. Further work in this direction would be to categorize technologies according to the adoption curve, to show if the system has important resistance to the previous technology (endogenous aging) or a balance between memory and external influence or advertisement (exogenous aging). Furthermore, the theoretical framework presented here gives a basis for further investigations of the memory effects and non-Markovian dynamics in networks, and in particular for binary-state models with aging. Still, a number of theoretical developments remain open for future work, such as the consideration of stochastic finite size effects (108). Also, proper approximations need to be developed to account for some of our numerical results for random-regular networks with high degree, as well as for high clustering, degree-degree correlations networks and for regular lattices, including continuous field equations for this latter case.

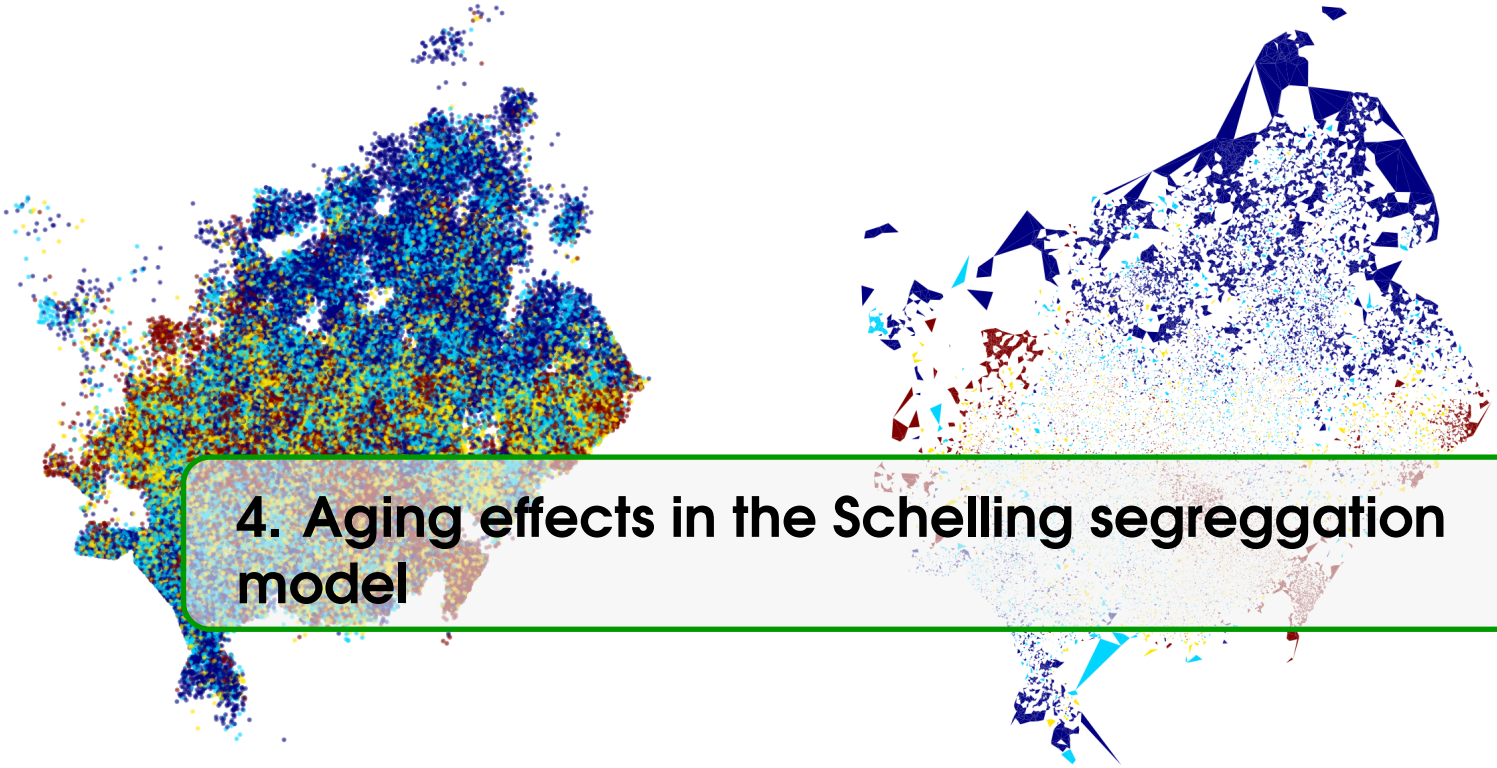

4. Aging effects in the Schelling segreggation model

The Schelling model has become a paradigm in social sciences to explain the emergence of residential spatial segregation, even in the presence of high tolerance to mixed neighborhoods by the side of citizens. In particular, we consider a noisy constrained version of the Schelling model, in which agents maximize its satisfaction, related to the composition of the local neighborhood, by infinite-range movements towards satisfying vacancies. We add to it an aging effect by making the probability of agents to move inversely proportional to the time they have been satisfied in their present location. This mechanism simulates the development of an emotional attachment to a location where an agent has been satisfied for a while. The introduction of aging has several major impacts on the model statics and dynamics: the phase transition between a segregated and a mixed phase of the original model disappears, and we observe segregated states with a high level of agent satisfaction even for high values of tolerance. In addition, the new segregated phase is dynamically characterized by a slow power-law coarsening process similar to a glassy-like dynamics.

4.1 Introduction

Thomas Schelling introduced a simple segregation model (71, 124, 125, 126) in which agents of two colors are distributed randomly on a chess-board, leaving some locations free. Agents are unsatisfied if more than a half of the eight nearest neighbors have different color. Randomly, the unsatisfied agents will move to available satisfying locations of the neighborhood. This model has had a very significant impact for several reasons: The "hand-made" simulations performed by T. Schelling by moving pawns on a chessboard are an early precedent of the use of agent-based simulations in Social Sciences. It is also one of the first social models to show emergent behavior as a result of simple interactions among agents, a characteristic of complex systems. A robust result of the model is that segregation occurs even when individuals have a very mild preference for neighbors of their own type, so collective behavior is not to be understood in terms of individual intentions. In addition, the model introduced the concept of behavioral threshold that inspired a number of other models of collective social behavior (61). But still currently, Schelling's model is at the basis of fundamental studies of the micro-macro paradigm in Social Sciences (64), while it continues to have important implications for social and economic policies addressing the urban segregation problem (29, 30, 88, 122). A main limitation of the Schelling model is that it has no history or memory by

which, for example, residents might prefer to maintain their present location (129). In this paper we address this limitation on the effects of memory.

As a result of the notable implications of this model and the robustness of the emerging segregation, there exists a vast literature around Schelling's results. Many variants of the original Schelling model have been reported modifying the rules that govern the dynamics, the satisfaction condition, or including other mechanisms, network effects, or specific applications (4, 5, 12, 33, 43, 50, 51, 60, 72, 73, 80, 89, 105, 106, 118, 127, 138, 139, 144, 145). In particular, the Schelling model has been studied from a Statistical Physics point of view due to its close relation to different forms of Kinetic Ising-like models (138, 139), and also addressing general questions of clustering and domain growth phenomena, as well as for the existence of phase transitions from segregated to non-segregated phases. For example, the relation with phase separation in binary mixtures has been considered (33, 145), as well as the connection with the phase diagram of spin-1 Hamiltonians (17, 50, 51, 123). In this context a useful classification of models is to distinguish between two possible types of dynamics (33): "constrained", where agents just move to satisfying vacancies (if possible), and "unconstrained", where agents' motion does not prevent them to remain unsatisfied. In addition, the motion can be short-range (only to neighboring sites, as in the original model) or long-range. Constrained motion has been named "solid-like" because it generally leads to frozen small clusters, while unconstrained motion has been considered "liquid-like" because it allows for large growing clusters (145). Including the motion of satisfied agents leads to a noisy effect playing the role of temperature in a statistical physics approach.

It is known that human interactions do not occur at a constant rate. They rather show a bursty character with a non-Poissonian inter-event time distribution that reflects a memory from past interactions. (10, 77, 87, 104, 121, 153) However, most social simulations, including simulations of variants of the Schelling model, implicitly assume a constant rate of interactions or state updating. "Aging" is one form of memory effect on which the rate of interactions depends on the persistence time of an agent in a state, modifying the transition to a different state (18, 45, 114). This concept of aging, or "social inertia" (135), constrains the transitions in a way that the longer an agent remains in a given state, the smaller the probability to change it. Aging has been already shown to modify social dynamics very significantly. For example, in opinion dynamics, aging is able to produce coarsening towards a consensus state in the voter model (45, 112) or to induce a continuous phase transition in the noisy voter model (9). With the motivation of established relevant effects of aging in opinion dynamics, our goal is to characterize how "aging" modifies the segregation dynamics of the Schelling model. In this context, aging must be understood as an emotional/economic attachment to a certain location linked to the persistence time in this location. This attachment balances the memory-less and purely rational considerations of the original model (63). The aging-induced inertia, which results in resistance to movement, is minimalist modeling of behavior with many different possible causes. Besides the moving out cost due to the housing market fluctuations, aging accounts for the links established with the neighborhood's public goods, venues, schools, etc, which are known to be highly relevant in this context (27, 129, 146). These urban elements are also a major consideration when households locate (28, 31, 34, 130) and aging also accounts for the memory of this decision.

In this paper, aging is introduced in the Schelling model by considering that agents are less prone to change their location as they get older in a satisfying place. In other words, aging is introduced giving a smaller probability for satisfied agents to "move-out" the longer they have remained in a satisfying neighborhood. We implement this aging mechanism in the long-range noisy constrained version of the Schelling Model (50),

for which a detailed phase diagram was reported. We study how this phase diagram is modified by the aging mechanism, finding that aging inhibits a segregated-mixed phase transition. This implies that aging favors segregation, a counter-intuitive result. We also describe the coarsening dynamics in the segregated phase showing that aging gives rise to a slower coarsening that breaks the time-translational invariance.

4.2 Model

The model considered in this work is a variant of the noisy constrained Schelling model (50) in which we explicitly include aging effects. For simplicity, we refer to this variant as the Schelling model during the rest of the paper to compare with the model presented here: the Schelling model with aging. For both, the system is established on a $L \times L$ Moore lattice with 8 neighbors per site and periodic boundary conditions, where agents of two kinds (representing, for instance, wealth levels, race, language, etc) occupy the sites. There are also empty sites (vacancies), where agents can move to, depending on their state and on the vacancy neighborhood. The condition of each site i of the lattice will be described with a variable σ_i that takes three possible values: $\sigma_i = \pm 1$ for the two kinds of agents and $\sigma_i = 0$ for vacancies. In addition, depending on the local environment, agents can be in two states: satisfied or unsatisfied. In our case, agents are satisfied if their neighborhood is constituted by a fraction of unlike agents lower than a fixed homogeneous parameter T. Otherwise, they are unsatisfied. Therefore, this control parameter T is a measure of how tolerant the population of the system is. We also need a non-zero vacancy density, $\rho_v > 0$, for agents to change their location. This ρ_v is understood as an extra parameter of the model. The initial configuration is built by randomly distributing the agents ($N_{\text{agents}} = L^2 (1 - \rho_v)$). We always consider one half of agents of each kind.

In the Schelling model considered, an agent chosen by chance moves to a random satisfying vacancy (if any exists) independently of his/her initial state and of the distance. This process is repeated until the system reaches a stationary state. The movement of unsatisfied agents behaves as a driver for the system dynamics, while the motion of satisfied agents plays the role of noise. When tolerance T becomes larger, more satisfying vacancies are present in the system and the noise consequently increases.

The aging mechanism in our model is introduced by considering an activation probability of the agents inversely proportional to the time spent at a satisfied location, motivated by the definition for opinion dynamics (9). This methodology was proposed to mimic the power-law like inter-event time distributions observed in real-world social systems (10, 45). If an agent j is initially satisfied in her neighborhood, the internal time is set $\tau_j = 0$. Then, in every time step, a randomly chosen agent j follows different rules depending on whether she is originally satisfied or not. If unsatisfied, j moves to any random satisfying vacancy of the system. Otherwise, she moves to another satisfying vacancy with an activation probability $p_j = 1/(\tau_j + 2)$. In both cases, if no vacancy has a satisfying neighborhood, the agent j remains in the initial site. As before, these rules are iterated until the system reaches a stationary state (if possible). The time is counted in Monte-Carlo steps; after each Monte-Carlo step, that is after N_{agents} iterations, the internal time increases for all satisfied agents in one unit, $\tau_j \to \tau_j + 1$. Notice that, when an unsatisfied agent becomes satisfied due to the neighbor's motion, an internal time $\tau_j = 0$ is set for that agent. As for the Schelling model, there is a noise effect associated with the motion of satisfied agents. In this case, the intensity of this noise is related not only to the tolerance parameter T, but to the presence of aging as well. In fact, aging introduces more constraints to the movements and contributes to decreasing the noise.

Given the number of neighbors available in the Moore lattice, numerical simulations

are only performed for a finite set of meaningful tolerance values: $\{1/8, 1/7, 1/6, \cdots, 6/7, 7/8\}$. During all our analysis, we focus on the low vacancy density region of the phase diagram. In this region, there is an even smaller number of meaningful T values $\{1/8, 2/8, ..., 7/8\}$, because the majority of agents do not see vacancies in their surroundings.

4.3 Metrics of segregation

Many metrics have been introduced in the literature to discern if the final state is segregated or not (50, 89, 133, 150). The number of clusters is known to be directly related to the segregation because a high presence of small clusters indicates a mixing between agents. As for the Schelling model(50), we compute the following metric related to the second moment of the cluster size distribution:

$$s = \frac{2}{\left(L^2\left(1-\rho_v\right)\right)^2} \sum_{\{c\}} n_c^2, \tag{4.1}$$

where the index of the sum c runs over all the clusters $\{c\}$ and n_c is the number of agents in the cluster c. The average of s over realizations after reaching a stationary state is defined as the segregation coefficient $\langle s \rangle$. This metric is bounded between 0 and 1: $\langle s \rangle \to 1$ if there are only 2 equally-sized clusters, and $\langle s \rangle \to 0$ if the number of clusters tends to the number of agents. The cluster detection is performed using the Hoshen-Kopelman algorithm (74).

Another metric of segregation is the interface density (33), defined as the fraction of links connecting agents of different kinds. The calculation is done in two steps: estimating the interface density for each agent j, ρ_j, and then the average over all the agents ρ:

$$\rho_j = \frac{1}{2}\left(1 - \frac{\sigma_j \sum_{k\in\Omega_j} \sigma_k}{\sum_{k\in\Omega_j} \sigma_k^2}\right) \quad \text{and} \quad \rho = \frac{1}{\mathrm{N_{agents}}} \sum_{\mathrm{j=1}}^{\mathrm{N_{agents}}} \rho_{\mathrm{j}}, \tag{4.2}$$

where the indices k run over the neighborhood of agent j, Ω_j. If an agent j is surrounded only by vacant sites, we define by convention $\rho_j = 0$. Performing a realization average of ρ, we obtain the average interface density $\langle \rho \rangle$ in the stationary state is denoted as $\langle \rho_{\mathrm{st}} \rangle$. The evolution of this metric allows us to study the coarsening process.

4.4 Results

4.4.1 Phase diagram

To discuss the phase diagram of our model, we focus on the region of parameters with a vacancy density $\rho_v < 50\%$ to avoid diluted states with a majority of vacancies. For this region, the Schelling model presents 3 different phases (50): frozen, segregated and mixed. For low tolerance values, the system freezes in a disordered state, given that there are no satisfying vacancies for any kind of agent. With increasing tolerance, the system undergoes a transition toward a segregated state, which is characterized by a 2-clusters dynamical final state. Finally, for high values of T, after another transition, we find a dynamical disordered (mixed) state, in which a vast majority of vacancies are satisfying for both kinds of agents, and small clusters are continuously created and annihilated.

These three phases are characterized by measuring the segregation coefficient $\langle s \rangle$ and the average interface density $\langle \rho_{\mathrm{st}} \rangle$ at the final state. The results for the original model are depicted as a function of the tolerance T in Fig. A.1a for the interface density and in Fig. A.1b for the segregation coefficient. At low values of T, both indicators show

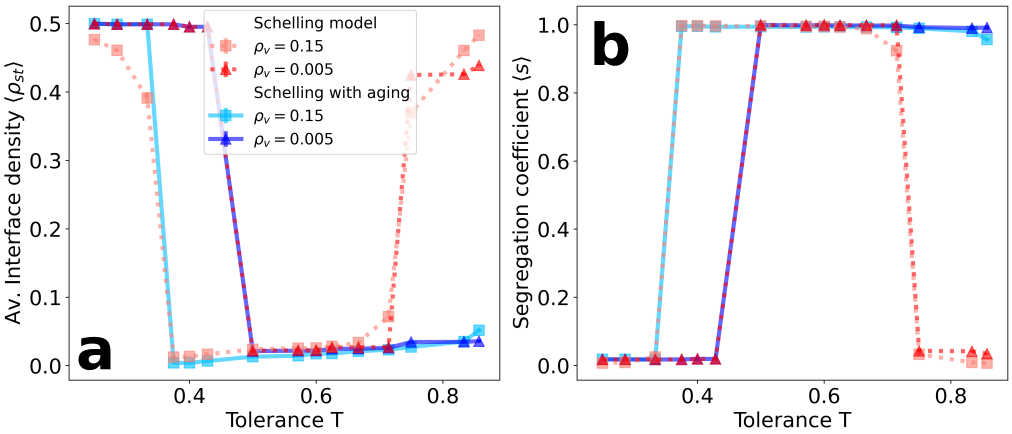

Figure 4.1: Average interface density $\langle \rho_{\mathrm{st}} \rangle$ (**a**) and segregation coefficient $\langle s \rangle$ (**b**) at the stationary regime as a function of the tolerance parameter T for two values of the vacancy density $\rho_v = 0.5\%$ and 15%. Results are shown for both the Schelling model and the variant with aging introduced in this paper. Simulations are performed on an 80×80 lattice and averaged over $5 \cdot 10^4$ realizations.

a disordered state that falls in the frozen phase. We also observe a dependence of the transition point with the vacancy density. On the other hand, for high T values, the transition point between segregated and mixed states has no dependence on the parameter ρ_v. Notice that mixed and frozen states present a very similar value of $\langle s \rangle$ but can be differentiated by the stationary value of the average interface density $\langle \rho_{\mathrm{st}} \rangle$. These results are in agreement with the results reported for the Schelling model(50), with the extra information provided by the average interface density.

The first quite dramatic effect of including aging in the system is the disappearance of the mixed state from the phase diagram. In both metrics, the difference between the models with and without aging is clearly manifested. For low T values, the frozen-segregated transition behaves similarly to the original model since aging has no implications as the system gets quickly frozen. Nevertheless, for high values of the tolerance $T > 0.5$, the segregated-mixed transition disappears, and the segregated phase is always present. This is not an intuitive effect and one would think that aging, contributing to difficult agent's mobility, should prevent the system from forming fully developed segregated clusters. However, it is just the opposite, and it favors cluster emergence.

4.4.2 Segregated phase: final state

To gain further insights into the differences in the system dynamics that lead to the extended segregated phase, we compute the fraction of unsatisfied agents at the stationary regime n_u (see Fig. A.2a). This metric plays a role as a marker for the frozen-segregated transition, as shown for the 1D Schelling model (33). The frozen phase presents a big majority of unsatisfied agents for both models. After the transition, this parameter decays to very low values in the segregated phase, where a majority of agents are satisfied. In this phase, we observe a step-like increasing behavior of the unsatisfied agents with T. As the tolerance grows, the number of satisfying vacancies increases and the noisy movement of satisfied agents drives the system evolution, creating eventual unsatisfied agents in the sites that they abandon or target. However, in the Schelling model, the transition to a mixed state at $T = 0.75$ inhibits the creation of clear fronts between agents of different kinds, and it is also associated to a sharp

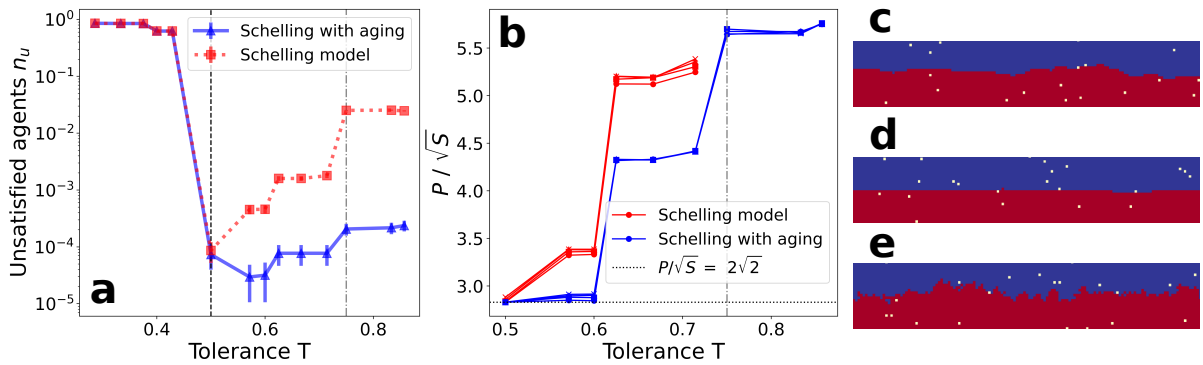

Figure 4.2: (**a**) Fraction of unsatisfied agents n_u at the stationary regime as a function of the tolerance parameter T. (**b**) Measure of the interface roughness between clusters of different kind of agents at the final stationary state $P/\sqrt{S}$ as a function of the tolerance parameter T. Different markers indicate different system sizes: $L = 40$ (circles), 60 (squares), 80 (triangles) and 100 (crosses). Results are shown for both the Schelling model with and without aging. Numerical simulations are performed for $\rho_v = 0.5\%$ and averaged over $5 \cdot 10^4$ realizations. The frozen-segregated transition (dashed black line) and the segregated-mixed transition (gray dot-dashed line) are highlighted to differentiate the phases that the Schelling model exhibits. There are no values of $P/\sqrt{S}$ for the Schelling model above $T = 3/4$ because the segregated-mixed transition occurs. (**c**) Final state interface zoom snapshot for $T = 0.57$ using the original model. (**d**) Final state interface zoom snapshot for $T = 0.57$ using the model with aging. (**e**) Same as c for $T = 0.86$.

increase of $n_u \simeq 0.05$ (red squares in Fig. A.2a). The Schelling model with aging, on the other hand, shows a lower fraction of unsatisfied agents during all values of the tolerance above the frozen-segregated transition (blue triangles in Fig. A.2a). So much so, that many realizations reach $n_u = 0$ and this causes the large error bars in Fig. A.2a after the transition. In a counterintuitive way, the introduction of aging causes a higher global satisfaction when compared with the original model in both the segregated and the mixed phases.

The creation of new unsatisfied agents at the final stationary state occurs at the interface between the segregated agent kinds. This is why we study the interface roughness (perimeter) P as a function of the tolerance parameter. To compute this measure, we compute the number of agents of one kind in contact with different kind agents. To perform this calculation, we smooth the interface by considering vacancies surrounded by a majority of agents of a certain kind as members of that kind. In our system of $L \times L$ with periodic boundary, the minimum interface size (perimeter) P between clusters of agents of different kind is $P = 2L$. To avoid the L dependency, we calculate an adimensional magnitude $P/\sqrt{S}$, where S is the number of agents of each kind $S = N_{\text{agents}}/2 = L^2(1-\rho_v)/2$ (surface). This metric $P/\sqrt{S}$ is computed starting from a flat interface as an initial condition and evolving it for $t_{\max} = 10^4$ MC steps to reach well within the stationary state. With the metric $P/\sqrt{S}$, we are able to estimate how close is the final state interface of our system to the flat interface ($P/\sqrt{S} = 2\sqrt{2}$). The results show an increasing dependence of roughness with the tolerance parameter T (see Fig. A.2b). This growth can be explained as an increase in tolerance means that agents are satisfied with fewer "same-kind" neighbors. Therefore, the interface is able to be rougher, keeping the agents in a satisfied state. In addition, notice that all values with different L collapse, so the dependence on the system size has been eliminated.

Comparing both models, one observes a lower interface roughness for the Schelling model with aging, regardless of the value of T. The closest value to the flat interface

occurs for the first values of T after the frozen-segregated phase transition (shown in Fig. A.2d). In the original model, we observe higher values of $P/\sqrt{S}$ due to the noise produced by the satisfied agents' behavior (see Fig. A.2c). Moreover, aging allows us to obtain a segregated phase with even larger interface roughness than the maximum observed in the original model for large values of T (see Fig. A.2e). We remark that, when aging is introduced, agents try to join those of their own kind but are less and less prone to change location as time passes. Thus, in the Schelling model with aging, agents in the bulk of the clusters mainly do not move and those moving more often are located at the interface between agent kinds. At medium and large scales, this phenomenon leads to ergodicity breaking in the final state dynamics.

4.4.3 Segregated phase: coarsening dynamics

Diverse versions of the original Schelling Model exhibit different behaviors in terms of coarsening dynamics. Recent publications report a power-law like domain growth (5, 33). We monitor here the evolution of the interface density $\langle\rho(t)\rangle$, which decreases as $\langle\rho(t)\rangle \sim t^{-\alpha}$ so the domains should grow in our model following a power-law with time.

The coarsening process of the Schelling model at the segregated phase ($0.5 \leq T < 0.75$) is displayed in Fig. A.3a and Fig. 4.4. We find that the average interface density follows a power-law decay with an exponent $\alpha \simeq 0.5$ for the limit of small vacancy density $\rho_v \to 0$, in agreement with the value reported for close variants of the Schelling model (33). This exponent value is curious since the coarsening in the presence of a conserved quantity (but with local interactions) exhibits an exponent $\alpha = 1/3$ (66). Nevertheless, the interactions in this model are not local, and the coarsening exponent is more similar to the one in systems with a non-conserved order-parameter ($\alpha = 1/2$). Fig. A.3a shows as well how coarsening changes with the tolerance parameter. Even though the exponent α does not depend on T, we observe a certain delay when increasing T from 0.6 to 0.62. In the system evolution of Fig. 4.4, one can see how the behavior of the satisfied agents for higher tolerance values is translated into rougher interfaces, causing such delay. For $T > 0.75$, the system exhibits a transition towards a mixed state where the interface density fluctuates around $\rho = 0.5$, indicating that the state is constantly disordered.

The Schelling model with aging shows very different behavior (Fig. A.3b). As predicted by the phase diagram, the average interface density exhibits a power-law decay with time for all values of the tolerance T after the frozen-segregated transition. Still, the decay is slower than for the Schelling model, with $\langle\rho(t)\rangle \sim t^{-0.2}$. A mechanism that could be behind this behavior is that the model with aging counts more satisfied agents than the original model, and their probability to move becomes lower as time goes by. Moreover, satisfied agents inside a cluster will not move and the dynamics in the model take place at the interface. It is, therefore, more difficult for separated clusters to collide and merge, an effect that slows down the decay of the interface density. The persistence of small clusters becomes clear when the snapshots' evolution is compared for both models at the same tolerance value $T = 0.71$ (see Fig. 4.4). Moreover, while for the original model the initial clustering for $t = 500$ steps does not determine the final state, in the case of aging the bigger clusters present at the beginning of the evolution are the ones that keep growing, determining the shape of the system configuration after 50000 time steps. This is a dynamical effect, because the system in both cases tends to a final configuration with 2-clusters.

In the case of the Schelling model with aging, we observe an early cross-over in the dynamics (Fig. A.3b). For $T < 0.75$, the coarsening starts with an initial decay of $\langle\rho(t)\rangle$ faster than $t^{-0.2}$. This occurs because in this regime it is necessary sometimes for the aging effects to become relevant, and initially the system behaves as in the original

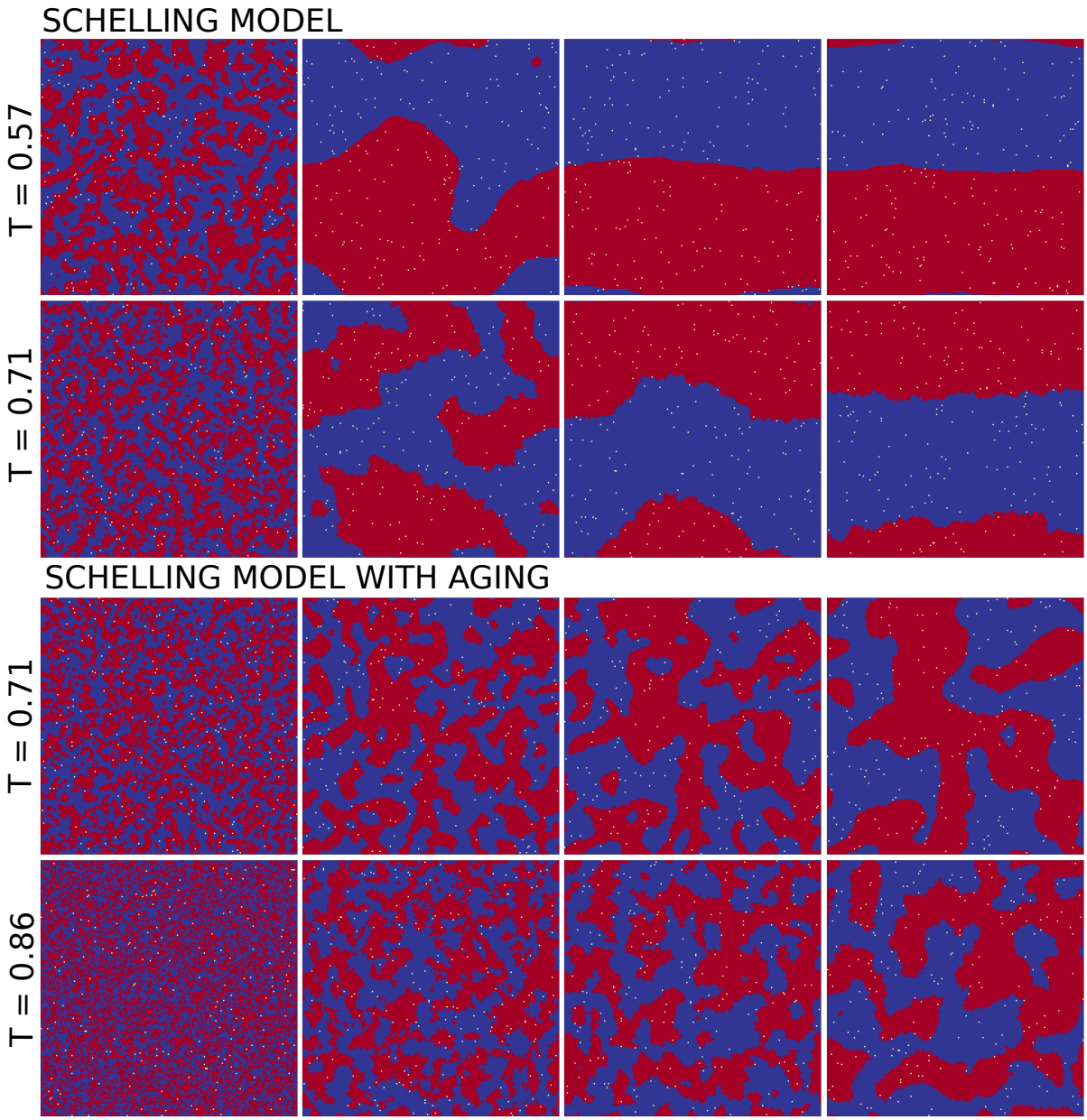

Figure 4.3: Average interface density $\langle \rho(t) \rangle$ as a function of time steps for different values of the tolerance parameter T using the Schelling model (**a**) and the version with aging (**b**). Average performed over $5 \cdot 10^3$ realizations. Fitted power-law in a black dashed line highlighting the estimated exponent value. We set system size $L = 200$ and $\rho_v = 0.005$.

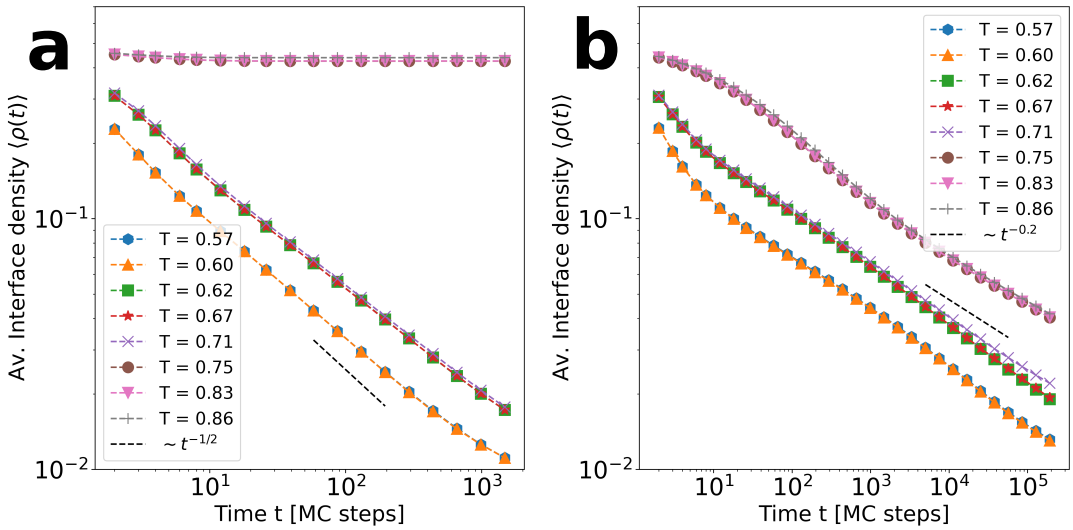

Figure 4.4: Coarsening towards the segregated state at two different values of T for both models. Snapshots are taken for 5, 500, 5000 and 50000 time steps ordered from left to right. We set system size $L = 200$ and $\rho_v = 0.005$.

model. Similarly, for $T \geq 0.75$, $\langle \rho(t) \rangle$ decays slowly for a moment before reaching the power-law behavior for large t values. Confirming this scenario, Fig. 4.4 shows that for $T = 0.86$, the system starts evolving similarly to a mixed state until some clusters are created. At this moment, aging prevents the clusters' desegregation, leading the system very slowly to coarsening dynamics and, eventually, to a fully segregated state.

Regarding the relaxation time to the final state, we see in Fig. 4.4 how for $T = 0.71$, the stationary state of the Schelling model is reached after approximately $t = 5000$ time steps. In contrast, the version with aging needs much more than 50000 steps to attain it. This highlights the important temporal difference between both models in terms of domain growth dynamics, which strongly increases the computational cost of the study of the stationary state of the model with aging. We have been thus able to study only medium and small system sizes in this final regime (see videos included as Supplementary Information S1 and S2).

The dynamics studied thus far are performed considering the limit $\rho_v \to 0$, but the analysis can be extended to higher vacancy densities. For the particular case of high ρ_v and low T, aging leads to the formation of a vacancy cluster at the interface between domains (see details in Supplementary information S3).

4.4.4 Aging breaks the asymptotic time-translational invariance

Here, we explore further time translational invariance (TTI) in the model dynamics. For this, we start by defining the two-time autocorrelation function $C(\tau, t_w)$ (151) as

$$C(\tau, t_w) = \left\langle \frac{1}{M} \sum_{i=1}^{N} \sigma_i(t_w + \tau)\, \sigma_i(t_w) \right\rangle, \tag{4.3}$$

where N is the system size, $\langle \cdot \rangle$ refers to averages over realizations, t_w is the waiting time to start the autocorrelation measurements, τ a time interval after t_w and M is a

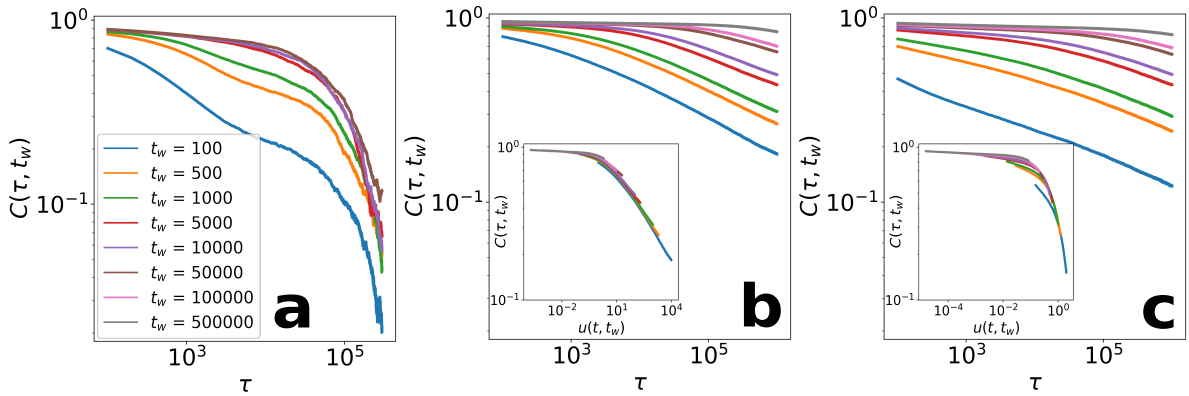

Figure 4.5: Two-times autocorrelation $C(\tau, t_{\rm w})$ as a function of the time period passed since the waiting time $t_{\rm w}$. First, the autocorrelation is shown for the Schelling model at $T = 0.71$ in **a**, and for the version with aging at $T = 0.71$ in **b** and $T = 0.86$ in **c**. The insets are the result of the collapse using $u(\tau, t_w) = \tau/t_w$ (**b**) and $u(\tau, t_w) = \log(\tau + t_w)/\log(t_w) - 1$ (**c**). The curves correspond to different values of the waiting time $t_{\rm w}$. Calculations performed on a 100×100 lattice averaged over $5 \cdot 10^4$ realizations.

normalization factor defined as

$$M = \sum_{i=1}^{N} (\sigma_i(t_{\rm w} + \tau)\, \sigma_i(t_{\rm w}))^2. \tag{4.4}$$

which is computed at each realization.

The autocorrelation function is displayed for the Schelling model with $T = 0.75$ in Fig. 4.5a. We observe the curves decreasing with τ as expected, and that after a characteristic time period ($t_{\rm w}^* \approx 5000$ for a system size of 80×80) they collapse into a single curve. This is the regime in which the dynamics becomes TTI, implying that the autocorrelation function does not depend any more on the waiting time, $C(\tau, t_{\rm w}) = C(\tau)$ for $t_{\rm w} > t_{\rm w}^*$.

For the Schelling model with aging, the dynamics show some different features (Figs. 4.5b and 4.5c). First, the autocorrelation functions decay slower with τ in all the cases, which is connected to the long-lived small clusters mentioned previously. We do not find in the simulations any value of $t_{\rm w}^*$ for the systems to fall into a TTI regime. Not only that, but a scaling relation including both τ and $t_{\rm w}$ can be applied to collapse the autocorrelation curves (see insets Figs. 4.5b and 4.5c). This behavior is similar to glassy systems (151), therefore it is useful to use the mathematical description for those systems in our case. In this type of dynamics, a final stationary state is not attainable in the thermodynamic limit, and it is possible to decompose the autocorrelation function into an equilibrium part and an "aging" part (aging in the sense of non-equilibrium dynamics in glassy systems) (15, 151):

$$C(\tau, t_{\rm w}) \simeq C_{\rm eq}(\tau)\, C_{\rm aging} u(\tau, t_w) = C_{\rm eq}(\tau)\, C_{\rm aging} \left(\frac{h(\tau)}{h(t_{\rm w})} \right), \tag{4.5}$$

where $C_{\rm eq}$ describes the fast relaxation of the system components within each domain (TTI term), $C_{\rm aging}$ is a scaling function and $u(\tau, t_w)$ is a normalization factor which, in some cases, can be written as the quotient of an unknown function $h(t)$ at the two times τ and $t_{\rm w}$. This function $h(t)$ is known to be related to the dynamical correlation length (15, 48). In our case, we use $h(t) = t$ to scale the results in Fig. 4.5b (see inset). This

scaling is valid for values of $T \in [0.5, 0.75)$. Nevertheless, higher values of T do not hold a linear scaling, and we need to turn to other functional forms as the normalization factor $u(\tau, t_w) = \log(\tau + t_w)/\log(t_w) - 1$ used in Fig. 4.5c. This indicates that for $T > 0.75$, the dynamical correlation length evolves in a different and slower way.

4.5 Summary and discussion

We have studied the effect of aging on a stochastic Threshold model, which combines long-range mobility with local short-range interactions. Specifically, taking as basis the noisy constrained Schelling model, we assign to the agents an internal clock counting the time spent in the same satisfying location. The probability of changing state decreases then inversely proportional to this time. Therefore, older satisfied agents are less prone to update resident locations. The original model displays a transition between a segregated phase and a mixed one as the tolerance control parameter T increases. This transition disappears when aging is introduced into the system, the mixed phase is replaced by a segregated phase even for high values of the tolerance parameter T. As a result, the model with aging presents a higher global satisfaction than without this effect for all values of the tolerance.

On the dynamical perspective, the relaxation towards the segregated phase features a coarsening phenomena characterized by a power-law decay of the average interface density with time $\langle \rho \rangle \sim t^{-\alpha}$. For the original model in the limit of low vacancy density, the exponent is around $\alpha = 1/2$. This exponent is also reported in other variants of the Schelling model (5, 33). Aging gives rise to long-lived small clusters and a slower coarsening, reducing the exponent to $\alpha \simeq 0.2$. We investigated the autocorrelation functions in the segregated phase and found that aging breaks the asymptotic time-translational invariance of the dynamics. This result, along with a nontrivial scaling of the autocorrelation functions, establish close similarities with low-coarsening systems, such as glassy systems, and our Schelling model with aging for high values of the tolerance parameter. Moreover, this work studies the case for equal size populations ignores effects arising from the competition between different population sizes. Further work would be to study a joint effect of minority population and aging.

As for the implications of our results from a social perspective, we must note that the fact that aging favors segregation, inhibiting the segregation-mixed phase transition, is rather counter-intuitive, but gives support to the argument that segregation is a stochastically stable state and may prevail in an all-integrationist world (152). Our model predicts the appearance of segregation even for tolerance values close to one. Additionally, the model relaxation time multiplies manifold, which implies that if aging is present the natural state of this system seems to be generically out of equilibrium.

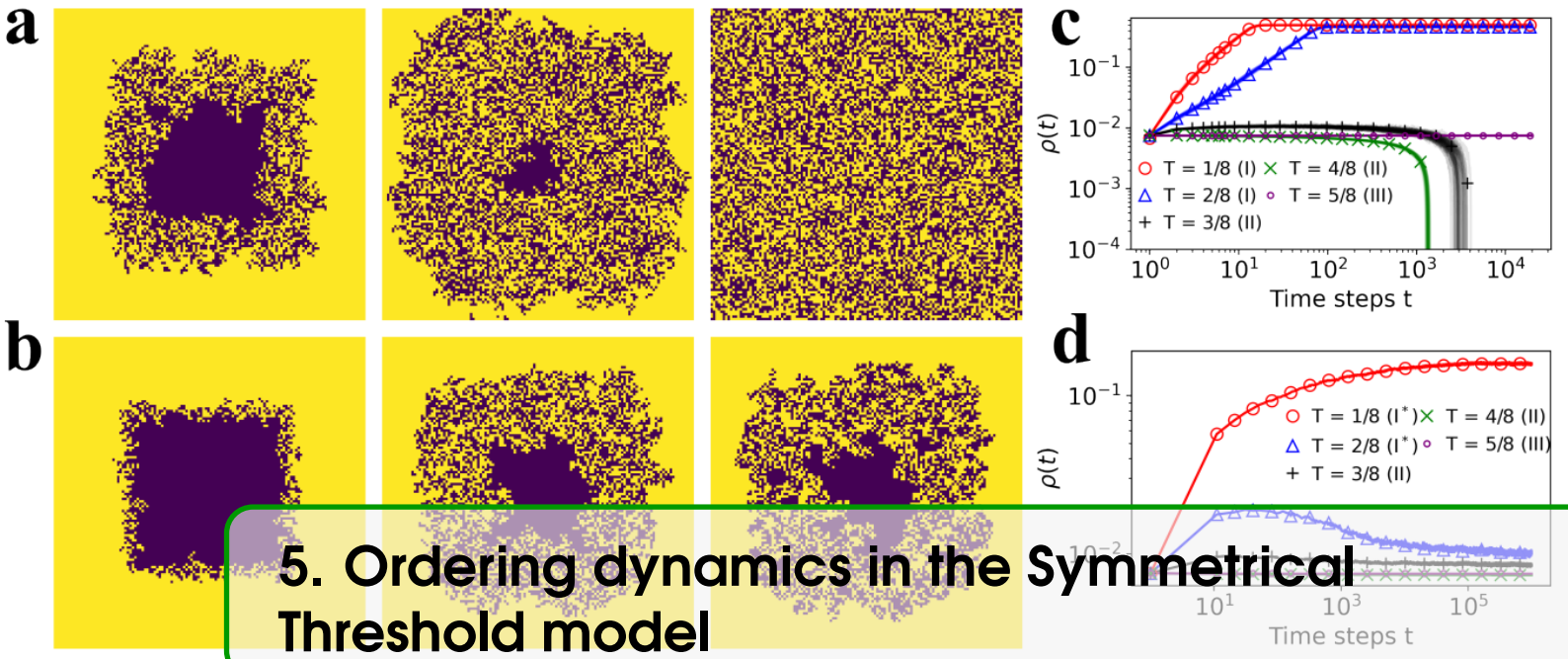

5. Ordering dynamics in the Symmetrical Threshold model

The so-called Granovetter-Watts model was introduced to capture a situation in which the adoption of new ideas or technologies requires a certain redundancy in the social environment of each agent to take effect. This model has become a paradigm for complex contagion. Here we investigate a symmetric version of the model: agents may be in two states that can spread equally through the system via complex contagion. We find three possible phases: a mixed one (dynamically active disordered state), an ordered one, and a heterogeneous frozen phase. These phases exist for several configurations of the contact network. Then, we consider the effect of introducing aging as a non-Markovian mechanism in the model, where agents become increasingly resistant to change their state the longer they remain in it. We show that when aging is present, the mixed phase is replaced, for sparse networks, by a new phase with different dynamical properties. This new phase is characterized by an initial disordering stage followed by a slow ordering process towards a fully ordered absorbing state. In the ordered phase, aging modifies the dynamical properties. For random contact networks, we develop a theoretical description based on an Approximate Master Equation that describes with good accuracy the results of numerical simulations for the model with and without aging.

5.1 Introduction

In recent decades, various techniques of probability and statistical physics have been employed to measure and explain social phenomena (16, 21, 81). A variety of social collective phenomena can be well understood through stochastic binary-state models of interacting agents. In these models, each agent is assumed to be in one of two possible states, such as susceptible/infected, adopters/non-adopters, etc., depending on the context of the model. The interaction among agents is determined by the underlying contact network and the dynamical rules of the model. There are various examples of binary-state models, including processes of opinion formation (47, 90, 116, 132, 140) and disease or social contagion (62, 107), among others. The consensus problem consists of determining under which circumstances the agents end up sharing the same state or when the coexistence of both states prevails. This is characterized by a phase diagram that provides the boundaries separating domains of different behaviors in the control parameter space. Macroscopic descriptions of these models in terms of mean-field, pair, and higher-order approximations are well established (55).

An important category of binary-state models are threshold models (147), which were originally introduced by M. Granovetter (62) to address problems of social contagion such as rumor propagation, innovation adoption, riot participation, etc. Multiple exposures, or group interaction, are necessary in these models to update the current state, a characteristic of complex contagion models (25, 75). The threshold model presents a discontinuous phase transition from a "global cascade" phase to a "no cascade" phase, which was analyzed in detail in Ref. (147). This model has been extensively studied on various network topologies, such as regular lattices, small-world (25), random (57), clustered (69, 70), modular (54), hypergraphs (7), homophilic (40) and coevolving (95) networks.

A main difference between the threshold model and other binary-state models, such as the Voter (90), majority vote (MV) (19, 103, 113), and nonlinear Voter model (23, 79, 92, 93, 96, 109), is the lack of symmetry between the two states. In the threshold model, changing state is only possible in one direction, representing the adoption forever of a new state that initially starts in a small minority of agents. A symmetric version of the threshold model, with possible changes of states in both directions, was introduced in Refs. (100, 101) to investigate the impact of noise and anticonformity. However, a complete characterization of the Symmetrical Threshold model and its ordering dynamics have not been addressed so far.

5.2 Symmetrical Threshold model

The system consists of a set of N agents located at the nodes of a network. The variable describing the state of each agent i takes one of the two possible values: $s_i = \pm 1$. Every agent has assigned a fixed threshold $0 \leq T \leq 1$, which determines the fraction of different neighbors required to change state. Even though this value might be agent-dependent, we will consider here only the case with a homogeneous T value for all the agents of the system. In each update attempt, an agent i (called active agent) is randomly selected, and if the fraction of neighbors with a different state is larger than the threshold T, the active agent changes state $s_i \to -s_i$. In other words, if m is the number of neighbors in state -1 out of the total number of neighbors k, the condition to change is $\theta(m/k - T)$, for a node in state $+1$, and $\theta((k-m)/k - T)$, for a node in state -1, where $\theta(x)$ is the Heaviside step function. Notice that this update rule is equivalent to "shifted" Glauber dynamics (53), with swapping probability $1/(1+\exp[\beta(\Delta E + C)]$ (where β is the inverse temperature, ΔE the energy loss to swap the state of a node according to Ising Hamiltonian and C a shifting constant), at the limit of zero temperature ($\beta \to \infty$). We analyze the model dynamics using numerical simulations. Simulation time is measured in Monte Carlo (MC) steps, i.e., N update attempts. Numerical simulations run until the system reaches a frozen configuration (absorbing state) or until the average magnetization, $m = (1/N)\sum_i s_i$, fluctuates around a constant value.

5.2.1 Mean-field

We first consider the mean-field case of the complete graph (all-to-all connections). We take an initial random configuration with magnetization m_0 and run numerical simulations for various values of T to construct the phase diagram (shown in Fig. 5.1a). We find three different phases based on the final state:

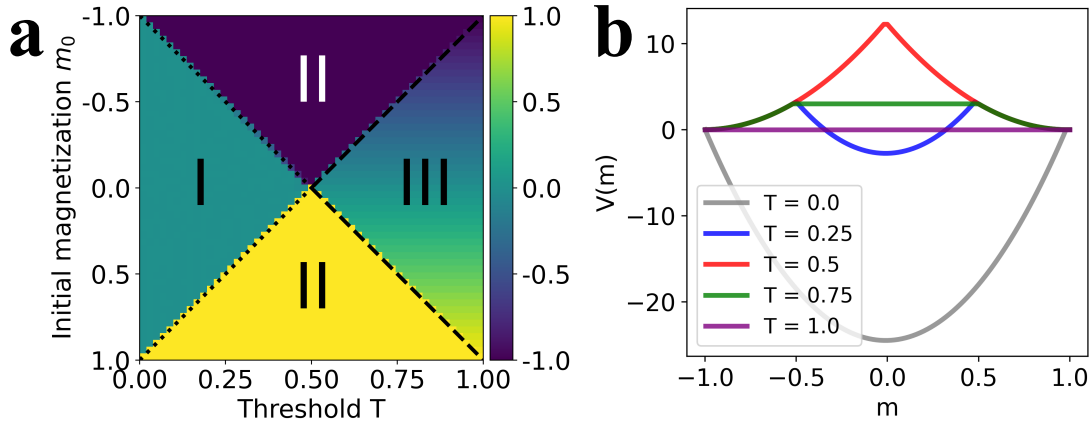

Figure 5.1: **Phases of the Symmetrical Threshold model.** (a) Phase diagram of the Symmetrical Threshold model in a Complete graph of $N = 2500$ nodes. Dotted and dashed lines correspond to $T = (1-|m_0|)/2$ and $T = (1+|m_0|)/2$, respectively. Average performed over 5000 realizations. (b) Potential representation from Eq. (**??**) for a set of values of the threshold T, shown in different colors.

- **Phase I or Mixed**: The system reaches an active disordered state (final magnetization $m_f = 0$) where the agents change their state continuously;
- **Phase II or Ordered**: The system reaches the ordered absorbing states ($m_f = \pm 1$) according to the initial magnetization m_0;
- **Phase III or Frozen**: The system freezes at the initial random state $m_f = m_0$.

For a given initial magnetization $m_0 \neq 0$ and increasing T, the system undergoes a mixed-ordered transition at a critical threshold $T_c = (1-|m_0|)/2$, and an ordered-frozen transition at a critical threshold $T_c^* = (1+|m_0|)/2 > T_c$ (indicated by dotted and dashed black lines in Fig. 5.1a, respectively). In this mean-field scheme, if the fraction of nodes in state $+1$ is denoted by x, the condition for a node in state -1 to change its state is given by $\theta(x-T)$, where θ is the Heaviside step function. Thus, in the thermodynamic limit ($N \to \infty$), the variable x evolves over time according to the following mean-field equation:<

$$\frac{dx}{dt} = (1-x)\,\theta(x-T) - x\,\theta(1-x-T) = -\frac{\partial V(x)}{\partial x}. \tag{5.1}$$

Here, $V(x)$ is the potential function. The stationary value of x, $x_{\rm st}$, is the solution of the implicit equation resulting from setting the time derivative equal to 0. The stationary solutions are $x_{\rm st} = 1/2$ ($m = 0$), the absorbing states $x_{\rm st} = 0, 1$ ($m = \pm 1$) or a degenerate continuum of solutions. The stability of these solutions can be understood in terms of the potential $V(x)$:

$$\begin{aligned} V(x) &= -\int (1-x)\,\theta(x-T) - x\,\theta(1-x-T)\,dx \\ &= \tfrac{x^2}{2} + \tfrac{1}{2}\left(T^2 - 2T - x^2 + 1\right)\,\theta(T+x-1) \\ &\quad -\tfrac{1}{2}\left(T^2 - 2T - x(x-2)\right)\,\theta(x-T) \end{aligned} \tag{5.2}$$

The minimum and maximum values of $V(x)$ correspond to stable and unstable solutions, respectively. Figure 5.1b shows the potential's dependence on the magnetization, obtained after a variable change $m = 2x-1$ in Eq. (5.2). For $T < 0.5$, $m = 0$ is a stable solution, but increasing the threshold reduces the range of values of the initial magnetization from which this solution is reached, enclosing Phase I between the unstable solutions $m = 1-2T$ and $2T-1$. In fact, if $m_0 > 1-2T$, the system reaches the absorbing solution

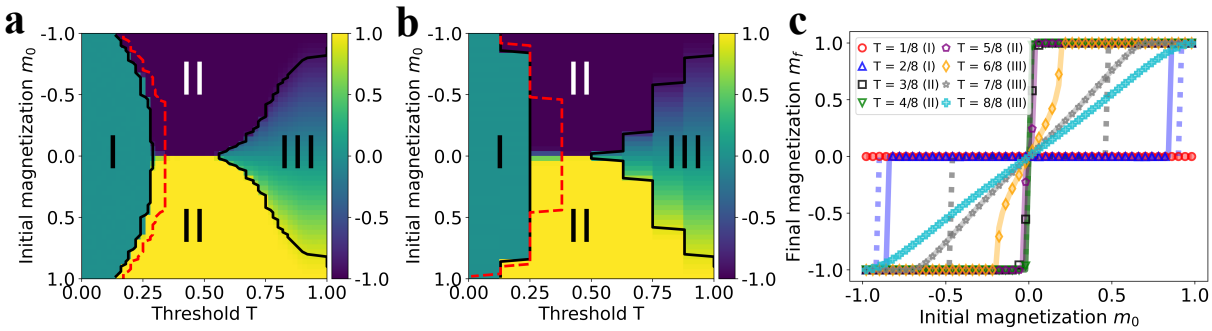

Figure 5.2: **Phase diagram in random networks.** Phase diagram of the Symmetrical Threshold model in an ER (a) and a RR (b) graph, both of $N = 4 \cdot 10^4$ nodes and mean degree $\langle k \rangle = 8$. The color map indicates the value of the average final magnetization m_f. The red dashed line is the HMF prediction of the mixed-ordered critical line. The black solid lines correspond to the AME prediction of the borders of Phase II. (c) Average final magnetization m_f as a function of the initial magnetization m_0 for different T values (indicated with different colors and markers) in the RR graph. The average is performed over 5000 realizations. The dotted and solid lines are the HMF (for $T = 1/8 - 4/8$) and AME predictions (for all T), respectively.

$m = +1$, while if $m_0 < -1 + 2T$, it reaches $m = -1$ (Phase II). For $T = 0.5$, there is just one unstable solution at $m = 0$, and all the initial magnetization values reach the absorbing states $m = \pm 1$. For $T > 0.5$, the potential is equal to a constant value for a range of m_0, which means that an initial condition will remain in this state forever (Phase III). The range of values of the initial condition from which this phase is reached grows linearly with T until $T = 1$, where all initial conditions fulfill $\frac{dm}{dt} = 0$.

Note that the mean-field Symmetrical Threshold model for $T = 1$ shows the same potential profile as the mean-field Voter model (22, 90, 140). The important difference is that for the Voter model, any initial magnetization is marginally stable, while in our model any initial magnetization is an absorbing state in Phase III. In the Voter model finite size fluctuations will take the system to the absorbing states $m = \pm 1$.

5.2.2 Random networks

We analyze the phase diagram of the Symmetrical Threshold model in two random networks: Erdős-Rényi (ER) (44) and random regular (RR) (149) graphs with mean degree $\langle k \rangle = 8$. Figures 5.2a and 5.2b show the phase diagram for both networks, where it is shown that the existence of the three phases previously described is robust to changes in network structure. The main difference from the all-to-all scenario is that Phase III does not freeze exactly at the same initial magnetization. Instead, the system reaches an absorbing state with a higher magnetization $m_f > m_0$. In this phase, the value of m_f depends on the threshold such that increasing T, increases the disorder in the system, until $T = 1$, where $m_f = m_0$ (see Fig. 5.2c). On the other hand, phases I and II reach the same stationary state as in the mean-field case. Furthermore, the critical thresholds T_c and T_c^* show a different dependence on m_0 depending on the network structure.

To explain the transitions exhibited by the model, we use a theoretical framework for binary-state dynamics in complex networks (56): the Approximate Master Equation (AME), which considers agents in both states ± 1 with degree k, m neighbors in state -1 that have been j time steps in the current state (called "internal time" or "age") as different sets in a compartmental model (see details of the AME derivation in (3, 56)). In

general, the AME is:

$$\begin{aligned}
\frac{d}{dt}x^{\pm}_{k,m,0}(t) = & \quad -x^{\pm}_{k,m,0}(t) + \textstyle\sum_l T^{\mp}_{k,m,l}\, x^{\mp}_{k,m,l}(t) - (k-m)\,\beta^{\pm}\, x^{\pm}_{k,m,0}(t) - m\,\gamma^{\pm}\, x^{\pm}_{k,m,0}(t), \\
\frac{d}{dt}x^{\pm}_{k,m,j}(t) = & \quad -x^{\pm}_{k,m,j}(t) + A^{\pm}_{k,m,j}\, x^{\pm}_{k,m,j-1}(t) - (k-m)\,\beta^{\pm}\, x^{\pm}_{k,m,j}(t) \\
& \quad +(k-m+1)\,\beta^{\pm}\, x^{\pm}_{k,m-1,j-1}(t) \\
& \quad +(m+1)\,\gamma^{\pm}\, x^{\pm}_{k,m+1,j-1}(t) - m\,\gamma^{\pm}\, x^{\pm}_{k,m,j}(t),
\end{aligned} \tag{5.3}$$

where variables $x^{+}_{k,m,j}(t)$ and $x^{-}_{k,m,j}(t)$ are the fractions of k-degree nodes that are in state $+1$ (respectively, -1), have m neighbours in state -1, and have age j. The configuration-dependent rates $\beta^{\pm}$ account for the change of state of neighbors ($\pm$) of a node in state $+1$. The rates $\gamma^{\pm}$ are equivalent but for nodes in state -1. To build the AME, we need to assume that these rates are equal for all nodes in the same state, as in Ref (56):

$$\begin{aligned}
\beta^{+} &= \frac{\sum_j \sum_k p_k \sum_{m=0}^{k} (k-m)\, T^{+}_{k,m,j}\, x^{+}_{k,m,j}}{\sum_j \sum_k p_k \sum_{m=0}^{k} (k-m)\, x^{+}_{k,m,j}}, \\
\beta^{-} &= \frac{\sum_j \sum_k p_k \sum_{m=0}^{k} m\, T^{+}_{k,m,j}\, x^{+}_{k,m,j}}{\sum_j \sum_k p_k \sum_{m=0}^{k} m\, x^{+}_{k,m,j}}, \\
\gamma^{+} &= \frac{\sum_j \sum_k p_k \sum_{m=0}^{k} (k-m)\, T^{-}_{k,m,j}\, x^{-}_{k,m,j}}{\sum_j \sum_k p_k \sum_{m=0}^{k} (k-m)\, x^{-}_{k,m,j}}, \\
\gamma^{-} &= \frac{\sum_j \sum_k p_k \sum_{m=0}^{k} m\, T^{-}_{k,m,j}\, x^{-}_{k,m,j}}{\sum_j \sum_k p_k \sum_{m=0}^{k} m\, x^{-}_{k,m,j}},
\end{aligned} \tag{5.4}$$

where the degree distribution of the chosen network is p_k. Notice that these equations are written using a dimensionless time t. The transition rate $T^{\pm}_{k,m,j}$ is for the probability of changing state ($\pm \to \mp$) for an agent of degree k, m neighbors in state -1 and age j, while the aging rate $A^{\pm}_{k,m,j}$ is for the probability of staying in the same state and increasing the internal time ($j \to j+1$). For the Symmetrical Threshold model, according to the update rules these rates do not depend on internal time j (Markovian dynamics):

$$\begin{aligned}
T^{+}_{k,m,j} = \theta(m/k - T) \qquad T^{-}_{k,m,j} = \theta((k-m)/k - T), \\
A^{\pm}_{k,m,j} = 1 - T^{\pm}_{k,m,j}.
\end{aligned} \tag{5.5}$$

Therefore, if we were not concerned with the internal time dynamics, we can simplify our AME to the one proposed by J. P. Gleeson in Ref. (56) for general binary-state models. Here we keep the internal times for a dynamical characterization of the different phases and as a reference frame for the aging studies in the next section.

The Approximate Master Equation is based is based in the same basic assumptions used in Ref. (56): an uncorrelated network with negligible levels of clustering created using the configuration model (99) (using a degree distribution p_k). The approximation also neglects finite size effects, being only valid in the thermodynamic limit ($N \to \infty$). Notice that we cannot use the AME to describe the Complete graph. For the complex networks considered in this section, these conditions are satisfied for large N, and the differential equations can be solved numerically using standard methods (a general script in Julia is available in the author's GitHub repository (52)). The mixed order and ordered frozen transitions predicted (solid black lines in Figs. 5.2a and 5.2b, respectively) are in agreement with the numerical simulations. The predicted lines represent the initial and final values of T at which the AME reaches the ordered absorbing states $m_f = \pm 1$. In Fig. 5.2c, we also observe a good agreement between numerically integrated solutions

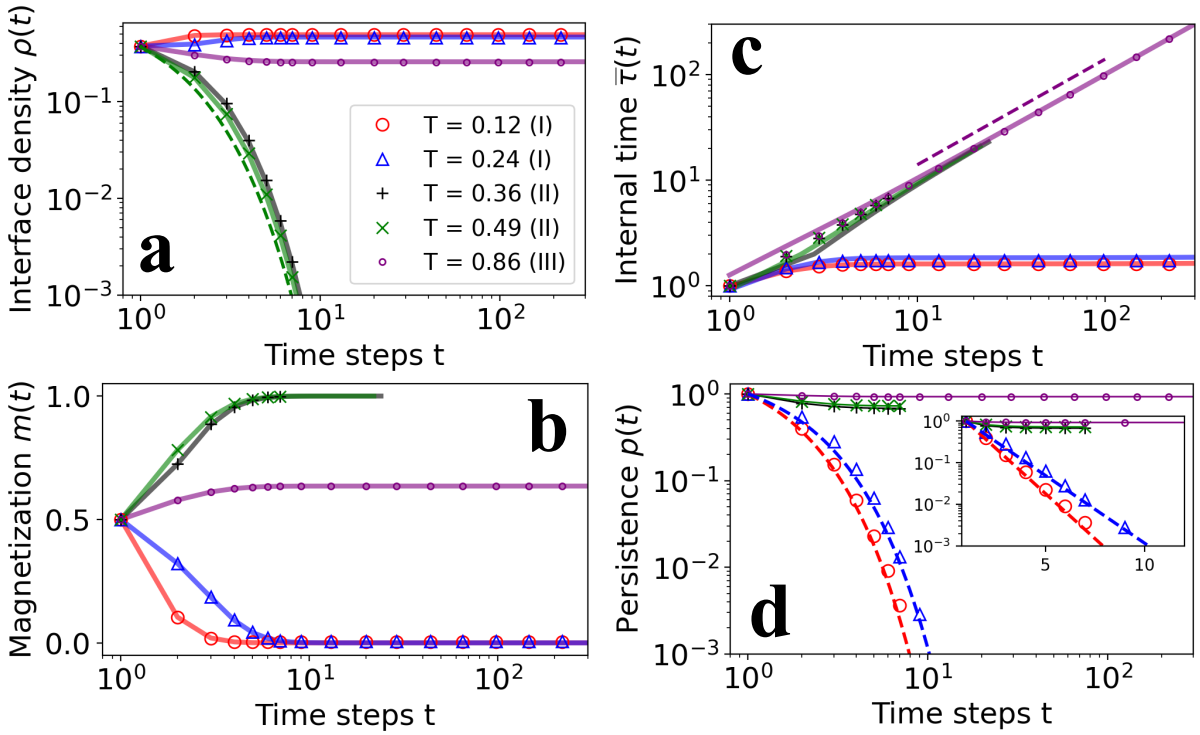

Figure 5.3: **Symmetrical Threshold model dynamics in random networks.** Evolution of the average interface density $\rho(t)$ (a), the average magnetization $m(t)$ (b), the mean internal time $\bar{\tau}(t)$ (c), and the persistence $p(t)$ (d) for the Symmetrical Threshold model. The average is computed over 5000 surviving trajectories (simulations stop when the system reaches the absorbing ordered states). Results for different values of T are plotted with diverse markers and colors: red ($T = 0.12$) and blue ($T = 0.24$) belong to Phase I, green ($T = 0.36$) and grey ($T = 0.49$) belong to Phase II and purple ($T = 0.86$) belongs to Phase III. Solid colored lines are the AME integrated solutions, using Eqs. (5.6)-(5.8). The initial magnetization is $m_0 = 0.5$. The system is on an ER graph with $N = 4 \cdot 10^4$ and mean degree $\langle k \rangle = 8$. The dashed green line in (a) shows $\rho(t) \sim \rho_0 e^{-t}$, the dashed purple line in (c) shows $\bar{\tau}(t) = t$ and the dashed lines in (d) show $p(t) \sim e^{-\alpha t}$, where $\alpha = 1$ (red) and $\alpha = 3/4$ (blue) We compute the relative difference, Δ, between the simulation and the integrated solution (until simulation ends): For all T, $\Delta_\rho < 5\%$, $\Delta_m < 1\%$ and $\Delta_{\bar{\tau}} < 5\%$ (except for $T = 0.86$ where $\Delta_{\bar{\tau}} = 11\%$).

(solid colored lines) and numerical simulations (markers), which is quantified via the relative difference Δ (see at figure captions).

An alternative simpler approximation is to consider a heterogeneous mean-field approximation (HMF) (refer to **??** for further details). This approximation is very useful when we work with networks with high clustering, close to the complete graph scenario ($\langle k \rangle / N \to 1$), a regime where the AME does not work properly because the clustering is not negligible. For our networks, HMF captures the qualitative behavior but the numerically integrated solutions do not agree with numerical simulations (see red dashed lines in Figs. 5.2a and 5.2b, and the colored dotted lines in Fig. 5.2c), and the frozen phase is not predicted by this framework. These findings demonstrate that threshold models (in networks far from $\langle k \rangle / N = 1$) need approximations beyond mean-field to achieve accuracy, in agreement with the findings in Refs. (3, 56, 57).

Beyond the stationary states, the previous phases can be characterized by their ordering dynamical regimes. To describe the coarsening process, we use the time-dependent average interface density $\rho(t)$ (fraction of links between nodes in different

states), the average magnetization $m(t)$, the mean internal time $\bar{\tau}(t)$ (mean time spent in the current state over all the nodes) and the persistence $p(t)$ (fraction of nodes that remain in their initial state at time t) (14). Fig. 5.3 shows the average results obtained from the numerical simulations, starting from an initial magnetization $m_0 = 0.5$. There are 3 regimes with different dynamical properties:

- **Mixed regime (Phase I):** It corresponds to Phase I in the static phase diagram and it is characterized by fast disordering dynamics, which is reflected by an exponential decay of the persistence. The interface density, the magnetization, and the mean internal time exhibit fast dynamics towards their asymptotic values in the dynamically active stationary state (see $T = 0.12, 0.24$ in Fig. 5.3);
- **Ordered regime (Phase II):** It coincides with Phase II in the static diagram and it is characterized by an exponential decay of the interface density. The magnetization tends to the ordered absorbing state based on the initial majority, and the mean internal time tends to scale as $\bar{\tau}(t) \sim t$. Persistence in this phase decays until a plateau that corresponds to the initial majority that reaches consensus (since this fraction of nodes does not change state from the initial condition). When consensus is reached, the surviving trajectory is stopped (see $T = 0.36, 0.49$ in Fig. 5.3);
- **Frozen regime (Phase III):** This regime corresponds to Phase III and it is characterized by an initial ordering process followed by the stop of the dynamics, with constant values of the metrics. The only exceptions are the mean internal time that grows as $\bar{\tau}(t) \sim t$ (see $T = 0.86$ in Fig. 5.3) and the persistence.

Using the numerically integrated solutions of AME ($x^{\pm}_{k,m,j}(t)$), we can compute the magnetization $m(t)$, the interface density $\rho(t)$, and the mean internal time $\bar{\tau}$:

$$\rho(t) = \frac{\sum_j \sum_k p_k \sum_m m x^{+}_{k,m,j}}{\frac{1}{2}\sum_j \sum_k p_k \sum_m k(x^{+}_{k,m,j} + x^{-}_{k,m,j})}, \tag{5.6}$$

$$\begin{aligned} m(t) &= 2\sum_j \sum_k p_k \sum_m x^{+}_{k,m,j} - 1 \\ &= -2\sum_j \sum_k p_k \sum_m x^{-}_{k,m,j} + 1, \end{aligned} \tag{5.7}$$

$$\bar{\tau}(t) = \sum_j \sum_k p_k \sum_m j \left(x^{+}_{k,m,j} + x^{-}_{k,m,j} \right). \tag{5.8}$$

All metrics exhibit a strong agreement between the numerical simulations and the integrated solutions (see solid lines in Fig. 5.3). However, the persistence cannot be directly calculated from the integrated solutions. This is because the fraction of persistent nodes at time t corresponds to the fraction of nodes with internal time $j = t$, which is at an extreme of the age distribution at each time step, since $x^{\pm}_{k,m,j}(t) = 0$ for $j > t$. Therefore, the computation of this measure requires a more sophisticated analysis using extreme value theory (68).

We note that the dynamical characterization discussed above holds for all possible m_0 except for the symmetric initial condition $m_0 = 0$. In this case, an order-disorder transition arises at a critical mean degree k_c, whose value depends on the size of the system N (115).

5.3 Symmetrical Threshold model in a Moore Lattice

We consider next the Symmetrical Threshold model in a Moore lattice, which is a regular 2-dimensional lattice with interactions among nearest and next-nearest neighbors ($k = 8$). From numerical simulations, we obtain a phase diagram (Fig. 5.5a) that is consistent with our previous results in random networks. The system undergoes a mixed-ordered

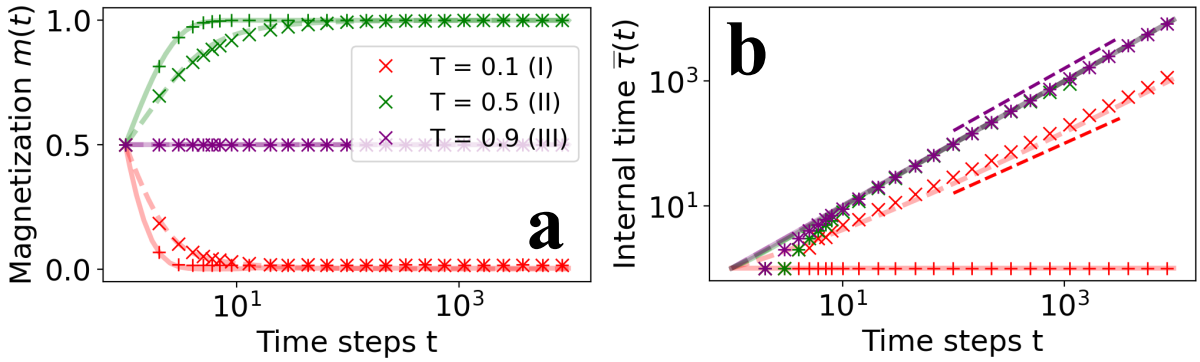

Figure 5.4: **Aging effects in the complete graph.** Evolution of the average magnetization $m(t)$ (a) and the mean internal time $\bar{\tau}(t)$ (b) in a complete graph of $N = 2500$ nodes. Results are shown for the Symmetrical Threshold Model (pluses) and the version with aging (crosses) obtained from simulations. Different colors correspond to different values of the threshold T: red ($T = 0.1$) belongs to Phase I, green ($T = 0.5$) belongs to Phase II, and purple ($T = 0.9$) to Phase III. The initial magnetization is fixed at $m_0 = 0.5$. The solid and dashed lines correspond to the numerically integrated solutions from Eq. 6.3 for the original model ($p_A(j) = 1$) and the version with aging ($p_A(j) = 1/(t+2)$), respectively. The dashed lines in (b) show $\bar{\tau}(t) = t$ (purple) and the solution from the recursive relation in Eq. (**??**) (red). As computed in Fig. 5.3, for the non-aging version, $\Delta_m, \Delta_{\bar{\tau}} < 4\%$ (except for $T = 0.86$ where $\Delta_{\bar{\tau}} = 10\%$) and for the aging version, $\Delta_m^a, \Delta_{\bar{\tau}}^a < 9\%$ (except for $T = 0.86$ where $\Delta_{\bar{\tau}}^a = 15\%$).

transition at a threshold value $T_c = 2/8$ which is independent of the value of the initial magnetization m_0. When $T > 4/8$, the system undergoes an ordered-frozen transition at a critical threshold T_c^*, which depends on m_0 (similarly to what happens in random networks). The final magnetization $m_f(m_0)$ (Fig. 5.5b) also shows a dependence on m_0 similar to the one found in RR networks (Fig. 5.2c).

5.3.1 Original model without aging

Fig. 5.6 shows the results from numerical simulations (for $m_0 = 0$ and 0.5) for the average interface density, the magnetization, and the persistence (the internal time shows the same results as in random graphs). Dynamical properties change significantly for different values of the threshold and initial magnetization m_0. Similarly to the case of random networks, we find three different regimes corresponding to the three phases, but with some properties different from the results on random networks:

- **Mixed regime (Phase I):** It is characterized by fast disordering dynamics with a persistence decay $p(t) \sim \exp(-\ln(t)^2)$, consistent with the results of the Voter model (14). The interface density and the magnetization exhibit fast dynamics towards their asymptotic values in the dynamically active stationary state (see $T = 1/8, 2/8$ in Fig. 5.6);
- **Ordered regime (Phase II):** It is characterized by an exponential or power-law decay of the interface density, depending on the initial condition (see details below). The magnetization tends to the absorbing ordered state (see $T = 3/8, 4/8$ in Fig. 5.6);
- **Frozen regime (Phase III):** It is characterized by an initial ordering process, but the system freezes fast (see $T = 5/8$ in Fig. 5.6).

In particular, in Phase II for $m_0 = 0$ the persistence and interface density decay are found to decay as a power law, $p(t) \sim t^{-0.22}$ and $\rho(t) \sim t^{-1/2}$, respectively (consistent with the results of the Ising model (35, 36, 37, 137)). For a biased initial condition ($m_0 = 0.5$),

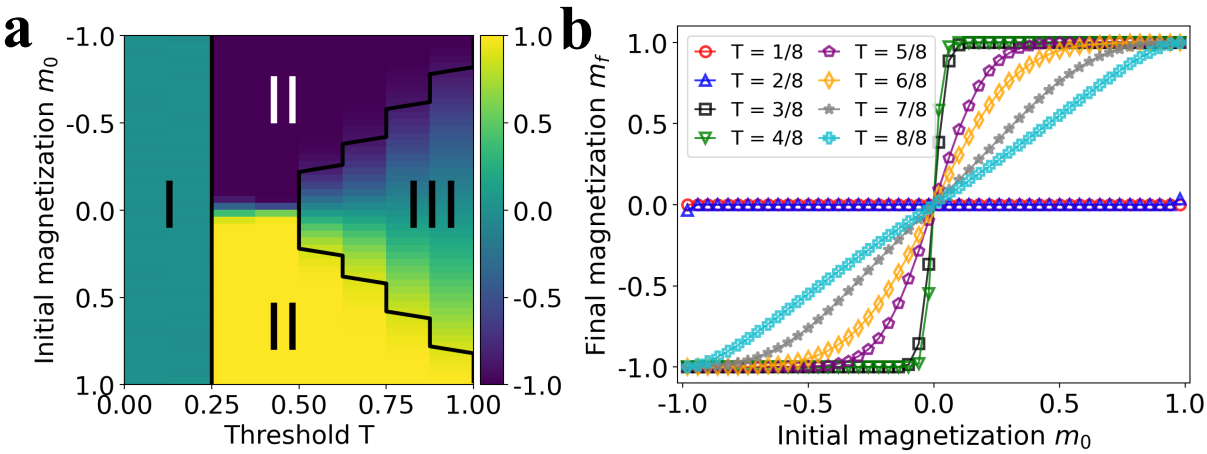

Figure 5.5: **Symmetrical Threshold model in a Moore lattice.** (a) Phase diagram of the Symmetrical Threshold model in a Moore lattice of size $N = L \times L$, with $L = 100$. The color map indicates the value of the average final magnetization m_f. Solid black lines are the borders of Phase II (first and last value of T where the system reaches the absorbing ordered state for each m_0), computed from the numerical simulations. (b) Average final magnetization m_f as a function of the initial magnetization m_0 for the discrete values of the threshold T (indicated with different colors and markers) in a Moore lattice of the same size. Average performed over 5000 realizations.

$p(t)$ decays to the initial majority fraction (which corresponds to the state reaching consensus), and $\rho(t)$ follows an exponential-like decay. Note that, for $m_0 = 0$, not all trajectories reach the ordered absorbing states ($m_f = \pm 1$). There exist other absorbing configurations as, for example, a flat interface configuration for $T = 4/8$, no agent will be able to change, and the system remains trapped in this state. This result is not observed for $m_0 > 0$.

Contrary, phases I and III show similar dynamics for balanced ($m_0 = 0$) and unbalanced ($m_0 = 0.5$) initial conditions. In Phase I, the system shows disordering dynamics with a persistence decay similar to the one exhibited for the Voter model in a lattice (14) while in Phase III, the system exhibited freezing dynamics with an initial tendency towards the majority consensus.

Due to the lattice structure and high clustering, the mathematical tools employed in the previous sections for random networks are inapplicable to regular lattices. Consequently, we limit ourselves to the results of numerical simulations. On the other hand, a regular structure facilitates easy modification of the geometry structure of the initial condition. **??** presents an analysis of how a compact initial condition influences the dynamics of the Symmetrical Threshold model (and its variant with aging).

5.4 Summary and conclusions

In this work, we have studied with Monte Carlo numerical simulations and analytical calculations the Symmetrical Threshold Model. In this model, the agents, nodes of a contact network, can be in one of the two symmetric states ± 1. System dynamics follows a complex contagion process in which a node changes state when the fraction of neighboring nodes in the opposite state is above a given threshold T. For $T = 1/2$, the model reduces to a majority rule or the zero temperature Spin Flip Kinetic Ising Model. When the change of state is only possible in one direction, say from 1 to -1, it reduces to the Granovetter-Watts Threshold model (3, 62, 147). We have considered the cases of a fully connected network, Erdős-Rényi, and random regular networks, as well as a

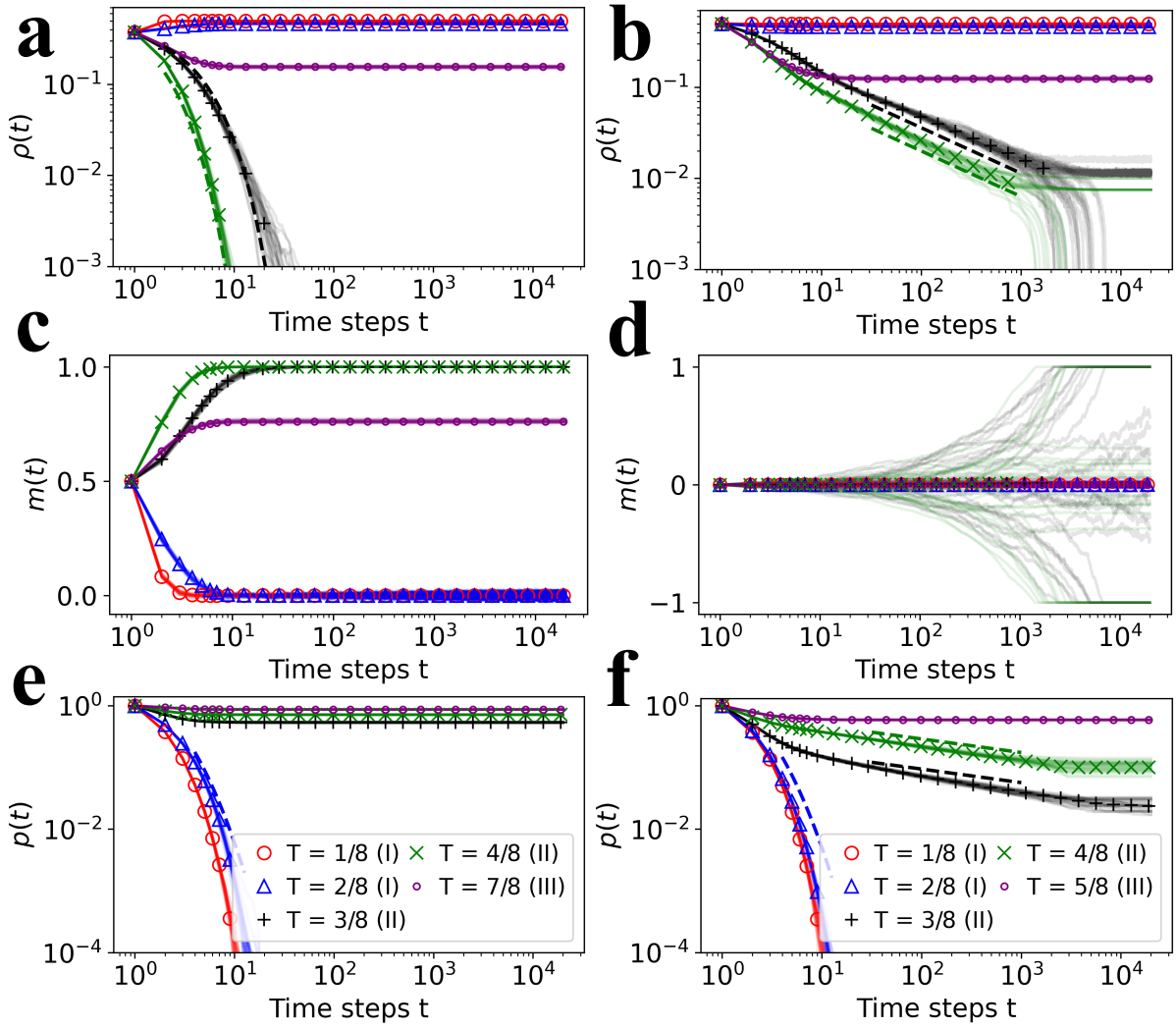

Figure 5.6: **Dynamical regimes in a Moore lattice.** Evolution of the average interface density $\rho(t)$ (a-b), the average magnetization $m(t)$ (c-d), and the persistence $p(t)$ (e-f) for the Symmetrical model in a Moore lattice starting from a random configuration with $m_0 = 0.5$ (a-c-e) and $m_0 = 0$ (b-d-f). We plot 50 different trajectories in solid lines and the average of 5000 surviving trajectories (simulations stop when the system reaches the absorbing ordered states) in different markers. Different colors and markers indicate different threshold values: red ($T = 1/8$) and blue ($T = 2/8$) belong to Phase I, green ($T = 3/8$) and black ($T = 4/8$), and purple ($T = 5/8, 7/8$) belong to Phase III. The average magnetization $m(t)$ is computed according to the two symmetric absorbing states. System size is fixed at $N = L \times L$, $L = 200$. The dashed lines in (a) are $\rho \sim \exp(-\alpha \cdot t)$ with $\alpha = 0.5$ (black) and $\alpha = 0.8$ (green), in (b) are $\rho(t) \sim at^{-1/2}$ with $a = 0.36$ (black) and $a = 0.2$ (green), in (e-f) is $p(t) \sim \exp(-\ln(t)^2)$ (blue).

regular two-dimensional Moore lattice.

We have found that, in the parameter space of threshold T and initial magnetization m_0, the model exhibits three distinct phases, namely Phase I or mixed, Phase II or ordered, and Phase III or frozen. The existence of these three phases is robust for different network structures. These phases are well characterized by the final state (m_f), and by dynamical properties such as the interface density $\rho(t)$, time-dependent average magnetization $m(t)$, persistence times $p(t)$, and mean internal time $\bar{\tau}(t)$. These phases can be obtained analytically in the mean-field case of a fully connected network. For the random networks considered, we derive an approximate master equation (AME) (3, 56) considering agents in each state according to their degree k, neighbors in state -1, m, and age j. From this AME, we have also derived a heterogeneous mean-field (HMF) approximation. While the AME reproduces with great accuracy the results of Monte Carlo numerical simulations of the model (both static and dynamic), the HMF shows an important lack of agreement, highlighting the importance of high-accuracy methods necessary for threshold models.

Aging is incorporated in the model as a decreasing probability to modify the state as the time already spent by the agent in that state increases. The key finding is that the mixed phase (Phase I), characterized by an asymptotically disordered dynamically active state, does not always exist: the aging mechanism can drive the system to an asymptotic absorbing ordered state, regardless of how low the threshold T is set. A similar effect of aging was already described for the Schelling model in Ref. (2). When the dynamics are examined in detail, a new Phase I*, defined in terms of dynamical properties, emerges in the domain of parameters where the model without aging displays Phase I. This phase is characterized by an initial disordering regime ($m \to 0$) followed by a slow ordering dynamics, driving the system toward the ordered absorbing states (including the one with spins opposite to the majoritarian initial option). This result is counter-intuitive since aging incorporates memory into the system, yet in this phase, the system "forgets" its initial state. The network structure plays an important role in the emergence of Phase I* since it does not exist for complete graphs. A detailed analysis reveals that Phase I* replaces Phase I only for sparse networks, including the case of the Moore lattice. For ER networks we find that, as the mean degree increases, Phase I reappears and there is a range of values of the mean degree for which phases I and I* coexist. Beyond a critical value of the mean degree, Phase I extends over the entire domain of parameters where Phase I* was observed.

While aging favors reaching an asymptotic absorbing ordered state for low values of T (Phase I), in Phase II the ordering dynamics are slowed down by aging, changing, both in random networks and in the Moore lattice, the exponential decay of the interface density by a power law decay with the same exponent. The aging mechanism is found not to be important in the frozen Phase III. All these effects of aging in the three phases are well reproduced for random networks by the AME derived in this work, which is general for any chosen activation probability $p_A(j)$.

For the Moore lattice, we have also considered in detail the special case of the initial condition $m_0 = 0$. In this case, Phase I* emerges, and Phase III is robust against aging effects. However, in Phase II aging destroys the characteristic power law decay of the interface density, $\rho(t) \sim at^{-1/2}$, associated with curvature reduction of domain walls. This would be a main effect of aging in the dynamics of the phase transition for the zero temperature spin flip Kinetic Ising model (67). Additionally, this regular structure allowed us to analyze the effects of a compact initial condition. We have shown that the joint effect of aging and a compact initial condition prevent the ordered phases from reaching the consensus state (see **??**).

As a final remark on the general effects of aging in different models of collective behavior, we note that the replacement of a dynamically active disordered stationary phase by a dynamically ordering phase is generic. In this paper, we find the replacement of Phase I by Phase I*. Likewise in the Voter model, aging destroys long-lived dynamically active states characterized by a constant value of the average interface density, and it gives rise to coarsening dynamics with a power law decay of the average interface density (45). In the same way, in the Schelling segregation model, a dynamically active mixed phase is replaced, due to the aging effect, by an ordering phase with segregation in two main clusters. Another aging effect that seems generic, in phases in which the system orders when there is no aging, is the replacement of dynamical exponential laws by power laws. This is what happens here in Phase II for the decay of the average interface density but, likewise, exponential cascades in the Granovetter-Watts model are replaced due to aging by a power-law growth with the same exponent (3).

Further research with the general AME used in this study would involve a new approach that considers the master equation, as described in Ref. (108). This approach aims to incorporate finite size effects, which are relevant when m_0 is close to zero, and would provide a mathematical framework for further analyisis of the results in Ref. (115). Regarding the model, this article reports the main features of the Symmetrical Threshold model dynamics and the aging effects. However, there are several areas for future research along this lines, such as investigating the impact of strongly heterogeneous (11) or coevolving networks (143, 154), exploring the dependence of the results on the aging activation function p_A, and examining the joint effect of aging and strongly heterogeneous degree distributions.

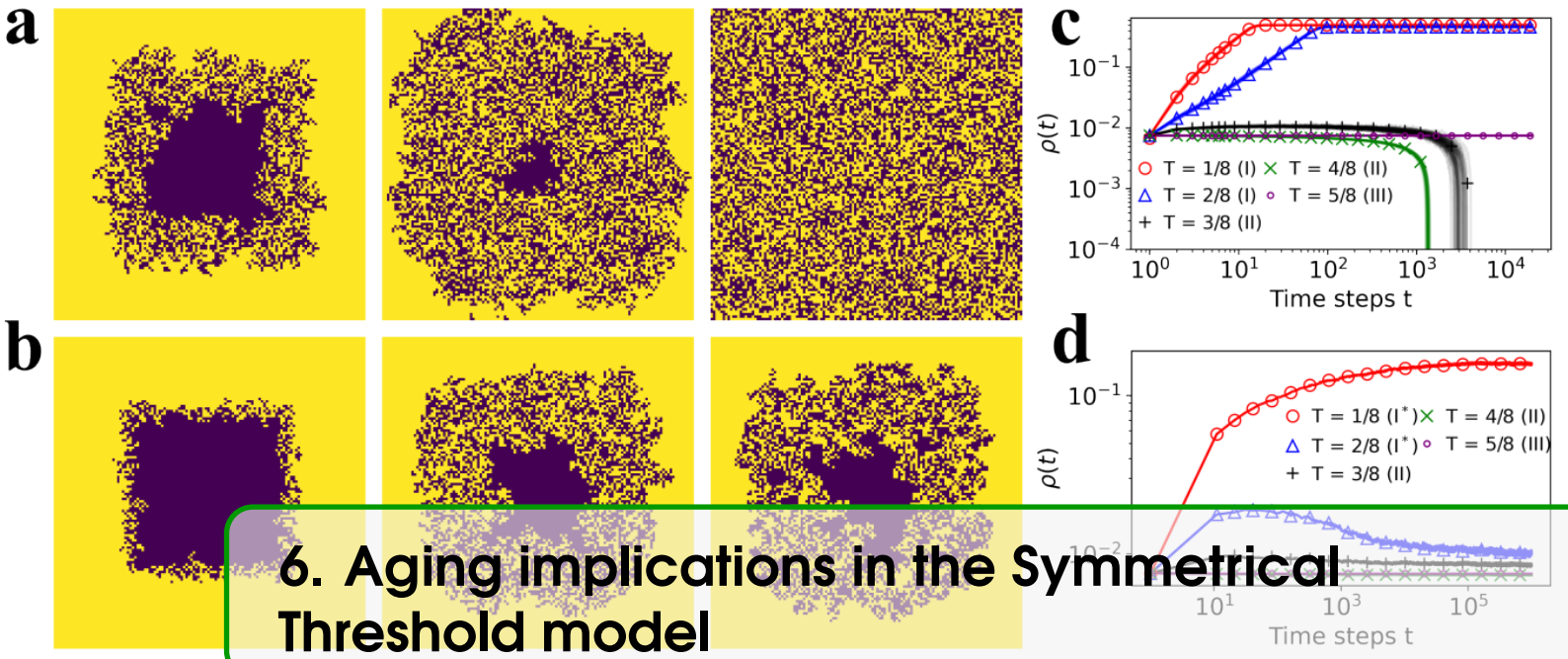

6. Aging implications in the Symmetrical Threshold model

6.1 Introduction

Aging is an important non-Markovian effect in binary-state models that has significant implications. It describes how the persistence time of an agent in a particular state influences the transition rate to a different state (18, 26, 45, 114, 134). As such, the longer an agent remains in the current state, the smaller the probability of changing. Aging has been shown to cause coarsening dynamics towards a consensus state in the Voter model (45, 111), to induce bona fide continuous phase transitions in the noisy Voter model (9, 110), modify the phase diagram and non-equilibrium dynamics of the Schelling segregation model (2), and to modify non-trivially the cascade dynamics of the threshold model (3). The introduction of aging is motivated by strong empirical evidence that human interactions do not occur at a constant rate and cannot be described using a Markovian assumption. Empirical studies have reported heavy-tail inter-event time distributions that reflect heterogeneous temporal activity patterns in social interactions (8, 83, 87, 120, 153).

In this work, we present a comprehensive analysis of the Symmetrical Threshold model, including its full phase diagram, and we investigate the effects of aging in the model. The model is examined in various network topologies, such as the complete graph, Erdős-Rényi (ER) (44), random regular (RR) (149), and a two-dimensional Moore lattice. The possible phases of the system are defined by the final stationary state as well as by the ordering/disordering dynamics characterized by the time-dependent magnetization, interface density, persistence, and mean internal time. For both the original model and the aging variant, the results of Monte Carlo numerical simulations are compared with results from the theoretical framework provided by an Approximate Master Equation (AME)(3, 56) which is general for any random network. We also derive a mean-field analysis to describe the outcomes in a complete graph.

6.2 Symmetrical Threshold model with aging

Aging refers to the property of agents becoming less likely to change their state the longer they have remained in that state (2, 3, 8, 9, 26, 110, 111, 134). In contrast to the original model, which assumes that agents update their state at a constant rate, this model introduces an activation function $p_A(j)$ that is inversely proportional to the agent's internal time j. At each time step, the following two steps are performed:

1. A node i with age j is selected at random and activated with probability $p_A(j)$;
2. If the fraction of neighbors in a different state is greater than the threshold T, the activated node changes its state from s_i to $-s_i$ and resets its internal time to $j=0$.

Following previous literature on aging effects (2, 3, 9, 45, 109) we make the choice of $p_A(j) = 1/(j+2)$ for the aging probability. This particular choice is motivated by the fact that it allows to reproduce inter-event time distributions observed empirically (8, 120).

6.2.1 Mean-field

Figure 5.4 compares the evolution of the average magnetization and mean internal time on a complete graph of the original Symmetrical Threshold model and the version with aging in phases I, II, and III. We observe that, for all considered threshold values, aging introduces a delay. However, the final stationary state coincides with the one observed for the original model. To explain these dynamics, we use a heterogeneous mean-field approach that considers the effects of aging (HMFA), as in Ref. (26) for other binary-state models (we use a general HMF description to be applied for a complete graph and to random networks in next section). In this case, the AME does not work well due to the high density of the network. For a general network with degree distribution p_k, we define the fraction of agents in state ± 1 with k neighbors and age j at time t as $x^{\pm}_{k,j}(t)$. The probability of finding a neighbor in state ± 1 is $\tilde{x}^{\pm}$, which can be written as

$$\tilde{x}^{\pm} = \sum_k p_k \frac{k}{\langle k \rangle} \sum_{j=0}^{\infty} x^{\pm}_{k,j}, \tag{6.1}$$

where $\langle k \rangle$ is the mean degree of the network. The transition rate $\omega^{\pm}_{k,j}$ for a node with state ± 1, degree k and age j to change state is given by

$$\omega^{\pm}_{k,j} = p_A(j) \sum_{m=0}^{k} \theta\left(\frac{m}{k} - T\right) B_{k,m}[\tilde{x}^{\mp}], \tag{6.2}$$

where $B_{k,m}[x]$ is the binomial distribution with k attempts, m successes, and with the probability of success x. In our model, there are two possible events for a node with degree k and age j:

- It changes state and the age is reset to $j=0$;
- It remains at its state and the age increases by one time step $j = j+1$.

According to these possible events, we can write the rate equations for the variables $x^{\pm}_{k,j}$ and $x^{\pm}_{k,0}$ as

$$\begin{aligned} \frac{dx^{\pm}_{k,0}}{dt} &= \textstyle\sum_{j=0}^{\infty} x^{\mp}_{k,j}\, \omega^{\mp}_{k,j} - x^{\pm}_{k,0}, \\ \frac{dx^{\pm}_{k,j}}{dt} &= x^{\pm}_{k,j-1}\,(1-\omega^{\pm}_{k,j-1}) - x^{\pm}_{k,j} \qquad j>0. \end{aligned} \tag{6.3}$$

It can be shown from Eq. (6.3) that the stationary solution for the fraction of agents in state $+1$, x_f, obeys the following implicit equation for a complete graph (see **??** for a detailed explanation):

$$x_f = \frac{F(1-x_f)}{F(x_f)+F(1-x_f)}, \tag{6.4}$$

where,

$$F(x) = 1 + \sum_{j=1}^{\infty} \prod_{a=0}^{j-1} \left(1 - p_A(a) \sum_{m=(N-1)T}^{N-1} B_{N-1,m}[x]\right). \tag{6.5}$$

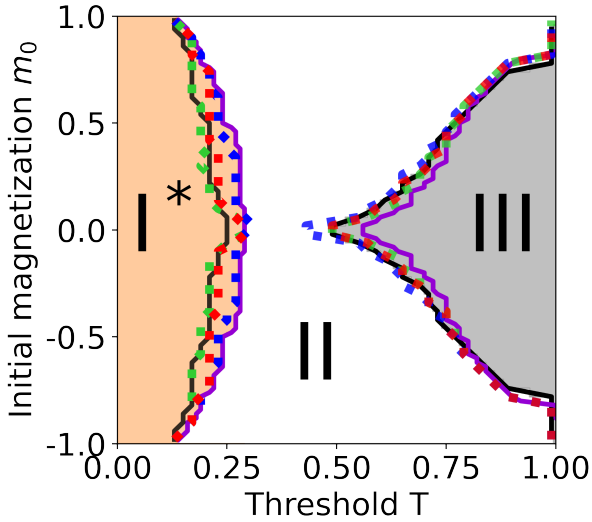

Figure 6.1: **Phase diagram modified by aging.** Phase diagram of the Symmetrical Threshold with aging model in an ER graph of $N = 4 \cdot 10^4$ nodes and $\langle k \rangle = 8$. The blue, red, and green dotted lines show the borders of Phase II (first and last value of T where the system reaches the absorbing ordered state for each m_0) computed from numerical simulations evolving until $t_{\max} = 10^3$, 10^4 and 10^5 time steps, respectively. Black solid lines show AME solution integrated 10^5 time steps. Phase I*, II and III correspond with the orange, white and gray areas, respectively. The solid purple lines are the mixed-ordered and ordered-frozen critical lines for the non-aging version of the model.

A solution of Eq. (6.4) can be obtained numerically using standard methods, as in Ref. (26). The final magnetization is calculated as $m_f = 2x_f - 1$. With this method, we obtain that the phase diagram for the model with aging is the same as for the original model (refer to Fig. 5.1a). As a technical point, we note that a truncation of the summation of the variable j in Eq. (6.5) is required for the numerical resolution of the implicit equation. The higher the maximum age considered $j_{\max}$, the higher the accuracy. With $j_{\max} = 5 \cdot 10^4$, the transition lines predicted by this mean-field approach show great accuracy. Moreover, by numerically integrating Eqs. (6.3), the dynamical evolution of the magnetization and mean internal time can be obtained. Fig. 5.4 shows the agreement between integrated solutions and Monte Carlo simulations of the system both for the aging and non-aging versions. It should be noted that, while aging introduces only a dynamical delay for the magnetization $m(t)$, the mean internal time $\bar{\tau}(t)$ in Phase I shows a different dynamical behavior with aging than in the original model. In this phase, due to the low value of T, the agents selected randomly will change their state (as they fulfill the threshold condition) and reset their internal time. Consequently, while the internal time fluctuates around a stationary value for the original model, when aging is incorporated, due to the activation probability $p_A(j)$ chosen, the mean internal time increases following a recursive relation (Eq. (**??**)). We refer to **??** for a derivation of this result.

6.2.2 Random networks

In contrast to the results obtained in a complete graph, aging effects have a significant impact on the phase diagram of the model on random networks. In Fig. 6.1, we show the borders of Phase II (first and last value of T where the system reaches the absorbing ordered state for each m_0) obtained from Monte Carlo simulations running up to a maximum time $t_{\max}$ (dotted colored lines). Reaching the stationary state in this model

requires a large number of steps (with a corresponding high computational cost). The two borders of Phase II exhibit different behavior as we increase the time cutoff $t_{\max}$: while the ordered-frozen border does not change with different $t_{\max}$, the mixed-ordered border is shifted to lower values of T as we increase the time cutoff $t_{\max}$. Our results suggest that Phase I is actually replaced in a good part of the phase diagram by an ordered phase in which the absorbing state $m_f = \pm 1$ is reached after a large number of time steps. Similar results are found for a RR graph (see **??**). The dependence of the results with $t_{\max}$ calls for a characterization of different phases in terms of dynamical properties rather than by the asymptotic value of the magnetization.

Figure 6.2 shows the time evolution of our ordering metrics. The dynamical properties are largely affected by the aging mechanism. In terms of the evolution, we find the following regimes:

- **Initial mixing regime (Phase I^*):** It is characterized by two dynamical transient regimes: a fast initial disordering dynamics followed by a slow ordering process. After the initial fast disordering stage, the average interface density exhibits a very slow (logarithmic-like) decay. Later, due to the finite size of the system, the average interface density follows a power law decay with time, where $\rho(t)$ scales as t^{-1}. This phase exists for the same domain of parameters (m_0, T) as Phase I (orange region in Fig. 6.1) in the model without aging (see $T = 0.12, 0.24$ in Fig. 6.2);
- **Ordered regime (Phase II):** According to the initial majority, the magnetization tends to the ordered absorbing state. This regime is characterized by a power-law interface decay, where $\rho(t)$ scales as t^{-1}. (see $T = 0.36, 0.49$ in Fig. 6.2);
- **Frozen regime (Phase III):** Each individual realization is characterized by an initial tendency towards the majority consensus, but very fast reaches an absorbing frozen configuration (see $T = 0.86$ in Fig. 6.2).

The main effect of aging is that the mixed states of Phase I are no longer present, at least not for the type of networks that we are analyzing here. We will show later that Phase I reemerges in denser graphs. Instead, for sparse graphs, we observe a new Phase I^* in which the system initially disorders and later orders until reaching the absorbing states $m_f = \pm 1$. This behavior is shown in Fig. 6.2 for $T = 0.12$ and 0.26. For $T = 0.12$, the system initially disorders, and then the interface density follows a logarithmic-like decay (see inset in Fig. 6.2a). Due to the slow decay, the system stays in this transient regime even after 10^6 time steps, and the fall to the absorbing states is not observed in this figure. Similarly, for $T = 0.26$ the disordering process stops and then the system gradually evolves towards a fully ordered state. For this value of T, the logarithmic-like decay is not appreciated and we just observe the power-law decay due to the finite size of the system. The difference between $T = 0.12$ and $T = 0.26$ comes from the fact that in this Phase I^*, the interface decay becomes faster as we increase the threshold T (see Fig. 6.3(a-c)). Notice the different interface decay in Fig. 6.3c (inset) between values of $T < 0.3$ (Phase I^*), where all trajectories show a logarithmic-like decay of $\rho(t)$ in a transient regime, and $T \geq 0.3$ (Phase II), where trajectories from the initial condition exhibit fast ordering dynamics towards the majority consensus. Moreover, we observe that in Phase I^*, the initial magnetization m_0 introduces a bias to the stochastic process, implying that the larger m_0 in absolute value, the larger the number of realizations that reach the absorbing state with the same sign of m_0. However, the system can still reach the absorbing state of the opposite sign of m_0 (initial minority), as shown in the trajectories with $T = 0.25$ in Fig. 6.3a. Due to the characteristic logarithmic decay of Phase I^*, a statistical analysis of the inversion process incurs a significant computational cost. In Fig. 6.3b, we present the final magnetization histogram for $T = 0.25$, a value proximal to the $\mathrm{I}^* - \mathrm{II}$ boundary where this analysis is computationally feasible. As depicted in this figure,

the proportion of realizations in which consensus is reached in the initial minority state is approximately 3.3%.

In Phase II, the system asymptotically orders for any initial condition as in the original model, but the dynamical properties are modified due to the presence of aging: the exponential decay of the interface density is replaced by a slow power-law decay, where the exponents of the exponential and the power-law are found to be similar. Contrary, the dynamical properties of Phase III are not affected by the presence of aging. The temporal magnitudes analysis (mean internal time and persistence) can be found in **??**.

As it occurred for the non-aging version of the model, the dynamical characterization discussed above holds for all possible m_0 except for the symmetric initial condition $m_0 = 0$. The implications of the order-disorder transition (that occurs at a critical mean degree $k_c(N)$) (115) are still present in the model with aging.

To account for the results of our Monte Carlo simulations, we use the same mathematical framework as described in Equation (5.3). According to the update rules of the Symmetrical Threshold Model with aging, the transition probabilities now depend on the age j, as given by the activation probability $p_A(j)$:

$$T^{+}_{k,m,j} = p_A(j)\,\theta(m/k - T) \qquad T^{-}_{k,m,j} = p_A(j)\,\theta((k-m)/k - T),$$
$$A^{\pm}_{k,m,j} = 1 - T^{\pm}_{k,m,j}. \tag{6.6}$$

We show in Figure 6.1 the mixed-ordered and ordered-frozen transition lines predicted by the integration of the AME equations until a time cutoff $t_{\max}$. We find good agreement between the theoretical predictions and the simulations both for ER and RR networks (see RR results in **??**). Regarding dynamical properties, the AME integrated solutions exhibit a remarkable concordance with the evolution of all the metrics as shown in Figure 6.2. Minor discrepancies between the numerical simulations and the integrated solutions are attributed to the different assumptions, discussed previously, on which the AME is based.

The numerical results discussed so far are for random networks with average degree $\langle k \rangle = 8$. According to them and to the analytical insights, one can conclude that aging significantly changes the phase diagram for sparse networks. However, we know that the model with aging shows the same phase diagram as the model without aging for a fully connected network. This implies that, for ER graphs, as the mean degree $\langle k \rangle$ approaches N, Phase I^* must disappear. Therefore, the combined effects of increasing the mean degree and introducing aging need to be investigated in more detail. Phase II is distinguishable from phases I and I^* because the system initially orders, i.e., $|\rho_0 - \rho_{\max}| = 0$, where $\rho_{\max}$ is the maximum value attained by the interface density during the dynamical evolution. In contrast, Phase I is distinguished from Phases I^* and II because the system remains disordered, i.e., $|\rho_{\max} - \rho(t_{\max})| \approx 0$. Thus, Phase I^* is the only phase among these three where $|\rho_0 - \rho_{\max}| > 0$ and $|\rho_{\max} - \rho(t_{\max})| > 0$. Using this criterion, we studied the dependence of the critical threshold T_c on the mean network degree defining the transition lines between phases I, I^*, and II (see Fig. 6.4). In the absence of aging, the red line in Fig. 6.4 gives the value of the mixed-ordered transition line T_c. When aging is included, at low degree values, Phase I is replaced by I^*, as expected. However, as the mean degree increases, Phase I emerges despite the presence of aging, leading to the coexistence of phases I and I^* in the same phase diagram over a range of mean degree values. As the mean degree is further increased, a critical value is reached where Phase I^* is no longer present, and the discontinuous transition I-II occurs at the same value than in the model without aging. Importantly, this critical mean degree at which Phase I^* disappears, depends significantly on the initial magnetization m_0.

6.3 Symmetrical Threshold model in a Moore Lattice

6.3.1 The role of aging

We show in Figure 6.5a the borders of Phase II obtained from numerical simulations running up to a time $t_{\max}$ (dotted colored lines). Similarly to the behavior observed in random networks, the mixed-ordered border is shifted to lower values of T as we increase the simulation time cutoff $t_{\max}$. Thus, Phase I is replaced by an ordered phase due to the aging mechanism. Examining the dependence of the final value of the magnetization on its initial condition $m_f(m_0)$ (Figure 6.5b), one can conclude that the mixed phase is still present, at least transiently, as in the initial disordering phase described in the previous section (Phase I^*). Phase II is again characterized by an asymptotically ordered state where the initial majority reaches consensus. However, for this specific structure, near $m_0 = 0$ and $T = 1/2$, the ordered state is not reached for any threshold value. Furthermore, comparing with Fig. 6.5b with the results from the model without aging (Fig. 5.5b), the discontinuous jump at $m_0 = 0$ for $T = 3/8, 4/8$ is replaced by a continuous transition, where a range of states with $0 < |m_f| < 1$ are present around $m_0 = 0$. To determine whether these states belong to Phase I^*, II or III, we need again a characterization of phases in terms of dynamical properties. According to the results in Figure 6.6, we find here the same regimes identified for random networks:

- **Initial mixing regime (Phase I^*):** After the initial disordering stage, the average interface density shows a very slow decay reflecting the slow growth of spatial domains in each binary state. The persistence in this phase shows a power-law decay $p(t) \sim t^{-1}$ (see $T = 1/8, 2/8$ in Fig. 6.6);
- **Ordered regime (Phase II):** It is characterized by coarsening dynamics that end in the absorbing states $m_f = \pm 1$. The form of the decay of the interface density depends on the value of m_0 (see $T = 3/8, 4/8$ in Fig. 6.6);
- **Frozen regime (Phase III):** It is characterized by an initial tendency to order but the system very fast reaches an absorbing frozen configuration (see $T = 5/8, 7/8$ in Fig. 6.6).

The implications of aging become explicit by comparing the dynamical properties of the cases with aging (Figure 6.6) and without aging (Figure 5.6). When the threshold is $T < 3/8$, Phase I is replaced by Phase I^* in which there is an initial disordering process very fast followed by a slow coarsening process that accelerates when we increase the threshold. Although the aging implications in this phase are similar to those observed in the ER graph, the coarsening process is slower (see insets in Fig. 6.6a-b).

In Phase II ($T = 3/8, 4/8$) and when $m_0 = 0.5$, the system exhibits coarsening towards the ordered state $m_f = \pm 1$. In this case, the interface decay $\rho \sim \exp(-\alpha t)$, observed in the absence of aging is replaced, due to aging, by a power law decay $\rho \sim t^{-\alpha}$, as noted in Ref. (3). We find $\alpha = 0.5$ and 0.8 for $T = 3/8$ and $4/8$, respectively. For $m_0 = 0$, the power law decay of the interface density vanishes with aging, and the system exhibits coarsening dynamics much slower than for an unbalanced initial condition. In this region of the phase diagram, spatial clusters start to grow from the initial condition, but once formed, it takes a long time for the system to reach the absorbing state $m_f = \pm 1$. We note that for these parameter values, the system is not able to reach $|m|$ over 0.1 even after 10^6 time steps, but since there is coarsening from the initial condition, the expected stationary state as $t \to \infty$ is $m_f = \pm 1$. There is neither initial disordering nor freezing, these values correspond to the defined Phase II, even though the system exhibits "long-lived segregation" long transient dynamics (see the difference with the dynamics of the model without aging in Fig. 6.7). In Fig. 6.5a, we differentiate Phase II from Phase III by analyzing the activity in the system: If agents are changing, even though the interface

decay is slow, the system is in Phase II. If agents are frozen, it lies in Phase III. When comparing the ordered-frozen critical line to the one from the original model (purple line), we notice that aging causes certain values (m_0, T) that were previously in Phase II near the critical line to enter the frozen phase.

Finally, it should be noted that in Phase I^*, the initial disordering dynamics drive the system towards $m = 0$. Therefore, the subsequent coarsening dynamics follow the slow interface decay observed in Phase II for $m_0 \sim 0$. Thus, the presence of aging implies that the system asymptotically orders for any initial condition, but due to the initial disordering, the coarsening dynamics fall into the "long-lived segregation" regime independently of the initial condition.

6.4 Summary and conclusions

In this work, we have studied with Monte Carlo numerical simulations and analytical calculations the Symmetrical Threshold Model. In this model, the agents, nodes of a contact network, can be in one of the two symmetric states ± 1. System dynamics follows a complex contagion process in which a node changes state when the fraction of neighboring nodes in the opposite state is above a given threshold T. For $T = 1/2$, the model reduces to a majority rule or the zero temperature Spin Flip Kinetic Ising Model. When the change of state is only possible in one direction, say from 1 to -1, it reduces to the Granovetter-Watts Threshold model (3, 62, 147). We have considered the cases of a fully connected network, Erdős-Rényi, and random regular networks, as well as a regular two-dimensional Moore lattice.

We have found that, in the parameter space of threshold T and initial magnetization m_0, the model exhibits three distinct phases, namely Phase I or mixed, Phase II or ordered, and Phase III or frozen. The existence of these three phases is robust for different network structures. These phases are well characterized by the final state (m_f), and by dynamical properties such as the interface density $\rho(t)$, time-dependent average magnetization $m(t)$, persistence times $p(t)$, and mean internal time $\bar{\tau}(t)$. These phases can be obtained analytically in the mean-field case of a fully connected network. For the random networks considered, we derive an approximate master equation (AME) (3, 56) considering agents in each state according to their degree k, neighbors in state -1, m, and age j. From this AME, we have also derived a heterogeneous mean-field (HMF) approximation. While the AME reproduces with great accuracy the results of Monte Carlo numerical simulations of the model (both static and dynamic), the HMF shows an important lack of agreement, highlighting the importance of high-accuracy methods necessary for threshold models.

Aging is incorporated in the model as a decreasing probability to modify the state as the time already spent by the agent in that state increases. The key finding is that the mixed phase (Phase I), characterized by an asymptotically disordered dynamically active state, does not always exist: the aging mechanism can drive the system to an asymptotic absorbing ordered state, regardless of how low the threshold T is set. A similar effect of aging was already described for the Schelling model in Ref. (2). When the dynamics are examined in detail, a new Phase I^*, defined in terms of dynamical properties, emerges in the domain of parameters where the model without aging displays Phase I. This phase is characterized by an initial disordering regime $(m \to 0)$ followed by a slow ordering dynamics, driving the system toward the ordered absorbing states (including the one with spins opposite to the majoritarian initial option). This result is counter-intuitive since aging incorporates memory into the system, yet in this phase, the system "forgets" its initial state. The network structure plays an important role in the emergence of Phase I^* since it does not exist for complete graphs. A detailed analysis

reveals that Phase I^* replaces Phase I only for sparse networks, including the case of the Moore lattice. For ER networks we find that, as the mean degree increases, Phase I reappears and there is a range of values of the mean degree for which phases I and I^* coexist. Beyond a critical value of the mean degree, Phase I extends over the entire domain of parameters where Phase I^* was observed.

While aging favors reaching an asymptotic absorbing ordered state for low values of T (Phase I), in Phase II the ordering dynamics are slowed down by aging, changing, both in random networks and in the Moore lattice, the exponential decay of the interface density by a power law decay with the same exponent. The aging mechanism is found not to be important in the frozen Phase III. All these effects of aging in the three phases are well reproduced for random networks by the AME derived in this work, which is general for any chosen activation probability $p_A(j)$.

For the Moore lattice, we have also considered in detail the special case of the initial condition $m_0 = 0$. In this case, Phase I^* emerges, and Phase III is robust against aging effects. However, in Phase II aging destroys the characteristic power law decay of the interface density, $\rho(t) \sim at^{-1/2}$, associated with curvature reduction of domain walls. This would be a main effect of aging in the dynamics of the phase transition for the zero temperature spin flip Kinetic Ising model (67). Additionally, this regular structure allowed us to analyze the effects of a compact initial condition. We have shown that the joint effect of aging and a compact initial condition prevent the ordered phases from reaching the consensus state (see **??**).

As a final remark on the general effects of aging in different models of collective behavior, we note that the replacement of a dynamically active disordered stationary phase by a dynamically ordering phase is generic. In this paper, we find the replacement of Phase I by Phase I^*. Likewise in the Voter model, aging destroys long-lived dynamically active states characterized by a constant value of the average interface density, and it gives rise to coarsening dynamics with a power law decay of the average interface density (45). In the same way, in the Schelling segregation model, a dynamically active mixed phase is replaced, due to the aging effect, by an ordering phase with segregation in two main clusters. Another aging effect that seems generic, in phases in which the system orders when there is no aging, is the replacement of dynamical exponential laws by power laws. This is what happens here in Phase II for the decay of the average interface density but, likewise, exponential cascades in the Granovetter-Watts model are replaced due to aging by a power-law growth with the same exponent (3).

Further research with the general AME used in this study would involve a new approach that considers the master equation, as described in Ref. (108). This approach aims to incorporate finite size effects, which are relevant when m_0 is close to zero, and would provide a mathematical framework for further analyisis of the results in Ref. (115). Regarding the model, this article reports the main features of the Symmetrical Threshold model dynamics and the aging effects. However, there are several areas for future research along this lines, such as investigating the impact of strongly heterogeneous (11) or coevolving networks (143, 154), exploring the dependence of the results on the aging activation function p_A, and examining the joint effect of aging and strongly heterogeneous degree distributions.

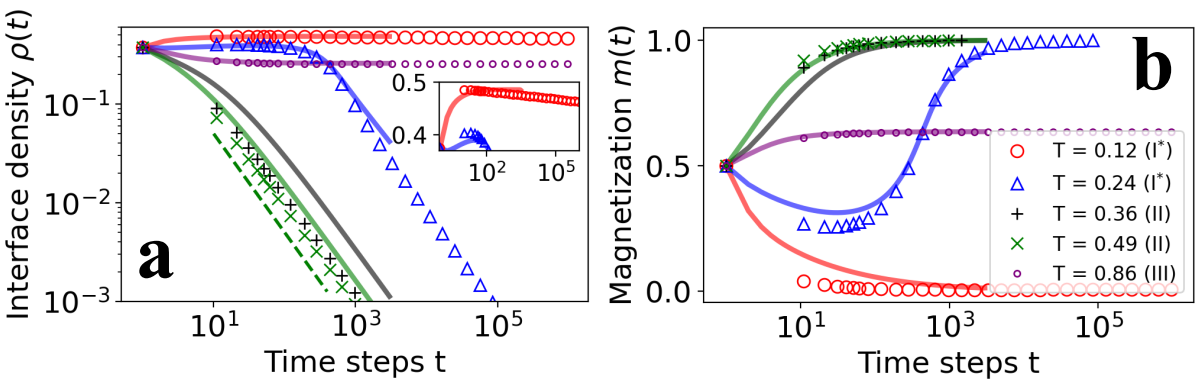

Figure 6.2: **Symmetrical threshold model with aging dynamics in random networks.** Evolution of the average interface density $\rho(t)$ (a) and the average magnetization $m(t)$ (b) for the Symmetrical Threshold model with aging. The average is computed over 5000 surviving trajectories (simulations stop when the system reaches the absorbing ordered states) for different values of T, shown by different markers and colors: red ($T = 0.12$) and blue ($T = 0.24$) belong to Phase I*, green ($T = 0.36$) and grey ($T = 0.49$) belong to Phase II and purple ($T = 0.86$) belong to Phase III. The inset in (a) shows a close look to the evolution for $T = 0.12$, in linear-log scale. Solid colored lines are the AME integrated solutions for 10^4 time steps, using Eqs. 5.6 - 5.7. The initial magnetization is $m_0 = 0.5$. The system is on an ER graph with $N = 4 \cdot 10^4$ and mean degree $\langle k \rangle = 8$. The dashed green line in (a) shows $\rho(t) \sim \rho_0 t^{-1}$. As computed in Fig. 5.3, for all T, $\Delta^a_\rho < 12\%$, $\Delta^a_m < 15\%$.

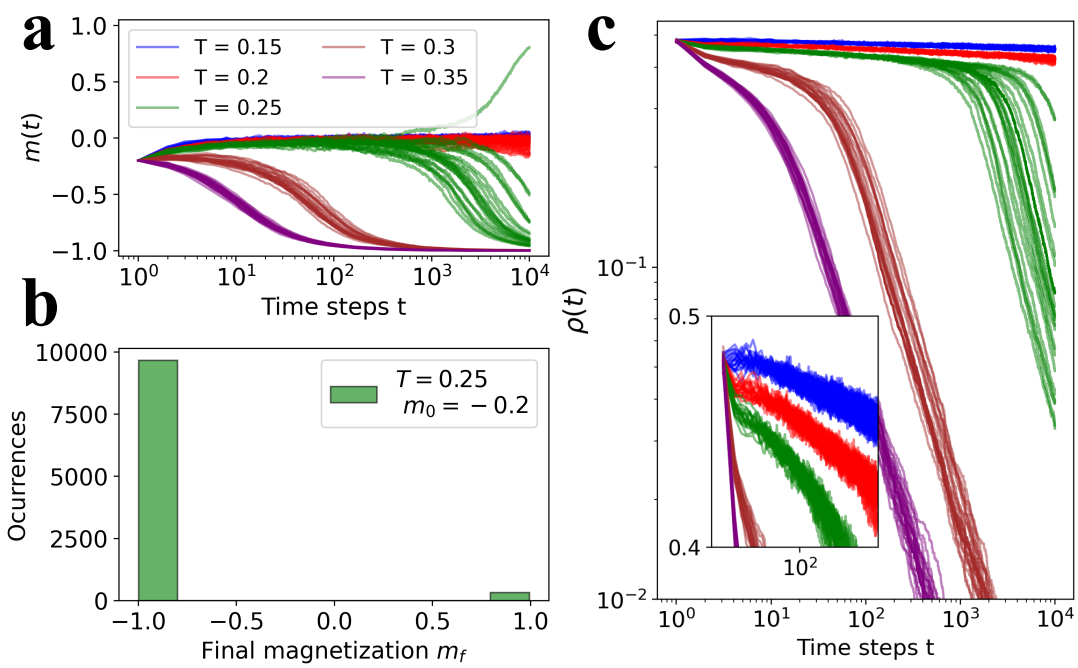

Figure 6.3: **Phase I* slow decay and minority consensus.** Magnetization $m(t)$ (a) and interface density $\rho(t)$ (c) trajectories for different values of the threshold T ($m_0 = -0.2$) using the Symmetrical Threshold model with aging. (b) Final magnetization histogram of 1000 trajectories for the same system at $T = 0.25$. Different colors indicate different values of T. The inset at (b) shows a close look at the logarithmic-like decay, shown in linear-log scale. The system is an ER graph with $N = 4 \cdot 10^4$ and mean degree $\langle k \rangle = 8$.

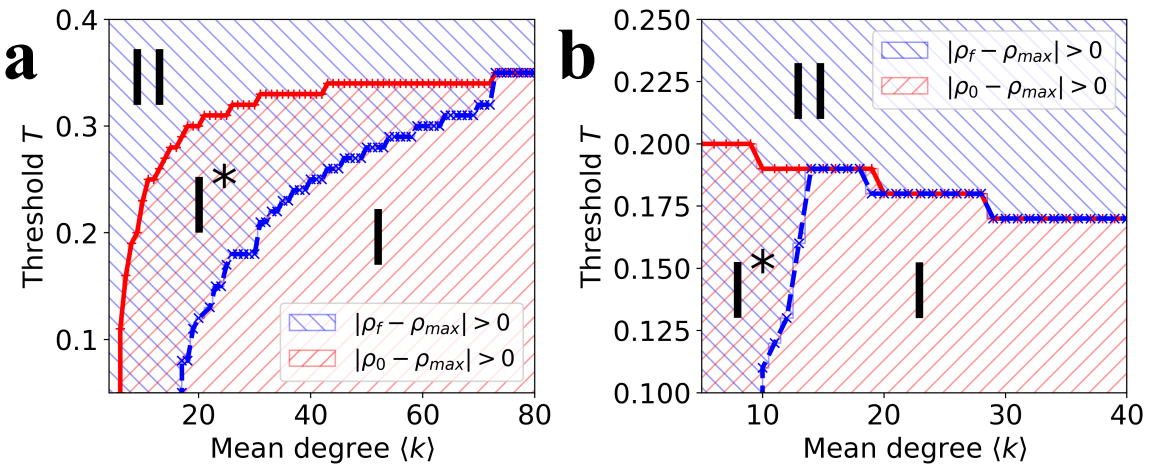

Figure 6.4: **Phase I* dependence with the network mean degree.** Critical threshold T_c dependence with the mean degree $\langle k \rangle$ for the Symmetrical Threshold model with aging for an ER graph with $N = 4 \times 10^4$ nodes for an initial magnetization of $m_0 = 0.25$ (a) and $m_0 = 0.75$ (b). The blue and red markers indicate the borders of phases I and II, which coincide for a sufficiently large value of the mean degree. The hatched area corresponds to the fulfillment of the inequality in the legend.

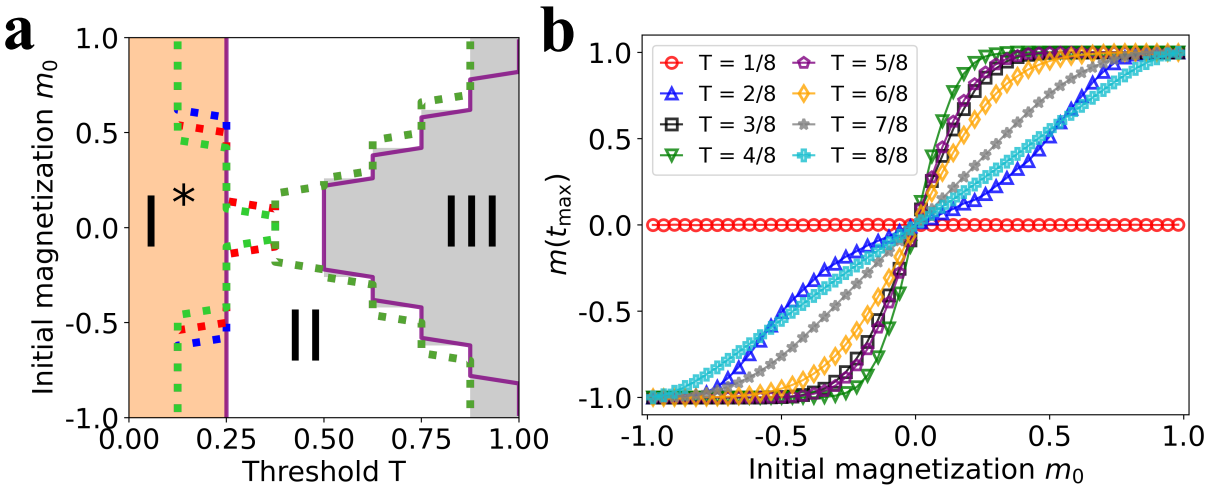

Figure 6.5: **Symmetrical Threshold model with aging in a Moore lattice.** (a) Phase diagram of the Symmetrical Threshold model with aging in a Moore lattice of $N = L \times L$, with $L = 100$. The blue, red and green dotted lines show the borders of Phase II (first and last value of T where the system reaches the absorbing ordered state for each m_0) from numerical simulations evolving until $t_{\max} = 10^3$, 10^4 and 10^5 time steps, respectively. Phase I*, II and III correspond with the orange, white and gray areas, respectively. The solid purple lines are the mixed-ordered and ordered-frozen critical lines for the Symmetrical threshold model (from Fig. 5.5) (b) Average magnetization at time $t_{\max}$ ($m_f(t_{\max})$) as a function of the initial magnetization m_0 for different values of the threshold T (indicated with different colors and markers) in a Moore lattice of $N = L \times L$, with $L = 100$. The numerical simulations are obtained until $t_{\max} = 10^4$ time steps. Average performed over 5000 realizations.

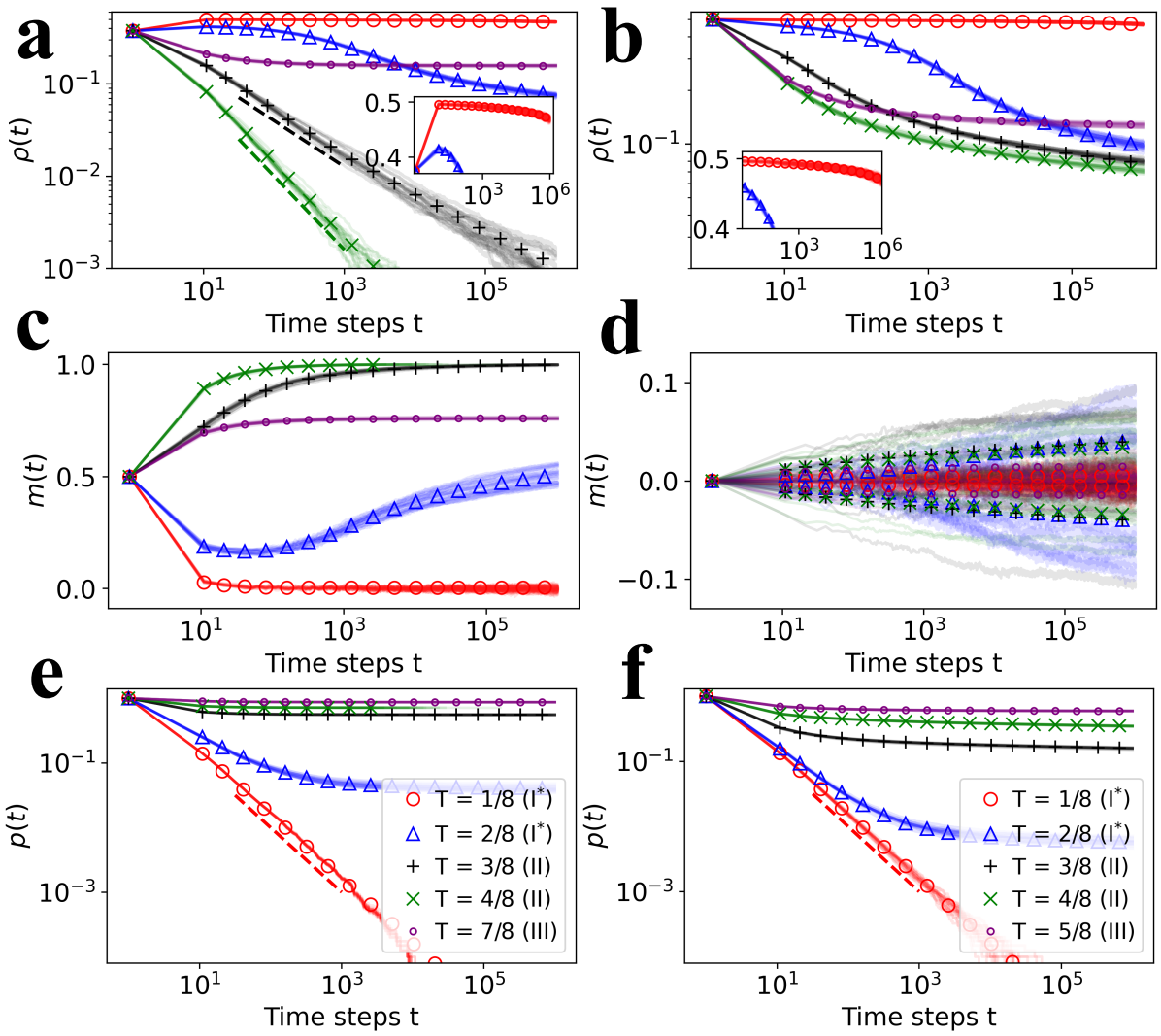

Figure 6.6: **Modified dynamical regimes by aging in a Moore lattice** Evolution of the average interface density $\rho(t)$ (a-b), the average magnetization $m(t)$ (c-d), and the persistence $p(t)$ (e-f) for the Symmetrical model with aging in a Moore lattice starting from a random configuration with $m_0 = 0.5$ (a-c-e) and $m_0 = 0$ (b-d-f). We plot 30 different trajectories in solid lines and the average of over 5000 surviving trajectories in symbols. Colors and symbols indicate different threshold values: red ($T = 1/8$) and blue ($T = 2/8$) belong to Phase I*, green ($T = 3/8$), and black ($T = 4/8$) belong to Phase II, and purple ($T = 5/8, 7/8$) belong to Phase III. The average magnetization is computed according to the two symmetric absorbing states. The insets in (a-b) show a close look at the evolution for $T = 0.12$, in linear-log scale. System size is fixed at $N = L \times L$, $L = 200$. The dashed lines in (a) are $\rho \sim t^{-\alpha}$ with $\alpha = 0.5$ (black) and $\alpha = 0.8$ (green), and in (c) are $p(t) \sim t^{-1}$ (red). Simulations stop when the system reaches the absorbing ordered states.

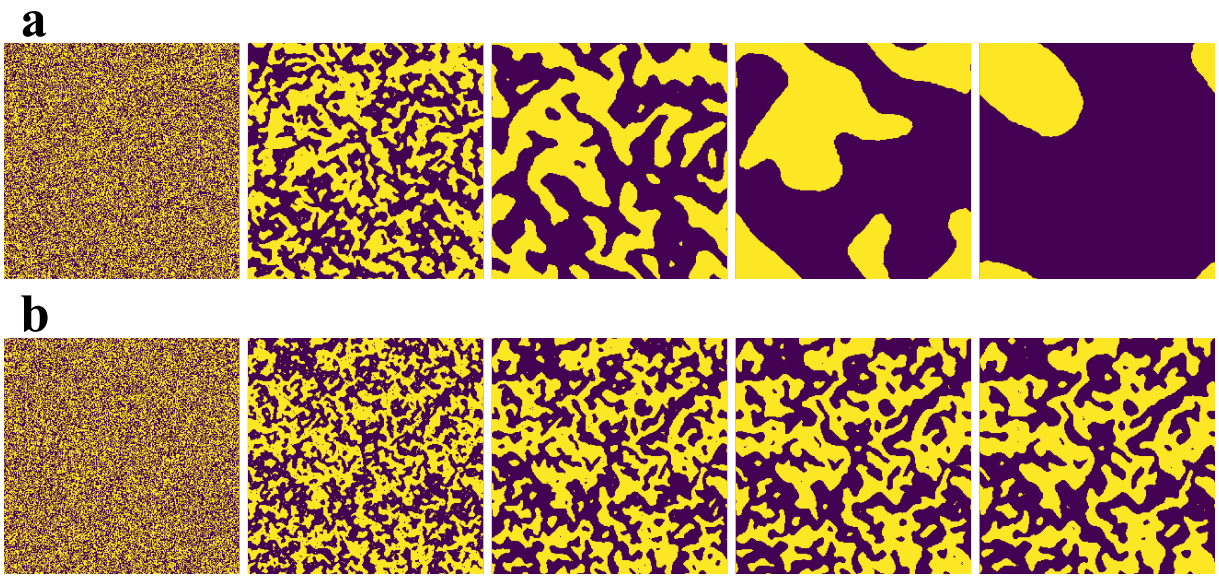

Figure 6.7: **System evolution at $T = 0.5$ and $m_0 = 0$.** Evolution of a single realization for $T = 0.5$ and $m_0 = 0$ using the Symmetrical threshold model (a) and the version with aging (b). Snapshots are taken after $1, 10, 60, 440$ and 3300 time steps in (a) and after $1, 60, 3300, 2 \cdot 10^5$ and $5 \cdot 10^6$ time steps in (b), increasing from left to right. System size is fixed to $N = L \times L$, $L = 256$.

II Real estate market dynamics

7 Dynamics of the real state market 65
7.1 Theorems 65
7.2 Definitions 65
7.3 Notations 65
7.4 Remarks 66
7.5 Corollaries 66
7.6 Propositions 66
7.7 Examples 66
7.8 Exercises 66
7.9 Problems 66
7.10 Vocabulary 67

8 Assessing the real state market segmentation 69
8.1 Table 69
8.2 Figure 69

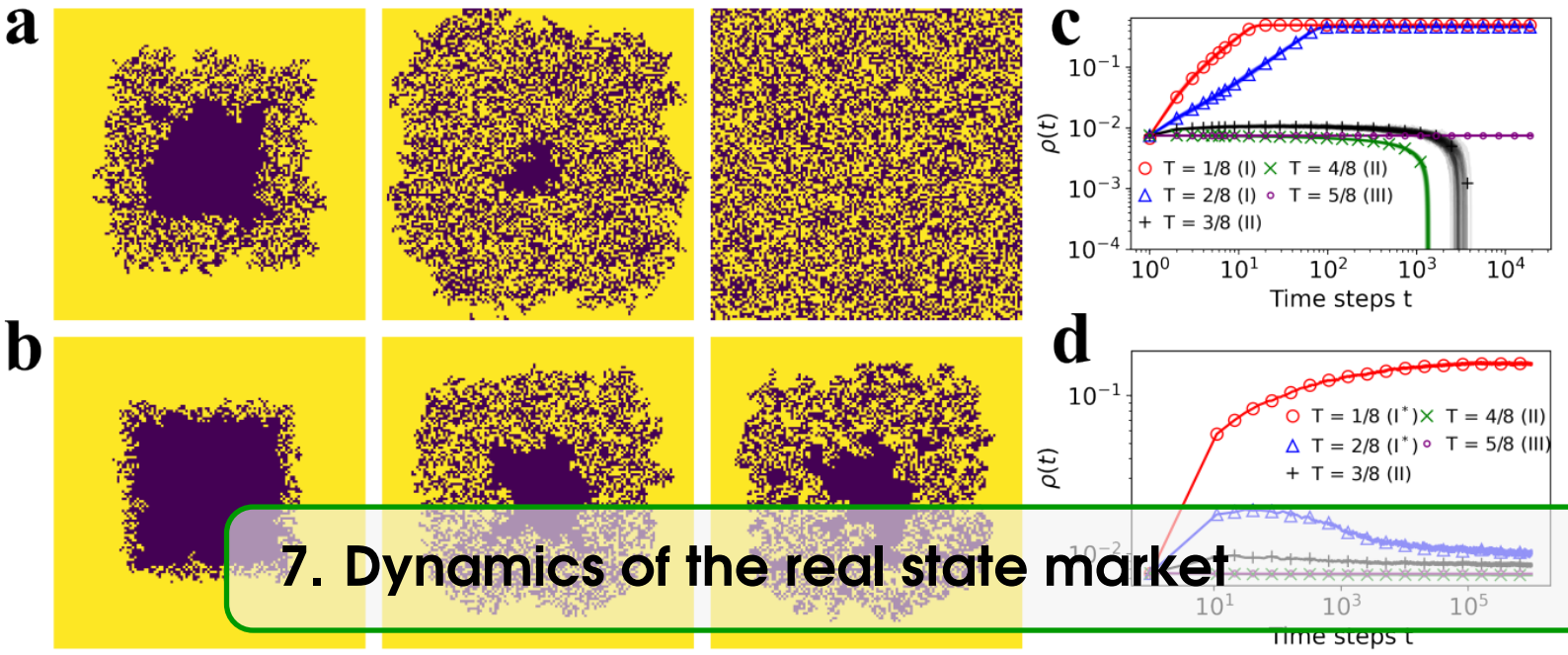

7. Dynamics of the real state market

7.1 Theorems

7.1.1 Several equations

This is a theorem consisting of several equations.

Theorem 7.1 — Name of the theorem. In $E = \mathbb{R}^n$ all norms are equivalent. It has the properties:

$$\big|\,||\mathbf{x}|| - ||\mathbf{y}||\,\big| \leq ||\mathbf{x} - \mathbf{y}|| \tag{7.1}$$

$$||\sum_{i=1}^{n} \mathbf{x}_i|| \leq \sum_{i=1}^{n} ||\mathbf{x}_i|| \quad \text{where } n \text{ is a finite integer} \tag{7.2}$$

7.1.2 Single Line

This is a theorem consisting of just one line.

Theorem 7.2 A set $\mathscr{D}(G)$ in dense in $L^2(G)$, $|\cdot|_0$.

7.2 Definitions

A definition can be mathematical or it could define a concept.

Definition 7.1 — Definition name. Given a vector space E, a norm on E is an application, denoted $||\cdot||$, E in $\mathbb{R}^+ = [0, +\infty[$ such that:

$$||\mathbf{x}|| = 0 \;\Rightarrow\; \mathbf{x} = \mathbf{0} \tag{7.3}$$

$$||\lambda \mathbf{x}|| = |\lambda| \cdot ||\mathbf{x}|| \tag{7.4}$$

$$||\mathbf{x} + \mathbf{y}|| \leq ||\mathbf{x}|| + ||\mathbf{y}|| \tag{7.5}$$

7.3 Notations

■ **Notation 7.1** Given an open subset G of $\mathbb{R}^n$, the set of functions φ are:

1. Bounded support G;
2. Infinitely differentiable;

a vector space is denoted by $\mathscr{D}(G)$.

7.4 Remarks

This is an example of a remark.

R The concepts presented here are now in conventional employment in mathematics. Vector spaces are taken over the field $\mathbb{K} = \mathbb{R}$, however, established properties are easily extended to $\mathbb{K} = \mathbb{C}$.

7.5 Corollaries

Corollary 7.1 — Corollary name. The concepts presented here are now in conventional employment in mathematics. Vector spaces are taken over the field $\mathbb{K} = \mathbb{R}$, however, established properties are easily extended to $\mathbb{K} = \mathbb{C}$.

7.6 Propositions

7.6.1 Several equations

Proposition 7.1 — Proposition name. It has the properties:

$$\big|||\mathbf{x}|| - ||\mathbf{y}||\big| \leq ||\mathbf{x} - \mathbf{y}|| \tag{7.6}$$

$$||\sum_{i=1}^{n} \mathbf{x}_i|| \leq \sum_{i=1}^{n} ||\mathbf{x}_i|| \quad \text{where } n \text{ is a finite integer} \tag{7.7}$$

7.6.2 Single Line

Proposition 7.2 Let $f, g \in L^2(G)$; if $\forall \varphi \in \mathscr{D}(G)$, $(f, \varphi)_0 = (g, \varphi)_0$ then $f = g$.

7.7 Examples

7.7.1 Equation Example

■ **Example 7.1** Let $G = \{x \in \mathbb{R}^2 : |x| < 3\}$ and denoted by: $x^0 = (1, 1)$; consider the function:

$$f(x) = \begin{cases} \mathrm{e}^{|x|} & \text{si } |x - x^0| \leq 1/2 \\ 0 & \text{si } |x - x^0| > 1/2 \end{cases} \tag{7.8}$$

The function f has bounded support, we can take $A = \{x \in \mathbb{R}^2 : |x - x^0| \leq 1/2 + \varepsilon\}$ for all $\varepsilon \in]0; 5/2 - \sqrt{2}[$.
■

7.7.2 Text Example

■ **Example 7.2 — Example name.** Aliquam arcu turpis, ultrices sed luctus ac, vehicula id metus. Morbi eu feugiat velit, et tempus augue. Proin ac mattis tortor. Donec tincidunt, ante rhoncus luctus semper, arcu lorem lobortis justo, nec convallis ante quam quis lectus. Aenean tincidunt sodales massa, et hendrerit tellus mattis ac. Sed non pretium nibh. Donec cursus maximus luctus. Vivamus lobortis eros et massa porta porttitor. ■

7.8 Exercises

Exercise 7.1 This is a good place to ask a question to test learning progress or further cement ideas into students' minds. ■

7.9 Problems

Problem 7.1 What is the average airspeed velocity of an unladen swallow?

7.10 Vocabulary

Define a word to improve a students' vocabulary.

■ **Vocabulary 7.1 — Word.** Definition of word.

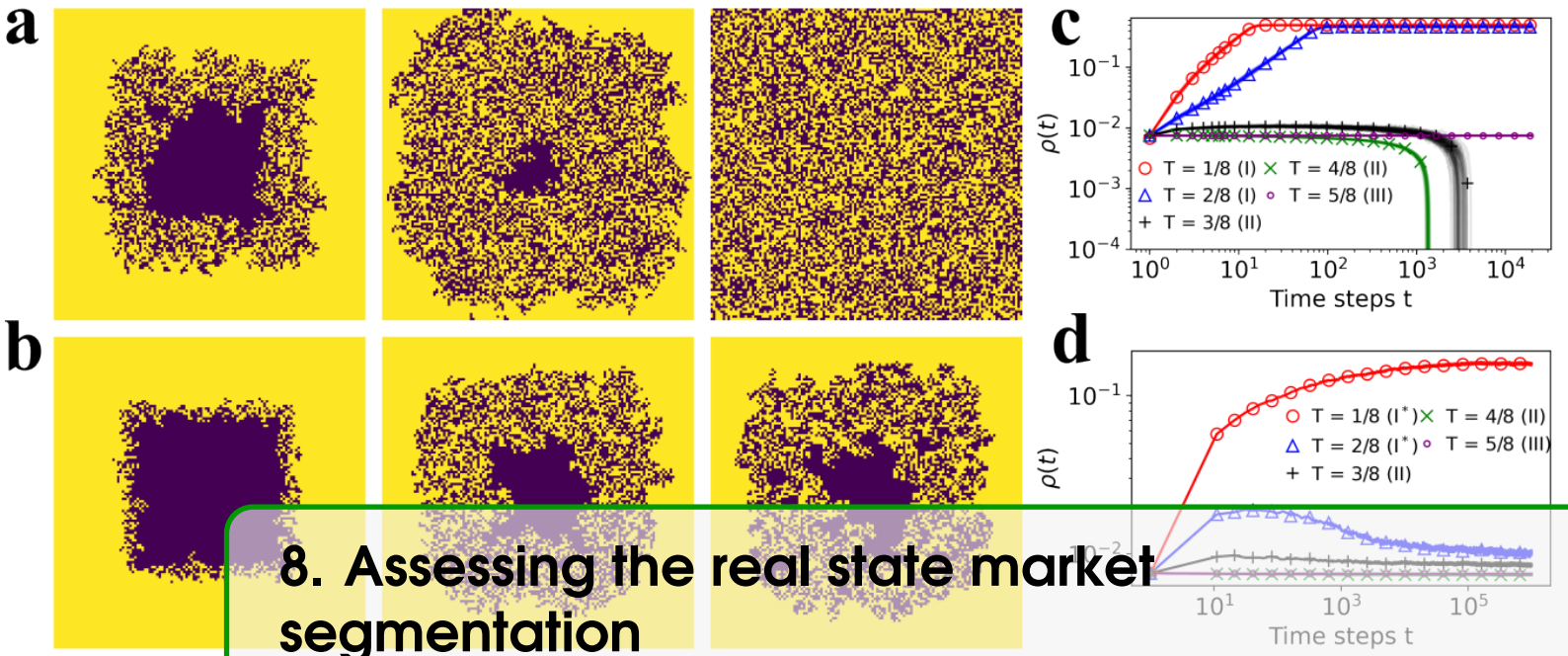

8. Assessing the real state market segmentation

8.1 Table

Lorem ipsum dolor sit amet, consectetur adipiscing elit. Praesent porttitor arcu luctus, imperdiet urna iaculis, mattis eros. Pellentesque iaculis odio vel nisl ullamcorper, nec faucibus ipsum molestie. Sed dictum nisl non aliquet porttitor. Etiam vulputate arcu dignissim, finibus sem et, viverra nisl. Aenean luctus congue massa, ut laoreet metus ornare in. Nunc fermentum nisi imperdiet lectus tincidunt vestibulum at ac elit. Nulla mattis nisl eu malesuada suscipit.

Treatments	Response 1	Response 2
Treatment 1	0.0003262	0.562
Treatment 2	0.0015681	0.910
Treatment 3	0.0009271	0.296

Table 8.1: Table caption.

Referencing Table 8.1 in-text using its label.

8.2 Figure

Lorem ipsum dolor sit amet, consectetur adipiscing elit. Praesent porttitor arcu luctus, imperdiet urna iaculis, mattis eros. Pellentesque iaculis odio vel nisl ullamcorper, nec faucibus ipsum molestie. Sed dictum nisl non aliquet porttitor. Etiam vulputate arcu dignissim, finibus sem et, viverra nisl. Aenean luctus congue massa, ut laoreet metus ornare in. Nunc fermentum nisi imperdiet lectus tincidunt vestibulum at ac elit. Nulla mattis nisl eu malesuada suscipit.

creodocs

Figure 8.1: Figure caption.

Referencing Figure 8.1 in-text using its label.

Treatments	Response 1	Response 2
Treatment 1	0.0003262	0.562
Treatment 2	0.0015681	0.910
Treatment 3	0.0009271	0.296

Table 8.2: Floating table.

Figure 8.2: Floating figure.

Bibliography

Bibliography

[1] David Abella, Maxi San Miguel, and José J. Ramasco. *Aging effects in Schelling Segregation model*. 2022. DOI: 10.48550/ARXIV.2204.01417. URL: https://arxiv.org/abs/2204.01417 (cited on pages 12, 13, 15).

[2] David Abella, Maxi San Miguel, and José J. Ramasco. "Aging effects in Schelling segregation model". In: *Scientific Reports* 12 (2022), page 19376. DOI: 10.1038/s41598-022-23224-7 (cited on pages 23, 49, 51, 52, 57).

[3] David Abella, Maxi San Miguel, and José J. Ramasco. "Aging in binary-state models: The Threshold model for complex contagion". In: *Phys. Rev. E* 107 (2 Feb. 2023), page 024101. DOI: 10.1103/PhysRevE.107.024101. URL: https://link.aps.org/doi/10.1103/PhysRevE.107.024101 (cited on pages 23, 42, 44, 47, 49–52, 56–58).

[4] Aishwarya Agarwal et al. "Swap Stability in Schelling Games on Graphs". In: *Proceedings of the AAAI Conference on Artificial Intelligence* 34.02 (2020), pages 1758–1765. DOI: 10.1609/aaai.v34i02.5541 (cited on page 28).

[5] Ezequiel Albano. "Interfacial roughening, segregation and dynamic behaviour in a generalized Schelling model". In: *Journal of Statistical Mechanics-theory and Experiment - J STAT MECH-THEORY EXP* 2012 (Mar. 2012). DOI: 10.1088/1742-5468/2012/03/P03013 (cited on pages 28, 33, 37).

[6] R Amato et al. "Opinion competition dynamics on multiplex networks". In: *New Journal of Physics* 19.12 (2017), page 123019. DOI: 10.1088/1367-2630/aa936a (cited on page 11).

[7] Guilherme Ferraz de Arruda, Giovanni Petri, and Yamir Moreno. "Social contagion models on hypergraphs". In: *Physical Review Research* 2.2 (2020). DOI: 10.1103/physrevresearch.2.023032 (cited on pages 11, 12, 40).

[8] Oriol Artime, José J. Ramasco, and Maxi San Miguel. "Dynamics on networks: competition of temporal and topological correlations". In: *Scientific Reports* 7.1 (2017). DOI: 10.1038/srep41627 (cited on pages 12, 13, 51, 52).

[9] Oriol Artime et al. "Aging-induced continuous phase transition". In: *Physical Review E* 98.3 (2018). DOI: 10.1103/physreve.98.032104 (cited on pages 12, 13, 15, 28, 29, 51, 52).

[10] A. L. Barabasi. "The origin of bursts and heavy tails in human dynamics". In: *Nature* 435 (2005), page 207 (cited on pages 28, 29).

[11] Albert-László Barabási. "Scale-free networks: a decade and beyond". In: *Science* 325.5939 (2009), pages 412–413 (cited on pages 13, 50, 58).

[12] George Barmpalias, Richard Elwes, and Andrew Lewis-Pye. "Minority Population in the One-Dimensional Schelling Model of Segregation". In: *Journal of Statistical Physics* 173.5 (2018), pages 1408–1458. DOI: 10.1007/s10955-018-2146-2 (cited on page 28).

[13] Frank M Bass. "A new product growth for model consumer durables". In: *Management science* 15.5 (1969), pages 215–227 (cited on page 12).

[14] E. Ben-Naim, L. Frachebourg, and P. L. Krapivsky. "Coarsening and persistence in the voter model". In: *Physical Review E* 53.4 (1996), pages 3078–3087. DOI: 10.1103/physreve.53.3078 (cited on pages 45–47).

[15] L. Berthier and A. P. Young. "Aging dynamics of the Heisenberg spin glass". In: *Physical Review B* 69.18 (May 2004). ISSN: 1550-235X. DOI: 10.1103/physrevb.69.184423. URL: http://dx.doi.org/10.1103/PhysRevB.69.184423 (cited on page 36).

[16] Ginestra Bianconi et al. "Complex systems in the spotlight: next steps after the 2021 Nobel Prize in Physics". In: *Journal of Physics: Complexity* 4.1 (2023), page 010201 (cited on page 39).

[17] M. Blume, V.J. Emery, and Robert B. Griffiths. "Ising Model for the Lambda Transition and Phase Separation in He3-He4 Mixtures". In: *Phys. Rev. A* 4 (1971), page 1071. DOI: https://doi.org/10.1103/PhysRevA.4.1071 (cited on page 28).

[18] Marian Boguñá et al. "Simulating non-Markovian stochastic processes". In: *Physical Review E* 90.4 (2014). DOI: 10.1103/physreve.90.042108 (cited on pages 12, 28, 51).

[19] Paulo RA Campos, Viviane M de Oliveira, and FG Brady Moreira. "Small-world effects in the majority-vote model". In: *Physical Review E* 67.2 (2003), page 026104 (cited on page 40).

[20] Adrián Carro, Raúl Toral, and Maxi San Miguel. "The noisy Voter model on complex networks". In: *Scientific Reports* 6.1 (2016). DOI: 10.1038/srep24775 (cited on page 11).

[21] Claudio Castellano, Santo Fortunato, and Vittorio Loreto. "Statistical physics of social dynamics". In: *Rev. Mod. Phys.* 81 (2 May 2009), pages 591–646. DOI: 10.1103/RevModPhys.81.591. URL: https://link.aps.org/doi/10.1103/RevModPhys.81.591 (cited on page 39).

[22] Claudio Castellano, Santo Fortunato, and Vittorio Loreto. "Statistical physics of social dynamics". In: *Rev. Mod. Phys.* 81 (2 May 2009), pages 591–646. DOI: 10.1103/RevModPhys.81.591. URL: https://link.aps.org/doi/10.1103/RevModPhys.81.591 (cited on page 42).

[23] Claudio Castellano, Miguel A. Muñoz, and Romualdo Pastor-Satorras. "Nonlinearq-Voter model". In: *Physical Review E* 80.4 (2009). DOI: 10.1103/physreve.80.041129 (cited on pages 11, 40).

[24] Giulia Cencetti et al. "Temporal properties of higher-order interactions in social networks". In: *Scientific Reports* 11.1 (2021). DOI: 10.1038/s41598-021-86469-8 (cited on page 11).

[25] Damon Centola, Víctor M. Eguíluz, and Michael W. Macy. "Cascade dynamics of complex propagation". In: *Physica A: Statistical Mechanics and its Applications* 374.1 (2007), pages 449–456. DOI: 10.1016/j.physa.2006.06.018 (cited on pages 11–13, 23, 40).

[26] Hanshuang Chen et al. "Non-Markovian majority-vote model". In: *Physical Review E* 102.6 (2020). DOI: 10.1103/physreve.102.062311 (cited on pages 11–13, 15, 51–53).

[27] Raj Chetty, Nathaniel Hendren, and Lawrence F. Katz. "The Effects of Exposure to Better Neighborhoods on Children: New Evidence from the Moving to Opportunity Experiment". In: *American Economic Review* 106.4 (Apr. 2016), pages 855–902. DOI: 10.1257/aer.20150572. URL: http://dx.doi.org/10.1257/aer.20150572 (cited on page 28).

[28] Terry Nichols Clark et al. "Amenities Drive Urban Growth". In: *Journal of Urban Affairs* 24.5 (Dec. 2002), pages 493–515. DOI: 10.1111/1467-9906.00134. URL: http://dx.doi.org/10.1111/1467-9906.00134 (cited on page 28).

[29] W. A. V. Clark and M. Fossett. "Understanding the social context of the Schelling segregation model". In: *Proceedings of the National Academy of Sciences* 105.11 (2008), pages 4109–4114. DOI: 10.1073/pnas.0708155105 (cited on page 27).

[30] W.A.V. Clark. "Residential preferences and neighborhood racial segregation: A test of the schelling segregation model". In: *Demography* 28.1 (1991), pages 1–19. DOI: 10.2307/2061333 (cited on page 27).

[31] William A.V. Clark, Youqin Huang, and Suzanne Withers. "Does commuting distance matter?" In: *Regional Science and Urban Economics* 33.2 (Mar. 2003), pages 199–221. DOI: 10.1016/s0166-0462(02)00012-1. URL: http://dx.doi.org/10.1016/s0166-0462(02)00012-1 (cited on page 28).

[32] Agnieszka Czaplicka, Raul Toral, and Maxi San Miguel. "Competition of simple and complex adoption on interdependent networks". In: *Physical Review E* 94.6 (2016). DOI: 10.1103/physreve.94.062301 (cited on page 12).

[33] L Dall'Asta, C Castellano, and M Marsili. "Statistical physics of the Schelling model of segregation". In: *Journal of Statistical Mechanics: Theory and Experiment* 2008.07 (July 2008), page L07002. ISSN: 1742-5468. DOI: 10.1088/1742-5468/2008/07/l07002. URL: http://dx.doi.org/10.1088/1742-5468/2008/07/L07002 (cited on pages 28, 30, 31, 33, 37).

[34] Nancy A Denton. "The persistence of segregation: Links between residential segregation and school segregation". In: *Minn. L. Rev.* 80 (1995), page 795 (cited on page 28).

[35] B Derrida. "Exponents appearing in the zero-temperature dynamics of the 1D Potts model". In: *Journal of Physics A: Mathematical and General* 28.6 (1995), pages 1481–1491. DOI: 10.1088/0305-4470/28/6/006 (cited on page 46).

[36] B. Derrida. "How to extract information from simulations of coarsening at finite temperature". In: *Phys. Rev. E* 55 (3 Mar. 1997), pages 3705–3707. DOI: 10.1103/PhysRevE.55.3705. URL: https://link.aps.org/doi/10.1103/PhysRevE.55.3705 (cited on page 46).

[37] Bernard Derrida, Vincent Hakim, and Vincent Pasquier. "Exact First-Passage Exponents of 1D Domain Growth: Relation to a Reaction-Diffusion Model". In: *Physical Review Letters* 75.4 (1995), pages 751–754. DOI: 10.1103/physrevlett.75.751 (cited on page 46).

[38] Marina Diakonova, Maxi San Miguel, and Víctor M. Eguíluz. "Absorbing and shattered fragmentation transitions in multilayer coevolution". In: *Physical Review E* 89.6 (2014). DOI: 10.1103/physreve.89.062818 (cited on page 11).

[39] Marina Diakonova et al. "Irreducibility of multilayer network dynamics: the case of the Voter model". In: *New Journal of Physics* 18.2 (2016), page 023010. DOI: 10.1088/1367-2630/18/2/023010 (cited on page 11).

[40] Fernando Diaz-Diaz, Maxi San Miguel, and Sandro Meloni. "Echo chambers and information transmission biases in homophilic and heterophilic networks". In: *Scientific Reports* 12.1 (2022). DOI: 10.1038/s41598-022-13343-6 (cited on pages 12, 40).

[41] Peter Sheridan Dodds, Kameron Decker Harris, and Christopher M. Danforth. "Limited Imitation Contagion on Random Networks: Chaos, Universality, and Unpredictability". In: *Physical Review Letters* 110.15 (2013). DOI: 10.1103/physrevlett.110.158701 (cited on page 12).

[42] Peter Sheridan Dodds and Duncan J. Watts. "Universal Behavior in a Generalized Model of Contagion". In: *Physical Review Letters* 92.21 (2004). DOI: 10.1103/physrevlett.92.218701 (cited on page 12).

[43] Nicolás Goles Domic, Eric Goles, and Sergio Rica. "Dynamics and complexity of the Schelling segregation model". In: *Physical Review E* 83.5 (2011). DOI: 10.1103/physreve.83.056111 (cited on page 28).

[44] Paul Erdős, Alfréd Rényi, et al. "On the evolution of random graphs". In: *Publ. Math. Inst. Hung. Acad. Sci* 5.1 (1960), pages 17–60 (cited on pages 13, 42, 51).

[45] J. Fernández-Gracia, V. M. Eguíluz, and M. San Miguel. "Update rules and interevent time distributions: Slow ordering versus no ordering in the voter model". In: *Physical Review E* 84.1 (2011). DOI: 10.1103/physreve.84.015103 (cited on pages 12, 13, 15, 28, 29, 50–52, 58).

[46] Juan Fernández-Gracia, Víctor M. Eguíluz, and Maxi San Miguel. "Timing Interactions in Social Simulations: The Voter Model". In: *Understanding Complex Systems* (2013), pages 331–352 (cited on pages 13, 15).

[47] Juan Fernández-Gracia et al. "Is the Voter Model a Model for Voters?" In: *Physical Review Letters* 112.15 (2014). DOI: 10.1103/physrevlett.112.158701 (cited on pages 11, 39).

[48] Daniel S. Fisher and David A. Huse. "Ordered Phase of Short-Range Ising Spin-Glasses". In: *Phys. Rev. Lett.* 56 (15 Apr. 1986), pages 1601–1604. DOI: 10.1103/PhysRevLett.56.1601. URL: https://link.aps.org/doi/10.1103/PhysRevLett.56.1601 (cited on page 36).

[49] SERGE GALAM. "SOCIOPHYSICS: A REVIEW OF GALAM MODELS". In: *International Journal of Modern Physics C* 19.03 (Mar. 2008), pages 409–440. DOI: 10.1142/s0129183108012297. URL: http://dx.doi.org/10.1142/s0129183108012297 (cited on page 12).

[50] L. Gauvin, J. Vannimenus, and J.-P. Nadal. "Phase diagram of a Schelling segregation model". In: *The European Physical Journal B* 70.2 (July 2009), pages 293–304. ISSN: 1434-6036. DOI: 10.1140/epjb/e2009-00234-0. URL: http://dx.doi.org/10.1140/epjb/e2009-00234-0 (cited on pages 28–31).

[51] Laetitia Gauvin, Jean-Pierre Nadal, and Jean Vannimenus. "Schelling segregation in an open city: A kinetically constrained Blume-Emery-Griffiths spin-1 system". In: *Physical Review E* 81.6 (June 2010). ISSN: 1550-2376. DOI: 10.1103/physreve.81.066120. URL: http://dx.doi.org/10.1103/PhysRevE.81.066120 (cited on page 28).

[52] *GitHub repository*. https://github.com/davidabbu/Aging-in-binary-state-models (cited on pages 43, 90).

[53] Roy J Glauber. "Time-dependent statistics of the Ising model". In: *Journal of mathematical physics* 4.2 (1963), pages 294–307 (cited on page 40).

[54] James P. Gleeson. "Cascades on correlated and modular random networks". In: *Physical Review E* 77.4 (2008). DOI: 10.1103/physreve.77.046117 (cited on pages 12, 18, 20, 40).

[55] James P. Gleeson. "High-Accuracy Approximation of Binary-State Dynamics on Networks". In: *Physical Review Letters* 107.6 (2011). DOI: 10.1103/physrevlett.107.068701 (cited on pages 12, 18, 39).

[56] James P. Gleeson. "Binary-State Dynamics on Complex Networks: Pair Approximation and Beyond". In: *Physical Review X* 3.2 (2013). DOI: 10.1103/physrevx.3.021004 (cited on pages 12, 18–20, 42–44, 49, 51, 57, 87, 89).

[57] James P. Gleeson and Diarmuid J. Cahalane. "Seed size strongly affects cascades on random networks". In: *Physical Review E* 75.5 (2007). DOI: 10.1103/physreve.75.056103 (cited on pages 12, 13, 18, 20, 40, 44).

[58] James P. Gleeson et al. "Effects of Network Structure, Competition and Memory Time on Social Spreading Phenomena". In: *Physical Review X* 6.2 (2016). DOI: 10.1103/physrevx.6.021019 (cited on page 12).

[59] S. Gonçalves, M. F. Laguna, and J. R. Iglesias. "Why, when, and how fast innovations are adopted". In: *The European Physical Journal B* 85.6 (June 2012). DOI: 10.1140/epjb/e2012-30082-6. URL: http://dx.doi.org/10.1140/epjb/e2012-30082-6 (cited on pages 12, 26).

[60] C. Gracia-Lázaro et al. "Residential segregation and cultural dissemination: An Axelrod-Schelling model". In: *Physical Review E* 80.4 (2009). DOI: 10.1103/physreve.80.046123 (cited on page 28).

[61] M. Granovetter. "Threshold models of collective behavior". In: *American Journal of Sociology* 83 (1978), page 1420 (cited on page 27).

[62] Mark Granovetter. "Threshold Models of Collective Behavior". In: *American Journal of Sociology* 83.6 (1978), pages 1420–1443. DOI: 10.1086/226707 (cited on pages 11, 13, 39, 40, 47, 57).

[63] Mark Granovetter. "Economic Action and Social Structure: The Problem of Embeddedness". In: *American Journal of Sociology* 91.3 (Nov. 1985), pages 481–510. DOI: 10.1086/228311. URL: http://dx.doi.org/10.1086/228311 (cited on page 28).

[64] S. Grauwin et al. "Competition between collective and individual dynamics". In: *Proceedings of the National Academy of Sciences* 106.49 (2009), pages 20622–20626. DOI: 10.1073/pnas.0906263106 (cited on page 27).

[65] Douglas Guilbeault and Damon Centola. "Topological measures for identifying and predicting the spread of complex contagions". In: *Nature Communications* 12.1 (2021). DOI: 10.1038/s41467-021-24704-6 (cited on page 12).

[66] D. Gunton, M. San Miguel, and P.S. Sahni. "The dynamics of first order phase transitions". In: *Phase transitions and critical phenomena* 8 (1983), pages 267–466 (cited on page 33).

[67] JD Gunton. "The dynamics of first-order phase transitions". In: *Phase transitions and critical phenomena* 8 (1983), page 267 (cited on pages 49, 58).

[68] Laurens Haan and Ana Ferreira. *Extreme value theory: an introduction*. Volume 3. Springer, 2006 (cited on page 45).

[69] Adam Hackett and James P. Gleeson. "Cascades on clique-based graphs". In: *Physical Review E* 87.6 (2013). DOI: 10.1103/physreve.87.062801 (cited on pages 12, 40).

[70] Adam Hackett, Sergey Melnik, and James P. Gleeson. "Cascades on a class of clustered random networks". In: *Physical Review E* 83.5 (2011). DOI: 10.1103/physreve.83.056107 (cited on pages 12, 40).

[71] Rainer Hegselmann. "Thomas C. Schelling and James M. Sakoda: The Intellectual, Technical,and Social History of a Model". In: *Journal of Artificial Societies and Social Simulation* 20.3 (2017), page 15. DOI: 10.18564/jasss.3511 (cited on page 27).

[72] A. D. Henry, P. Pralat, and C.-Q. Zhang. "Emergence of segregation in evolving social networks". In: *Proceedings of the National Academy of Sciences* 108.21 (2011), pages 8605–8610. DOI: 10.1073/pnas.1014486108 (cited on page 28).

[73] Nina Holden and Scott Sheffield. "Scaling limits of the Schelling model". In: *Probability Theory and Related Fields* 176.1-2 (2019), pages 219–292. DOI: 10.1007/s00440-019-00918-0 (cited on page 28).

[74] J. Hoshen and R. Kopelman. "Percolation and cluster distribution. I. Cluster multiple labeling technique and critical concentration algorithm". In: *Phys. Rev. B* 14 (8 Oct. 1976), pages 3438–3445. DOI: 10.1103/PhysRevB.14.3438. URL: https://link.aps.org/doi/10.1103/PhysRevB.14.3438 (cited on page 30).

[75] "How Behavior Spreads: The Science of Complex Contagions How Behavior Spreads: The Science of Complex Contagions Damon Centola Princeton University Press, 2018. 308 pp." In: *Science* 361.6409 (2018), pages 1320–1320. DOI: 10.1126/science.aav1974 (cited on pages 11, 40).

[76] Iacopo Iacopini et al. "Simplicial models of social contagion". In: *Nature Communications* 10.1 (2019). DOI: 10.1038/s41467-019-10431-6 (cited on page 11).

[77] J. L. Iribarren and E. Moro. "Impact of human activity patterns on the dynamics of information diffusion." In: *Physical Review Letters* 103 (2009), page 038702 (cited on page 28).

[78] José Luis Iribarren and Esteban Moro. "Impact of Human Activity Patterns on the Dynamics of Information Diffusion". In: *Physical Review Letters* 103.3 (2009). DOI: 10.1103/physrevlett.103.038702 (cited on page 12).

[79] A Jedrzejewski. "Pair approximation for the q-voter model with independence on complex networks". In: *Phys. Rev. E* 95 (1 Jan. 2017), page 012307. DOI: 10.1103/PhysRevE.95.012307. URL: https://link.aps.org/doi/10.1103/PhysRevE.95.012307 (cited on page 40).

[80] Pablo Jensen et al. "Giant Catalytic Effect of Altruists in Schelling's Segregation Model". In: *Physical Review Letters* 120.20 (2018). DOI: 10.1103/physrevlett.120.208301 (cited on page 28).

[81] Marko Jusup et al. "Social physics". In: *Physics Reports* 948 (2022), pages 1–148 (cited on page 39).

[82] Fariba Karimi and Petter Holme. "Threshold model of cascades in empirical temporal networks". In: *Physica A: Statistical Mechanics and its Applications* 392.16 (2013), pages 3476–3483. DOI: 10.1016/j.physa.2013.03.050 (cited on page 12).

[83] M. Karsai et al. "Small but slow world: How network topology and burstiness slow down spreading". In: *Physical Review E* 83.2 (2011). DOI: 10.1103/physreve.83.025102 (cited on pages 12, 51).

[84] Márton Karsai et al. "Complex contagion process in spreading of online innovation". In: *Journal of The Royal Society Interface* 11.101 (2014), page 20140694. DOI: 10.1098/rsif.2014.0694 (cited on page 12).

[85] Márton Karsai et al. "Local cascades induced global contagion: How heterogeneous thresholds, exogenous effects, and unconcerned behaviour govern online adoption spreading". In: *Scientific Reports* 6.1 (2016). DOI: 10.1038/srep27178 (cited on page 12).

[86] Leah A. Keating, James P. Gleeson, and David J. P. O'Sullivan. "Multitype branching process method for modeling complex contagion on clustered networks". In: *Phys. Rev. E* 105 (3 Mar. 2022), page 034306. DOI: 10.1103/PhysRevE.105.034306. URL: https://link.aps.org/doi/10.1103/PhysRevE.105.034306 (cited on page 22).

[87] Pinaki Kumar et al. "On interevent time distributions of avalanche dynamics". In: *Scientific Reports* 10.1 (2020). DOI: 10.1038/s41598-019-56764-6 (cited on pages 12, 28, 51).

[88] Fabio Lamanna et al. "Immigrant community integration in world cities". In: *PLOS ONE* 13.3 (2018), e0191612. DOI: 10.1371/journal.pone.0191612 (cited on page 27).

[89] Maxime Lenormand et al. "Comparing and modelling land use organization in cities". In: *Royal Society Open Science* 2.12 (2015), page 150449. DOI: 10.1098/rsos.150449 (cited on pages 28, 30).

[90] Thomas M Liggett et al. *Stochastic interacting systems: contact, Voter and exclusion processes*. Volume 324. springer science & Business Media, 1999 (cited on pages 11, 39, 40, 42).

[91] Quan-Hui Liu et al. "Impacts of opinion leaders on social contagions". In: *Chaos: An Interdisciplinary Journal of Nonlinear Science* 28.5 (2018), page 053103. DOI: 10.1063/1.5017515 (cited on page 12).

[92] Andrew Mellor, Mauro Mobilia, and RKP Zia. "Characterization of the nonequilibrium steady state of a heterogeneous nonlinear q-voter model with zealotry". In: *EPL (Europhysics Letters)* 113.4 (2016), page 48001 (cited on page 40).

[93] Byungjoon Min and Maxi San Miguel. "Fragmentation transitions in a coevolving nonlinear voter model". In: *Scientific Reports* 7 (2017), page 12864. DOI: 10.1038/s41598-017-13047-2 (cited on page 40).

[94] Byungjoon Min and Maxi San Miguel. "Competing contagion processes: Complex contagion triggered by simple contagion". In: *Scientific Reports* 8.1 (2018). DOI: 10.1038/s41598-018-28615-3 (cited on page 12).

[95] Byungjoon Min and Maxi San Miguel. "Threshold Cascade Dynamics in Coevolving Networks". In: *Entropy* 25.6 (2023), page 929 (cited on page 40).

[96] Mauro Mobilia. "Nonlinear q-voter model with inflexible zealots". In: *Physical Review E* 92.1 (2015), page 012803 (cited on page 40).

[97] Michael Molloy and Bruce Reed. "A critical point for random graphs with a given degree sequence". In: *Random Structures and Algorithms* 6.2-3 (1995), pages 161–180. DOI: 10.1002/rsa.3240060204 (cited on pages 18, 87).

[98] Bjarke Mønsted et al. "Evidence of complex contagion of information in social media: An experiment using Twitter bots". In: *PLOS ONE* 12.9 (2017), e0184148. DOI: 10.1371/journal.pone.0184148 (cited on page 12).

[99] M. E. J. Newman, S. H. Strogatz, and D. J. Watts. "Random graphs with arbitrary degree distributions and their applications". In: *Physical Review E* 64.2 (2001). DOI: 10.1103/physreve.64.026118 (cited on pages 18, 43, 87).

[100] B. Nowak and Katarzyna Sznajd-Weron. "Homogeneous Symmetrical Threshold Model with Nonconformity: Independence versus Anticonformity". In: *Complexity* 2019 (Apr. 2019), pages 1–14. DOI: 10.1155/2019/5150825. URL: https://doi.org/10.1155/2019/5150825 (cited on page 40).

[101] Bartłomiej Nowak and Katarzyna Sznajd-Weron. "Symmetrical threshold model with independence on random graphs". In: *Physical Review E* 101.5 (2020), page 052316 (cited on page 40).

[102] Se-Wook Oh and Mason A. Porter. "Complex contagions with timers". In: *Chaos: An Interdisciplinary Journal of Nonlinear Science* 28.3 (2018), page 033101. DOI: 10.1063/1.4990038 (cited on page 12).

[103] Mario J de Oliveira. "Isotropic majority-vote model on a square lattice". In: *Journal of Statistical Physics* 66.1 (1992), pages 273–281 (cited on page 40).

[104] Maxi San Miguel Oriol Artine Jose J. Ramasco. "Dynamics on networks: competition of temporal and topological correlations." In: *Scientific Reports* 7 (2017), page 41627 (cited on page 28).

[105] Diego Ortega, Javier Rodríguez-Laguna, and Elka Korutcheva. "A Schelling model with a variable threshold in a closed city segregation model. Analysis of the universality classes". In: *Physica A: Statistical Mechanics and its Applications* 574 (2021), page 126010. DOI: 10.1016/j.physa.2021.126010 (cited on page 28).

[106] Diego Ortega, Javier Rodríguez-Laguna, and Elka Korutcheva. "Avalanches in an extended Schelling model: An explanation of urban gentrification". In: *Physica A: Statistical Mechanics and its Applications* 573 (2021), page 125943. DOI: 10.1016/j.physa.2021.125943 (cited on page 28).

[107] Romualdo Pastor-Satorras et al. "Epidemic processes in complex networks". In: *Reviews of Modern Physics* 87.3 (2015), pages 925–979. DOI: 10.1103/revmodphys.87.925 (cited on pages 11, 39).

[108] A. F. Peralta and R. Toral. "Binary-state dynamics on complex networks: Stochastic pair approximation and beyond". In: *Physical Review Research* 2.4 (2020). DOI: 10.1103/physrevresearch.2.043370 (cited on pages 18, 26, 50, 58).

[109] A. F. Peralta et al. "Analytical and numerical study of the non-linear noisy Voter model on complex networks". In: *Chaos: An Interdisciplinary Journal of Nonlinear Science* 28.7 (2018), page 075516. DOI: 10.1063/1.5030112 (cited on pages 11, 40, 52).

[110] Antonio F Peralta, Nagi Khalil, and Raúl Toral. "Reduction from non-Markovian to Markovian dynamics: the case of aging in the noisy-Voter model". In: *Journal of Statistical Mechanics: Theory and Experiment* 2020.2 (2020), page 024004. DOI: 10.1088/1742-5468/ab6847 (cited on pages 11–13, 15, 18, 51, 87).

[111] Antonio F. Peralta, Nagi Khalil, and Raúl Toral. "Ordering dynamics in the Voter model with aging". In: *Physica A: Statistical Mechanics and its Applications* 552 (2020), page 122475. DOI: 10.1016/j.physa.2019.122475 (cited on pages 12, 13, 15, 18, 51, 87).

[112] Antonio F. Peralta, Nagi Khalil, and Raúl Toral. "Ordering dynamics in the voter model with aging". In: *Physica A: Statistical Mechanics and its Applications* 552 (2020), page 122475. DOI: 10.1016/j.physa.2019.122475 (cited on page 28).

[113] Luiz FC Pereira and FG Brady Moreira. "Majority-vote model on random graphs". In: *Physical Review E* 71.1 (2005), page 016123 (cited on page 40).

[114] Toni Pérez, Konstantin Klemm, and Víctor M. Eguíluz. "Competition in the presence of aging: dominance, coexistence, and alternation between states". In: *Scientific Reports* 6.1 (2016). DOI: 10.1038/srep21128 (cited on pages 12, 13, 15, 28, 51).

[115] Armin Pournaki et al. *Order-disorder transition in the zero-temperature Ising model on random graphs*. May 2023. DOI: 10.1103/PhysRevE.107.054112. URL: https://link.aps.org/doi/10.1103/PhysRevE.107.054112 (cited on pages 45, 50, 55, 58).

[116] Sidney Redner. "Reality-inspired Voter models: A mini-review". In: *Comptes Rendus Physique* 20.4 (2019), pages 275–292. DOI: 10.1016/j.crhy.2019.05.004 (cited on pages 11, 39).

[117] Everett M Rogers, Arvind Singhal, and Margaret M Quinlan. "Diffusion of innovations". In: *An integrated approach to communication theory and research*. Routledge, 2014, pages 432–448 (cited on page 12).

[118] Tim Rogers and Alan J McKane. "A unified framework for Schelling's model of segregation". In: *Journal of Statistical Mechanics: Theory and Experiment* 2011.07 (July 2011), P07006. ISSN: 1742-5468. DOI: 10.1088/1742-5468/2011/07/p07006. URL: http://dx.doi.org/10.1088/1742-5468/2011/07/P07006 (cited on page 28).

[119] Sara Brin Rosenthal et al. "Revealing the hidden networks of interaction in mobile animal groups allows prediction of complex behavioral contagion". In: *Proceedings of the National Academy of Sciences* 112.15 (2015), pages 4690–4695. DOI: 10.1073/pnas.1420068112 (cited on page 12).

[120] Diego Rybski et al. "Scaling laws of human interaction activity". In: *Proceedings of the National Academy of Sciences* 106.31 (2009), pages 12640–12645. DOI: 10.1073/pnas.0902667106. eprint: https://www.pnas.org/doi/pdf/10.1073/pnas.0902667106. URL: https://www.pnas.org/doi/abs/10.1073/pnas.0902667106 (cited on pages 51, 52).

[121] Diego Rybski et al. "Communication activity in a social network: relation between long-term correlations and inter-event clustering". In: *Scientific Reports* 2.1 (2012). DOI: 10.1038/srep00560 (cited on pages 12, 28).

[122] S. Sassen. "The global city: introducing a concept". In: *Brown Journal of World Affairs* 11 (2005), pages 27–43 (cited on page 27).

[123] D. M. Saul, Michael Wortis, and D. Stauffer. "Tricritical behavior of the Blume-Capel model". In: *Phys. Rev. B* 9 (11 June 1974), pages 4964–4980. DOI: 10.1103/PhysRevB.9.4964. URL: https://link.aps.org/doi/10.1103/PhysRevB.9.4964 (cited on page 28).

[124] T Schelling. *Micromotives and Macrobehavior*. Norton, New York, 1978 (cited on page 27).

[125] Thomas Schelling. "Models of Segregation". In: *American Economic Review* 59.2 (1969), page 488 (cited on page 27).

[126] Thomas C Schelling. "Dynamic models of segregation". In: *The Journal of Mathematical Sociology* 1.2 (1971), pages 143–186. DOI: 10.1080/0022250X.1971.9989794. URL: https://doi.org/10.1080/0022250X.1971.9989794 (cited on page 27).

[127] Egemen Sert, Yaneer Bar-Yam, and Alfredo J. Morales. "Segregation dynamics with reinforcement learning and agent based modeling". In: *Scientific Reports* 10.1 (2020). DOI: 10.1038/s41598-020-68447-8 (cited on page 28).

[128] Munik Shrestha and Cristopher Moore. "Message-passing approach for threshold models of behavior in networks". In: *Physical Review E* 89.2 (2014). DOI: 10.1103/physreve.89.022805 (cited on page 12).

[129] Daniel Silver, Ultan Byrne, and Patrick Adler. "Venues and segregation: A revised Schelling model". In: *PLOS ONE* 16.1 (Jan. 2021), e0242611. DOI: 10.1371/journal.pone.0242611. URL: http://dx.doi.org/10.1371/journal.pone.0242611 (cited on page 28).

[130] Daniel Aaron Silver and Terry Nichols Clark. *Scenescapes: How qualities of place shape social life*. University of Chicago Press, 2016 (cited on page 28).

[131] P. Singh et al. "Threshold-limited spreading in social networks with multiple initiators". In: *Scientific Reports* 3.1 (2013). DOI: 10.1038/srep02330 (cited on pages 12, 13).

[132] V. Sood and S. Redner. "Voter Model on Heterogeneous Graphs". In: *Physical Review Letters* 94.17 (2005). DOI: 10.1103/physrevlett.94.178701 (cited on pages 11, 39).

[133] Sandro Sousa and Vincenzo Nicosia. *Quantifying ethnic segregation in cities through random walks*. 2020. arXiv: 2010.10462 [physics.soc-ph] (cited on page 30).

[134] Hans-Ulrich Stark, Claudio J. Tessone, and Frank Schweitzer. "Decelerating Microdynamics Can Accelerate Macrodynamics in the Voter Model". In: *Physical Review Letters* 101.1 (2008). DOI: 10.1103/physrevlett.101.018701 (cited on pages 12, 13, 15, 51).

[135] Hans-Ulrich Stark, Claudio J. Tessone, and Frank Schweitzer. "Decelerating Microdynamics Can Accelerate Macrodynamics in the Voter Model". In: *Phys. Rev. Lett.* 101 (1 June 2008), page 018701. DOI: 10.1103/PhysRevLett.101.018701. URL: https://link.aps.org/doi/10.1103/PhysRevLett.101.018701 (cited on page 28).

[136] Michele Starnini, James P. Gleeson, and Marián Boguñá. "Equivalence between Non-Markovian and Markovian Dynamics in Epidemic Spreading Processes". In: *Physical Review Letters* 118.12 (2017). DOI: 10.1103/physrevlett.118.128301 (cited on pages 11, 12).

[137] D Stauffer, J Adler, and A Aharony. "Universality at the three-dimensional percolation threshold". In: *Journal of Physics A: Mathematical and General* 27.13 (1994), pages L475–L480. DOI: 10.1088/0305-4470/27/13/003 (cited on page 46).

[138] D. Stauffer and S. Solomon. "Ising, Schelling and self-organising segregation". In: *The European Physical Journal B* 57.4 (2007), pages 473–479. DOI: 10.1140/epjb/e2007-00181-8 (cited on page 28).

[139] Dietrich Stauffer. "A Biased Review of Sociophysics". In: *Journal of Statistical Physics* 151.1-2 (2013), pages 9–20. DOI: 10.1007/s10955-012-0604-9 (cited on page 28).

[140] Krzysztof Suchecki, V1**********ctor M. Egu1********** and Maxi San Miguel. "Voter model dynamics in complex networks: Role of dimensionality, disorder, and degree distribution". In: *Phys. Rev. E* 72 (3 Sept. 2005), page 036132. DOI: 10.1103/PhysRevE.72.036132. URL: https://link.aps.org/doi/10.1103/PhysRevE.72.036132 (cited on pages 39, 42).

[141] Samuel Unicomb, Gerardo Iñiguez, and Márton Karsai. "Threshold driven contagion on weighted networks". In: *Scientific Reports* 8.1 (2018). DOI: 10.1038/s41598-018-21261-9 (cited on page 12).

[142] P. Van Mieghem and R. van de Bovenkamp. "Non-Markovian Infection Spread Dramatically Alters the Susceptible-Infected-Susceptible Epidemic Threshold in Networks". In: *Physical Review Letters* 110.10 (2013). DOI: 10.1103/physrevlett.110.108701 (cited on pages 11, 12).

[143] Federico Vazquez, Víctor M. Eguíluz, and Maxi San Miguel. "Generic Absorbing Transition in Coevolution Dynamics". In: *Physical Review Letters* 100.10 (2008). DOI: 10.1103/physrevlett.100.108702 (cited on pages 11, 50, 58).

[144] André P Vieira, Eric Goles, and Hans J Herrmann. "Dynamics of extended Schelling models". In: *Journal of Statistical Mechanics: Theory and Experiment* 2020.1 (2020), page 013212. DOI: 10.1088/1742-5468/ab5b8d (cited on page 28).

[145] D. Vinkovic and A. Kirman. "A physical analogue of the Schelling model". In: *Proceedings of the National Academy of Sciences* 103.51 (2006), pages 19261–19265. DOI: 10.1073/pnas.0609371103 (cited on page 28).

[146] Henry Wasserman and Gary Yohe. "Segregation and the Provision of Spatially Defined Local Public Goods". In: *The American Economist* 45.2 (Oct. 2001), pages 13–24. DOI: 10.1177/056943450104500202. URL: http://dx.doi.org/10.1177/056943450104500202 (cited on page 28).

[147] D. J. Watts. "A simple model of global cascades on random networks". In: *Proceedings of the National Academy of Sciences* 99.9 (2002), pages 5766–5771. DOI: 10.1073/pnas.082090499 (cited on pages 11–13, 15, 18, 40, 47, 57).

[148] N. C. Wormald. "Models of Random Regular Graphs". In: *Surveys in Combinatorics, 1999*. Edited by J. D. Lamb and D. A.Editors Preece. London Mathematical Society Lecture Note Series. Cambridge University Press, 1999, pages 239–298. DOI: 10.1017/CBO9780511721335.010 (cited on page 22).

[149] Nicholas C Wormald et al. "Models of random regular graphs". In: *London Mathematical Society Lecture Note Series* (1999), pages 239–298 (cited on pages 13, 42, 51).

[150] Yang Xu et al. "Quantifying segregation in an integrated urban physical-social space". In: *Journal of the Royal Society Interface* 16.160 (2019), page 20190536. ISSN: 17425662. DOI: 10.1098/rsif.2019.0536. URL: https://royalsocietypublishing.org/doi/abs/10.1098/rsif.2019.0536 (cited on page 30).

[151] A P Young. *Spin glasses and random fields*. World Scientific, 1997. URL: libgen.li/file.php?md5=5941f917f91576aa2f77de1c40712f2c (cited on pages 35, 36).

[152] Junfu Zhang. "Residential segregation in an all-integrationist world". In: *Journal of Economic Behavior and Organization* 54.4 (2004), pages 533–550. ISSN: 0167-2681. DOI: https://doi.org/10.1016/j.jebo.2003.03.005. URL: https://www.sciencedirect.com/science/article/pii/S0167268103001768 (cited on page 37).

[153] Matteo Zignani et al. "Walls-in-one: usage and temporal patterns in a social media aggregator". In: *Applied Network Science* 1.1 (2016). DOI: 10.1007/s41109-016-0009-9 (cited on pages 12, 28, 51).

[154] Martı**********n G. Zimmermann, Vı**********
M. Egu**********luz, and Maxi San Miguel. "Coevolution of dynamical states and interactions in dynamic networks". In: *Phys. Rev. E* 69 (6 June 2004), page 065102. DOI: 10.1103/PhysRevE.69.065102. URL: https://link.aps.org/doi/10.1103/PhysRevE.69.065102 (cited on pages 50, 58).

Index

Corollaries, 66

Definitions, 65

Examples, 66
    Equation, 66
    Text, 66
Exercises, 66

Figure, 69

Notations, 65

Problems, 66
Propositions, 66
    Several Equations, 66
    Single Line, 66

Remarks, 66

Table, 69
Theorems, 65
    Several Equations, 65
    Single Line, 65

Vocabulary, 67

A. Effect of a higher vacancy density ρ_v in the coarsening dynamics of the Schelling model

Since we restrain ourselves to the region $\rho_v < 0.5$, the increase/decrease of the number of vacancies does not change dramatically the behaviour. Above this value, we approach the segregated-dilute transition ($\rho_v \sim 0.62$). Nevertheless, it is worth to mention a few features we observe on the coarsening dynamics.

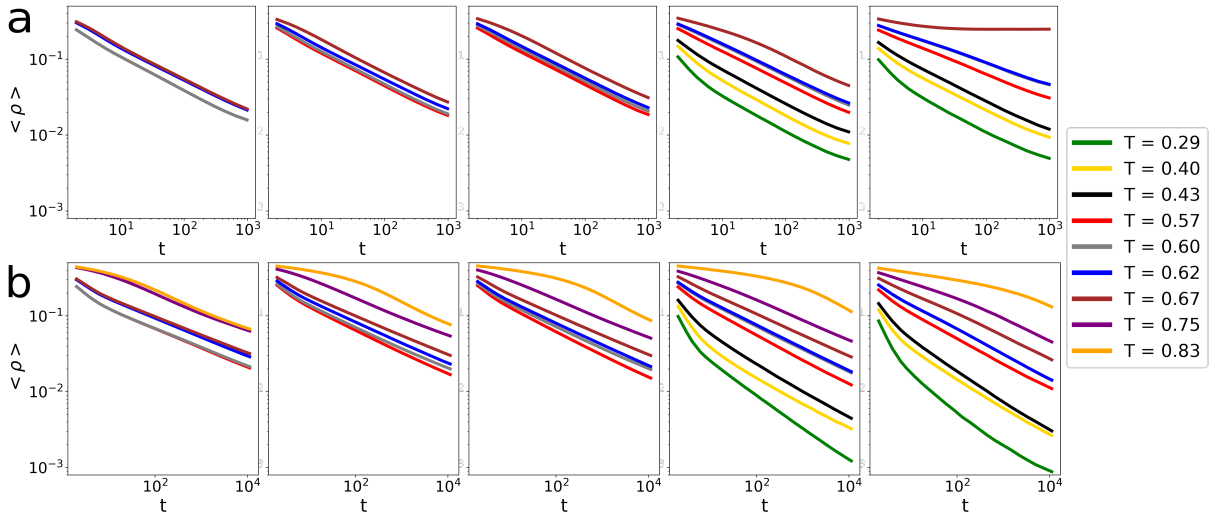

Figure A.1: Average interface density $\langle \rho(t) \rangle$ as a function of time steps for different values of the tolerance parameter T fr the Schelling model (**a**) and the version with aging (**b**). The different plots show a the evolution at a different value of the vacancy density, increasing from left to right $\rho_v = 0.005$, 0.15, 0.2, 0.3 and 0.45. Average performed over 10^3 realisations with system size 100 x 100.

Essentially, when we set a higher vacancy density, the number of agents which see vacancies at their surroundings increases. This results in a family of similar power-law decays towards the segregated state for every meaningful value of T (see Fig. A.1).

Moreover, a higher ρ_v allows us to study the coarsening phenomena for lower values of T according to the phase diagram for the original Schelling model. For those particular cases, when the aging is introduced, we observe a power law decay faster than without aging (Fig. A.1b). Therefore, the aging effect accelerates segregation in this region of the phase diagram, contrary as for lower values of ρ_v. This acceleration is

not caused by reaching the 2-clusters state in less time. Since there is a large presence of vacancies, aging causes a formation of vacancy clusters at the interface. Fig. A.2 shows the final segregated state with and without aging. This spontaneous behaviour is result of the low tolerance combined with the persistence of clusters (once formed) due to aging effect and the large number of vacancies that allows the possibility of the formation of clusters at the interface.

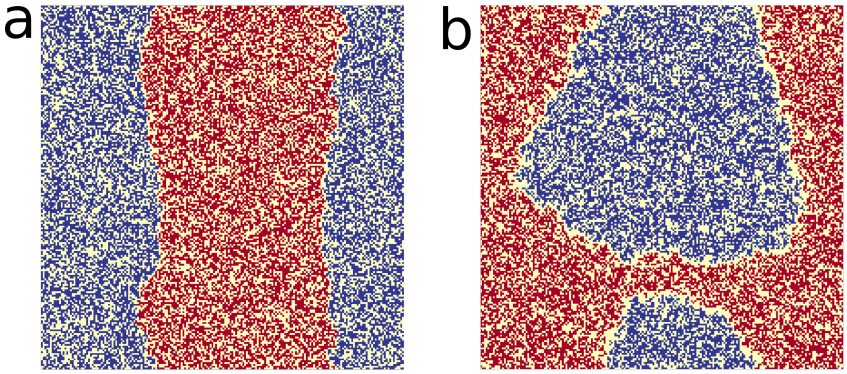

Figure A.2: Snapshots of the system at the final segregated state (after 10^6 MC steps) for the Schelling model (**a**) and the version with (**b**). System size 200 x 200 with $\rho_v = 0.45$ and $T = 0.29$.

In order to quantify this vacancy cluster formation, we define a measure inspired in the segregation coefficient:

$$s_v = \frac{1}{(L^2\rho_v)^2}\sum_{\{c\}} n_c^2 \tag{A.1}$$

where c is the size of a vacancy cluster and n_c is the number of clusters with size c. The sample average of s_v after reaching equilibrium is called the cluster coefficient of vacancies $\langle s_v \rangle$.

The results of this measure as a function of ρ_v for a few values of T are represented in Fig.A.3 for the Schelling model with and without aging. We observe an increasing dependence of $\langle s_v \rangle$ with ρ_v for both models, but the effect reducing tolerance changes dramatically the behaviour for the case with aging, highlighting the vacancy cluster formation.

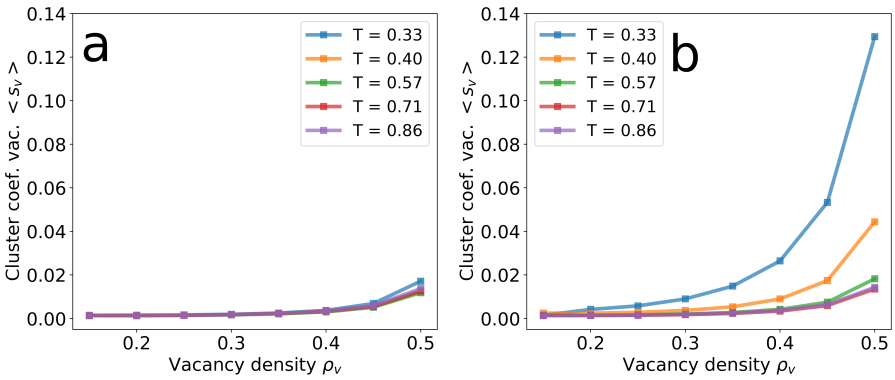

Figure A.3: Cluster coefficient of vacancies as a function of the vacancy density ρ_v for the Schelling model (**a**) and the version with (**b**) for different values of the tolerance T.

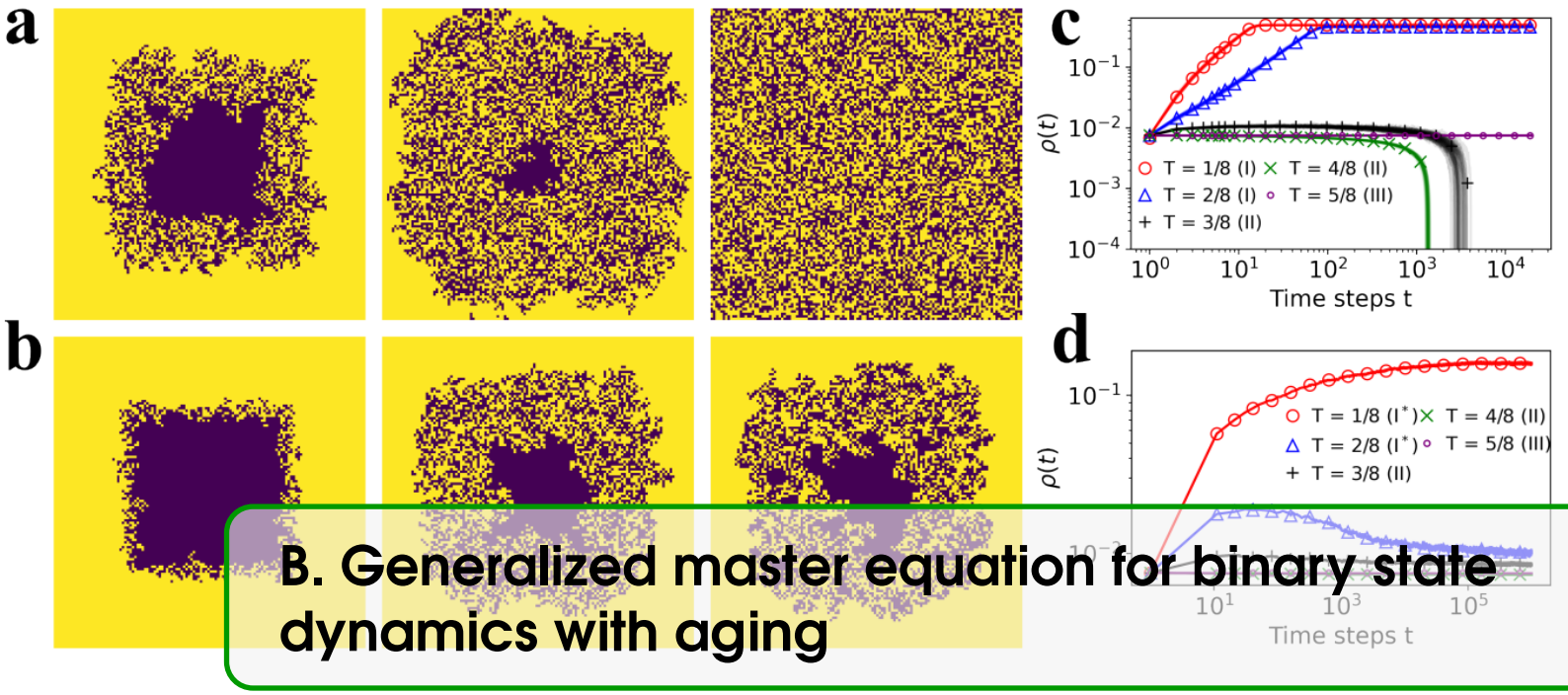

B. Generalized master equation for binary state dynamics with aging

We consider binary-state dynamics on static, undirected, connected networks assuming a locally tree-like structure and in the limit of $N \to \infty$, following closely the approach used in Ref. (56) for binary-state dynamics in complex networks. The new ingredient is to consider the nodes with different age as different sets, what allows us to treat as Markovian the memory effects introduced by aging (110, 111). We define $s_{k,m,j}(t)$ ($i_{k,m,j}(t)$) as the fraction of nodes that are susceptible (infected) and have degree k, m infected neighbors and age j at time t. The networks have degree distribution p_k and have been generated by the configuration model (97, 99). The initial condition is set such that all agents have age $j=0$ and there is a randomly chosen fraction ρ_0 of nodes infected:

$$\begin{aligned} &\text{For } j>0 \quad s_{k,m,j}(0)=0 \quad i_{k,m,j}(0)=0, \\ &\text{For } j=0 \quad s_{k,m,0}(0)=(1-\rho_0)\,B_{k,m}[\rho_0] \\ &\qquad\qquad\;\; i_{k,m,0}(0)=\rho_0\,B_{k,m}[\rho_0], \end{aligned} \tag{B.1}$$

where $B_{k,m}[\rho_0]$ is the binomial distribution with k attempts, m successes and ρ_0 is the initial fraction of infected agents that as the probability of success of the binomial. Now, we examine how $s_{k,m,j}$ changes in a time step. We consider separately the case $j=0$ since its evolution is different from $j>0$. See Fig. B.1 for a schematic representation of transitions involving $s_{k,m,j}$.

This is the way to reach the expressions of Eq. (B.2):

$$\begin{aligned} s_{k,m,j}(t+dt) =& s_{k,m,j}(t) - F(k,m,j)\,s_{k,m,j}\,dt - F_R(k,m,j)\,s_{k,m,j}\,dt - F_A(k,m,j)\,s_{k,m,j}\,dt \\ &+ F_A(k,m,j-1)\,s_{k,m,j-1}\,dt - \omega(s_{k,m,j}\to s_{k,m+1,j+1})\,s_{k,m,j}\,dt \\ &- \omega(s_{k,m,j}\to s_{k,m-1,j+1})\,s_{k,m,j}\,dt + \omega(s_{k,m+1,j-1}\to s_{k,m,j})\,s_{k,m+1,j-1}\,dt \\ &+ \omega(s_{k,m-1,j-1}\to s_{k,m-1,j-1})\,s_{k,m-1,j-1}\,dt, \\ s_{k,m,0}(t+dt) =& s_{k,m,0}(t) - F(k,m,0)\,s_{k,m,0}\,dt + \sum_{l=0}^{\infty} R(k,m,l)\,i_{k,m,l}\,dt + \sum_{l=1}^{\infty} F_R(k,m,l)\,s_{k,m,l}\,dt \\ &- F_A(k,m,0)\,s_{k,m,0}\,dt - \omega(s_{k,m,0}\to s_{k,m+1,1})\,s_{k,m,0}\,dt - \omega(s_{k,m,0}\to s_{k,m-1,1})\,s_{k,m,0}\,dt. \end{aligned} \tag{B.2}$$

Similar equations can be found considering transitions for $i_{k,m,j}$. In these equations, the transition probabilities (described in detail in section 3.3.2) allow agents to change

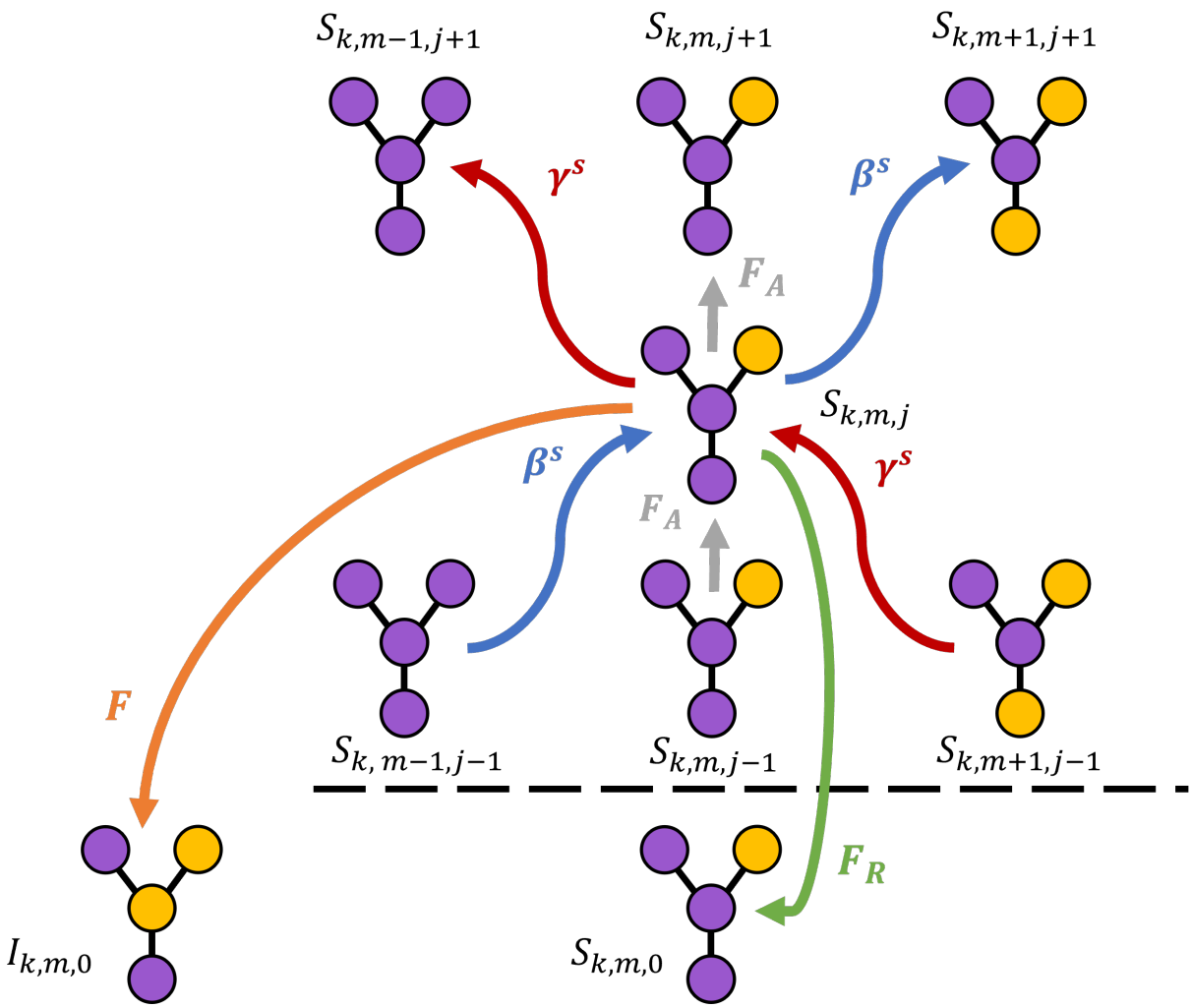

Figure B.1: Schematic representation of the transitions to or from the set $s_{k,m,j}$ $(j > 0)$. We show the central node with some neighbors for different values m and j. Purple nodes are susceptible or non-adopters or spin-down, and yellow are infected or adopters or spin-up.

state (F and R), reset internal time ($j \to 0$) (F_R and R_R and age ($j \to j+1$) (F_A and R_A). Notice that we have considered no transition increasing (or decreasing) the number of infected neighbors m, keeping constant the age j. This is because the age j is defined as the time spent in the current state (or since a reset). Therefore, if a node remains susceptible and the number of infected neighbors changes ($m \to m \pm 1$), the age of the node must increase ($j \to j+1$). To determine the rate of these events, we use the same assumption as in Ref. (56): we assume that the number of S-S edges change to S-I edges at a time-dependent rate β^s. Therefore, the transition rates are:

$$\begin{aligned} \omega(s_{k,m,j} \to s_{k,m+1,j+1}) &= (k-m)\,\beta^s, \\ \omega(s_{k,m-1,j-1} \to s_{k,m,j}) &= (k-m+1)\,\beta^s. \end{aligned} \tag{B.3}$$

To determine the rate β^s, we count the change of S-S edges that change to S-I in a time step. This change is produced by a neighbor changing state from susceptible to infected. Thus, we can extract this information from the infection probability $F(k,m,j)$:

$$\beta^s = \frac{\sum_{j=0}^{\infty}\sum_{k=0}^{\infty} p_k \sum_{m=0}^{k}(k-m)\,F(k,m,j)\,s_{k,m,j}}{\sum_{j=0}^{\infty}\sum_{k=0}^{\infty} p_k \sum_{m=0}^{k}(k-m)\,s_{k,m,j}}. \tag{B.4}$$

A similar approximation is used to determine the transition rates at which S-I edges change to S-S edges. We write:

$$\begin{aligned} \omega(s_{k,m,j} \to s_{k,m-1,j+1}) &= m\,\gamma^s, \\ \omega(s_{k,m+1,j-1} \to s_{k,m,j}) &= (m+1)\,\gamma^s, \end{aligned} \tag{B.5}$$

where the rate γ^s is computed using the recovery probability $R(k,m,j)$:

$$\gamma^s = \frac{\sum_{j=0}^{\infty}\sum_{k=0}^{\infty} p_k \sum_{m=0}^{k}(k-m)\,R(k,m,j)\,i_{k,m,j}}{\sum_{j=0}^{\infty}\sum_{k=0}^{\infty} p_k \sum_{m=0}^{k}(k-m)\,i_{k,m,j}}. \tag{B.6}$$

For standard models, one natural assumption is to consider the probability to age as the probability of neither changing state nor resetting:

$$\begin{aligned} F(k,m,j) + F_A(k,m,j) + F_R(k,m,j) &= 1, \\ R(k,m,j) + R_A(k,m,j) + R_R(k,m,j) &= 1. \end{aligned} \tag{B.7}$$

With this condition, taking the limit $dt \to 0$ of Eq. (B.2) we obtain the approximate master

equation (AME) for the evolution of the different sets $s_{k,m,j}$, $s_{k,m,0}$ $i_{k,m,j}$ and $i_{k,m,0}$:

$$\begin{aligned}
\frac{ds_{k,m,j}}{dt} &= -s_{k,m,j} - (k-m)\,\beta^s\, s_{k,m,j} - m\,\gamma^s\, s_{k,m,j} \\
&\quad + (k-m+1)\,\beta^s\, s_{k,m-1,j-1} \\
&\quad + (m+1)\,\gamma^s\, s_{k,m+1,j-1} \\
&\quad + F_A(k,m,j-1)\, s_{k,m,j-1}, \\
\frac{ds_{k,m,0}}{dt} &= -s_{k,m,0} - (k-m)\,\beta^s\, s_{k,m,0} - m\,\gamma^s\, s_{k,m,0} \\
&\quad + \sum_{l=0}^{\infty} R(k,m,l)\, i_{k,m,l} + \sum_{l=0}^{\infty} F_R(k,m,l)\, s_{k,m,l}, \\
\frac{di_{k,m,j}}{dt} &= -i_{k,m,j} - (k-m)\,\beta^i\, i_{k,m,j} - m\,\gamma^i\, i_{k,m,j} \\
&\quad + (k-m+1)\,\beta^i\, i_{k,m-1,j-1} \\
&\quad + (m+1)\,\gamma^i\, i_{k,m+1,j-1} \\
&\quad + R_A(k,m,j-1)\, i_{k,m,j-1}, \\
\frac{di_{k,m,0}}{dt} &= -i_{k,m,0} - (k-m)\,\beta^i\, i_{k,m,0} - m\,\gamma^i\, i_{k,m,0} \\
&\quad + \sum_{l=0}^{\infty} F(k,m,l)\, s_{k,m,l} + \sum_{l=0}^{\infty} R_R(k,m,l)\, i_{k,m,l},
\end{aligned} \tag{B.8}$$

where β^i and γ^i are similar rates as β^s (Eq. (B.4)) and γ^s (Eq. (B.6)), exchanging terms $s_{k,m,j}$ by $i_{k,m,j}$ and vice versa. These equations define a closed set of deterministic differential equations that can be solved numerically using standard computational methods for any complex network and any model aging via the infection/recovery, reset and aging probabilities (a general script in Julia is available in the author's GitHub repository (52)).

The model is introduced via the transition probabilities $(F, R, F_A, R_A, F_R, R_R)$, which may depend on the degree k, the number of infected neighbors m and the time spent in the actual state (or since a reset) j. For the Threshold model with aging, dynamics are monotonic and there are no age dynamics once the agent is infected $R(k,m,j) = R_A(k,m,j) = R_R(k,m,j) = 0$. Therefore, the equations for $s_{k,m,0}$ decouples from the equations for the variables $i_{k,m,j}$, reducing Eq.(B.8) to:

$$\begin{aligned}
\frac{ds_{k,m,j}}{dt} &= -s_{k,m,j} - (k-m)\,\beta^s\, s_{k,m,j} \\
&\quad + (k-m+1)\,\beta^s\, s_{k,m-1,j-1} \\
&\quad + F_A(k,m,j-1)\, s_{k,m,j-1}, \\
\frac{ds_{k,m,0}}{dt} &= -s_{k,m,0} - (k-m)\,\beta^s\, s_{k,m,0} \\
&\quad + \sum_{l=0}^{\infty} F_R(k,m,l)\, s_{k,m,l}.
\end{aligned} \tag{B.9}$$